UCLouvain
Institute of NeuroScience

On delays and decisions: The influence of temporal and spatial uncertainties on oculomotor anticipation.

Dominika Drążyk

Thesis submitted in fulfillment of the requirement for the degree of
Doctor in Biomedical and Pharmaceutical Sciences

Thèse présentée en vue de l'obtention du grade de
Docteur en Science Biomédicales et Pharmaceutiques

Secteur des Sciences de la Santé - SSS
Institut des NeuroSciences – IoNS

Dissertation committee:

Prof. Marcus Missal (UCLouvain, Belgium, *advisor*)
Prof. Sylvie Nozaradan (UCLouvain, Belgium, *secretary*)
Prof. Nicolas Tajeddine (UCLouvain, Belgium, *chair*)
Prof. André Moraux (UCLouvain, Belgium)
Prof. Jennifer Coull (Aix-Marseille University, France)
Prof. Peter Janssen (KU Leuven, Belgium)

July 2025

Table of Contents

Abstract [ENG]

An important differentiation can be drawn between temporal and other types of information that humans collect from the environment. Indeed, no receptors are intended to process the passage of time or the temporal variability of stimuli. At the same time, constructing temporal expectations is crucial for the preparation of movement. Most studies of anticipation use manual responses, such as a key press, to probe the strategies involved in processing stimulus-bound uncertainties. However, it is the oculomotor activity that usually precedes any reaching or withdrawing movement. Furthermore, oculomotor reactions, highly susceptible to changes in inhibitory control, could be a useful marker of uncertainty-induced impulsivity.

The current doctoral project tested the sensitivity of human oculomotor responses to spatial and temporal uncertainty. Results of four consecutive experiments indicate that to produce optimal and stable oculomotor performance, the available resources must be strategically allocated. The cautious strategy used by the oculomotor system in most experimental contexts favours increased resource allocation only in predictable environments. At the same time, spatially or temporally uncertain situations likely cause increased oculomotor inhibition. Studies presented here suggest a difference between manual and oculomotor responses. Results stress the need to further explore all types of eye movements as a valuable probe of human reactions to uncertainty.

Abstract [FR]

Une distinction fondamentale peut être établie entre l' information temporelle et les autres types d'informations que les êtres humains recueillent de leur environnement. En effet, il n'existe pas de récepteur sensoriel temporel. Néanmoins, la construction d'attentes temporelles demeure essentielle à la préparation de l'action motrice. La majorité des études sur l'anticipation temporel s'appuient sur des réponses manuelles. Toutefois, ce sont les activités oculomotrices qui précèdent habituellement les autres mouvements. En outre, les mouvements des yeux sont, particulièrement sensibles aux variations du contrôle inhibiteur, pourraient constituer un indicateur pertinent de l'impulsivité induite par l'incertitude temporelle.

La présente thèse de doctorat a examiné la sensibilité des réponses oculomotrices humaines à l'incertitude spatiale et temporelle. Les résultats issus de quatre expériences consécutives suggèrent que, pour garantir une performance oculomotrice optimale et stable, les ressources cognitives disponibles doivent être allouées de manière stratégique. La stratégie prudente adoptée par le système oculomoteur dans la plupart des contextes expérimentaux privilégie une allocation accrue des ressources uniquement dans des environnements prédictibles. En revanche, les situations caractérisées par une incertitude spatiale ou temporelle entraînent vraisemblablement une augmentation de l'inhibition oculomotrice. Les études présentées mettent en évidence une dissociation entre les réponses manuelles et les réponses oculomotrices. Les résultats soulignent ainsi la nécessité d'approfondir l'étude de l'ensemble des mouvements oculaires en tant qu'outil d'exploration pertinent des réactions humaines face à l'incertitude.

Acknowledgements

Finishing this thesis would not have been possible without the persistent support of others. Firstly, I would like to thank Aicha, Julien, Antoinette, and Anissa for the scientific collaboration and camaraderie, which brightened my time at the office.

I am also grateful to an esteemed team of researchers who provided invaluable guidance along the way. I would like to thank Professors Nozaradan, Mouraux, Tajeddine, and Goffaux for taking active roles as members of my steering committee. My sincere thanks also go to Professors Coull and Janssen who complemented the project with valuable insight during the defense.

I am especially thankful to my supervisor, Professor Marcus Missal, for offering me the opportunity to undertake this project in Belgium. I deeply appreciate his guidance and his encouragement to make the most of the networking opportunities that academia has to offer.

My tremendous thanks also go to the entire UCLouvain Administration Team, who navigated me through the formal aspects of this process with competence and a remarkable degree of patience.

Above all, the greatest amount of strength needed for this long-term project came from Family and Friends.

Moim Rodzicom dziękuję za wielkie wsparcie i niezachwiane przekonanie, że dam sobie radę wszędzie i ze wszystkim. Użyczałam sobie tej wiary bardzo często przez ostatnie lata.

Wreszcie moim Przyjaciołom: Weronice, Agnieszce, Monice, Urte i Magdzie, Karolowi, Adiemu i Mateuszowi, za wieloletnią cierpliwość i za powtarzanie mi, niezmiennie, że powinnam *robić to, co mnie uszczęśliwia*. Nie ma większej oznaki Przyjaźni.

List of Abbreviations

ACh	acetylcholine
ANOVA	analysis of variance
BG	basal ganglia
BIC	Bayes information criterion
BN	burst neurons
CB	cued box
CBPT	cluster-based permutation test
CDF	cumulative density function
CI	confidence intervals
CNV	contingent negative variation
CV	coefficient of variation
DA	dopamine
DDM	drift-diffusion models
EEG	electroencephalography
FEF	frontal eye fields
fMTP	formalised multiple trace theory of temporal preparation
FP	foreperiod
GLMM	generalised linear mixed model
HR	hazard rate
ICD	impulse control disorders
IRR	incidence rate ratio
IS	imperative signal
ITI	inter-trial interval
KW	Kruskal-Wallis rank sum test
LATER	linear approach to threshold with ergodic rate
LC	locus coeruleus
LIP	lateral intraparietal area
LL	log-likelihood
LM	linear model

LMM	linear mixed model
ML	maximum likelihood
NE	norepinephrine
OPN	omnipause neurons
PD	Parkinson's disease
PDF	probability density function
PPR	psycho-sensory pupil response
REML	restricted maximum likelihood
ROI	region of interest
RSS	residual sum of squares
SC	superior colliculus
SD	standard deviation
SE	standard error
SEF	supplementary eye fields
SET	scalar expectancy theory
SMA	supplementary motor area
SMC	supplementary motor cortex
SNr	substantia nigra pars reticulata
SU	spatial uncertainty
TB	target box
TU	temporal uncertainty
VG	visually guided
WS	warning signal

List of Figures

List of Tables

1

Chapter 1

1.1 The "fine cup of coffee" problem

It is remarkable how the human brain makes the most complex tasks seem easy and effortless, at least from the perspective of our conscious experience. Imagine a caffeine lover who wakes up every day and thinks only about his favourite coffee, made exactly how he likes. He puts the coffee pot on the flame and waits. Now, the desired outcome depends partially on how fast he removes the coffee pot from the flame. This must be done just in time for the coffee to be fully brewed and before it is burnt. For him, coffee-making is a ritual that he performs semi-automatically. However, upon closer examination of the process, the actions that he must take are based on a series of perceptual, cognitive, and motor decisions. Those decisions are founded on explicit knowledge, such as the brewing time suggested by the coffee producer, the previous experience of coffee-making, and the current state of the environment, e.g., the temperature. Therefore, to get a fine cup of coffee, one must acquire various types of knowledge, make a sequence of informed decisions, and execute well-timed movements. Or withdraw from those actions that would be too hasty.

However, there are some dangers along the way. The time suggested by the brewing recipe is ultimately just an approximation. Our acquired knowledge could be overridden by the strong need for caffeine. Finally, the variable temperature in the room could blur the perfect brewing interval. Many uncertainties are introduced into an already complex process. For us, it is a

simple morning ritual, but our brain is busy with optimisation.

How is a fine cup of coffee made in an uncertain world? How do we encode the implicit variability of the environment and uncertainty embedded in explicit recommendations? How do we use our previous experiences and integrate the new ones to create the dynamic movement protocol? It could be argued that what connects visual encoding, decision-making, and motor control is temporal processing.

1.2 Explicit and implicit usage of temporal information

1.2.1 Explicit and implicit information processing

Time perception requires the encoding and processing of temporal information [391]. However, temporal information differs from other data usually collected from the environment. Unlike for the visual or auditory input, there are no separate receptors for temporal information. What we know about time is rather an abstract or conceptual representation of its passage, with the arrival and disappearance of stimuli creating the sense of a changing environment [391, 397].

Temporal information can be either explicit or implicit [82, 268]. For example, temporal information is overtly presented when the label on the package indicates that the coffee should be brewed for 3 minutes. This type of information is usually used in *explicit* timing tasks when subjects, as accurately as possible, estimate the length of a given time interval. Subjects can do so by comparing it to a shorter or longer one (perceptual discrimination tasks) or by representing the given interval with a button press (motor timing tasks) [241]. In explicit timing, the fact that the subject must use a temporal perception to execute the task is evident [83].

However, temporal information can be presented and used more covertly or implicitly. With the same goal of making a good cup of coffee, we could base the brewing time on previous experience. Having made one hundred

coffees in the past, we could learn to approximate the appropriate reaction time. When the task is not directly related to time estimation but only requires temporal information to achieve the goal, it is called an *implicit* timing task [83].

1.2.2 Statistical learning

It has already been shown that temporal regularities could be implicitly learned by humans [93]. The process, called *statistical* or *implicit learning*, is executed without a person's intention or explicit awareness [90, 75, 359]. It occurs, for example, when we learn sequences of perceptual and motor actions [334]. It was suggested that such learning engages the basal ganglia, cerebellum, and neocortex [32, 122]. It is also highly dependent on the plasticity and engagement of modality-specific neuronal networks in creating statistics [75]. O'Reilly et al. [279] demonstrated that incidental learning of temporal regularities is strongly bound to performing the movement. This could be due to the fact that when temporal information is implicitly needed for the execution of the motor task, its learning process is facilitated by attention [20]. Indeed, the study of Damsma et al. [92] indicates that the implicit temporal pattern is ignored when it is not part of a task goal. However, recent findings of Salet et al. [317] suggested that, under certain circumstances, a strict bounding of the temporal regularity to the task is not indispensable for its acquisition.

Implicit information could be advantageous in perceptual tasks, as it provides precise knowledge of when the next sensory evidence will be available [267, 269, 270, 382, 76]. Some even suggest that implicitly acquired knowledge could be used in reinforcement learning. Every prediction and knowledge update could be rewarding for the system in itself [44, 396].

Implicit learning of temporal regularities is usually based on repeatable exposition to an event. This exposure gives us information about the possible variability of its occurrence time (*stimulus-bound variability* [170]). The occurrence of most events is influenced by environmental factors. We may

observe that the coffee is ready after 3 minutes most of the time, but sometimes the brewing will be prolonged by the lower temperature in the room or accelerated by the level of the coffee roast. When the experience is repeated, the brain can gather information about the underlying temporal regularity. Some researchers suggest that the brain represents temporal data in the form of probability distributions of the occurrence of an event. In such a distribution, the mean brewing time is represented by the *central tendency*, while the influence of the changing environment (aka noise) is described by the *variance* of the distribution. Subjects can estimate the intended brewing time based on the state of their implicit knowledge (*prior distribution*) and update their knowledge with new data once the brewing is over (*posterior distribution* [125], for review, see [358] and [224]). Every motor behaviour that humans repeatedly and successfully execute must be based on the current knowledge about our individual abilities and the changing environment [399]. The hypothesis that implicit learning informs human behaviour was supported by some recent electrophysiological studies [155, 210] (for review, see [75]).

1.3 Foreperiod task

1.3.1 Variants of the foreperiod task

A *foreperiod task* is an implicit temporal task where the main goal is non-temporal [400, 267]. In this task, a *warning signal* (further abbreviated as 'WS') appears first. It can be a dot on the screen or a sound. It precedes the appearance of a 'go' signal (otherwise called *imperative signal*, 'IS') to which the subject has to respond quickly. This response can be, for example, a button press or a saccade executed with specific instructions. Crucially, the delay between the WS and 'go' signals is referred to as the *foreperiod* (further abbreviated as 'FP'). The warning signal can also be preceded by a *cue* (cued foreperiod task) describing specific parameters of the FP or the 'go' signal [9, 102, 109, 45]. Finally, in some experiments, the WS itself could serve as a cue [1]. If the cue somehow indicates the possible duration of the incoming FP, temporal information in a given task is offered explicitly [9, 45]. This can

be true even if the time estimation is not a direct goal of the task.

The experiment can be further modified to a *constant foreperiod task* [109], where the delay duration between the WS and 'go' signals does not change throughout the trials. Otherwise, when the duration of the FP varies throughout the trials in a block the task is called a *variable foreperiod task* [166, 110, 45]. Based on the structure of the foreperiod task, two time points deserve special attention. First, the *critical moment* describes a possible moment of presentation of the 'go' signal, existing in relation to the entire task. For example, if the 'go' signal could be observed after 400 ms, 900 ms and 1400 ms from the WS in previous trials, those time points represent critical moments in future trials. Secondly, the *imperative moment* is the moment of presentation of the 'go' signal in a given trial. If in a given trial, the 'go' signal appeared 400 ms after the WS, this time point is called imperative moment. In the constant FP task, the critical and imperative moments are exactly the same. In the variable FP task, several critical moments occur, but only one of them will be the imperative moment in any particular trial [216, 214].

1.3.2 Foreperiod effects

In reaction time tasks, where the motor response is triggered by a 'go' signal, the duration of the FP partly determines the latency of responses [400]. Several general rules of that relationship have so far been established:

- *latency-FP effect*: the relationship between the duration of the FP and the latency of motor responses depends on the type of task: a in constant FP task, the mean latency increases with the duration of the FP interval (*fixed foreperiod effect*, [33, 376, 216]); in the variable FP task, the mean latency decreases with the duration of the FP (*variable foreperiod effect*), both when the duration of the FP is previously cued [9] and not cued to subjects [166, 216, 366, 217, 368]. This decrease usually takes the form of an exponential decay and flattens for the longest available FP durations [214]. Interestingly, when the probe, or catch trials are present in the variable foreperiod task, the increasing latency-FP effect is observed for

the cued [9] as well as uncued foreperiod durations [61, 149];

- *sequential FP effect*: observed only in the variable foreperiod task, where the latency on the current trial 'n' is dependent not only on FP duration in that current trial ('FP_n') but also on the preceding FP duration ('FP_{n-1}'). The shape of the relationship is asymmetric. For the short FP_n, the latency of movement strongly decreases with increasing FP_{n-1}. However, the longer the FP_n, the weaker the effect [377, 60, 61]. Furthermore, the typical pattern of the sequential effect can be disrupted if the variability of FP duration in a given block is low [345];

- *transfer effect*: refers to the modulation of the movement latency over the course of the blocks of trials or the experimental sessions. The character of the modulation depends on the distribution of the FP used in the first block or session. Crucially, the modulation can be long-lasting [217, 218, 242]. However, transfer effects do not depend on the subjects' explicit knowledge about the character of the currently used FP distribution [217, 242] (for review, see [318]).

Several theories of temporal preparation aimed to explain the foreperiod effects for the presented types of the task (constant or variable, cued or uncued, with or without catch trials). The subsection *Temporal expectation* will describe the most influential hypotheses. However, the fact that humans can respond to the changing duration of the FP means that they must effectively encode, represent, and track the passage of time. Therefore, the next subsection will explore the evolution of theories of the human internal clock and its neuronal correlates.

1.4 Theories of temporal perception

Early reports indicated that humans have a tendency to overestimate short durations (below 2 s) and underestimate long durations (above 3 s), with the point of most precise estimation falling within the range of 2 to 3 seconds (*indifference point*). This rule, called Vierordt's law (for review, see [207]), was es-

pecially prominent in temporal production and reproduction tasks, where the response was not corrected by any type of feedback [392]. However, further studies demonstrated that Vierordt's law is, in fact, only a deviation from a much more general set of rules. For example, a *central tendency effect* [160, 174] suggested that the indifference point is not fixed but dependent on the average of all experienced durations (for review, see [207]).

1.4.1 Oscillator models

The Scalar Expectancy Theory ('SET') was based on the work of Gibbon and Church [134, 135, 73] (for review, see [392]). It assumed that the behaviour that conforms to SET obeys two main assumptions:

- *mean accuracy*: when subjects produce time intervals based on a specific target duration, the mean accuracy of that production is equal to this duration. This assumption is congenial to the central tendency effect presented before;
- *scalar property of variance*: a form of Weber's law in psychophysics. When we estimate time, the variability (standard deviation, 'σ') of those estimates increases linearly with the target duration to be timed ('t'). The ratio of estimation variability to time is a constant value 'k' (also called *Weber fraction*: $k = \frac{\sigma}{t}$; for review, see [241]).

The scalar property of variance can be confirmed in three ways:

- a regression of standard deviation ('σ') against the mean ('μ') of the behavioural measure (e.g., movement latency) should be described by a linear function with a high coefficient of determination ('r^2');
- a coefficient of variation ('CV') calculated from the standard deviation and the mean of the behavioural measure, $CV = \frac{\sigma}{\mu}$, should remain constant as 't' is varied;
- total variance of responses should be linearly related to the target duration. This can be tested using slope analysis [171]. It assumes that the

total variance has two origins: a duration-dependent source ('c') and a duration-independent source ('k'). As it was shown by Getty et al. [132], total variance ('σ^2Total') is linearly related to the target interval, $\sigma^2 Total = kt + c$. This work was also a basis for the *generalised* form of Weber's law ($\sigma^2 Total = k^2t^2 + c$).

SET was constructed with the assumption that there is, embedded in our perceptual system, some sort of *internal clock* mechanism that keeps track of time. This clock could be of a Poisson *pacemaker-counter* type (see Information Processing Implementation of SET [367, 85], for review, see [236]). During a given target duration, a theoretical pacemaker module generates regular pulses that are further counted by the accumulator. A switch operates the starting and ending point of this counting. Furthermore, the pulses counted for a given duration could be stored in the memory modules (read-out) and then compared with a newly counted interval in the comparator. Once the durations are compared, the output can inform the subsequent decision-making process and the production of an overt response [299].

How does such a straightforward system implement the scalar property? Although the pacemaker and counter modules are non-scalar, they remain under the influence of internal errors and scalar sources of variance from memory or decision-making mechanisms [8, 392]. Some variance could arise from the activity of the switch, influenced by the amount of attention given to an onset stimulus [206]. It could also originate from the decay process that affects the accumulated pulses, depending on the amount of secondary events in the environment that require additional computational power [55]. Finally, the fluctuating level of arousal could influence the pacemaker and change the tempo of emitting pulses [367].

According to SET, the pacemaker-counter approach can be applied to a variety of duration ranges and tasks. Nevertheless, the main assumptions of scalar expectancy remain violated under specific circumstances. For example, interval production without feedback, temporal reproduction, and verbal estimation tasks could deviate from the mean accuracy and the scalar prop-

erty of variance, with the CV decreasing as timed intervals increase [40, 145] (for review, see [392], but see [305] for a possible explanation of the CV-based violations). Furthermore, response variability can be reduced by the amount of training or subjects' experience with specific durations to be timed [146, 240, 237].

1.4.2 Population clock models

The accumulator-counter model of the internal clock assumes a modular structure of the system, where information about counted pulses is calculated by one entity. Then, the information is sent from one module to the other for storage and comparison [299]. Although different claims were made about the possible neuronal localisation of these entities [54], it was also postulated that many such internal clocks could exist at the same time [56].

The more recent model of internal time-keeping incorporated the idea of multiple clocks while abandoning the system's modularity assumption. *Population clocks* [57] are based on the idea that time is encoded in changing populations of neural activity triggered by a stimulus or behaviour. A population clock can be defined as a neural trajectory in a N-dimensional space, where 'N' represents the number of neurons included in the clock. The activity of a single neuron was suggested to obey Weber's law [246, 364]. Temporal information is embedded in the temporal position of each neuron in an activation sequence or the geometrical characteristics of evoked neural trajectories (for review, see [314]). As these neurons are not time-specific, the population can also encode the stimulus itself, combining temporal and spatial processing. This last feature cannot be attributed to ramping models (for review, see [285]). The population clock hypothesis assumes that such a time-keeping mechanism will coexist with the sensory and motor neuronal activity within similar areas (e.g., cortico-thalamic-basal ganglia circuit hypothesis [263]). There is also a duration-dependent specialisation. Protopapa et al. [298] proposed the chronotopic map of human SMA with the activation pattern that was differentiated by the range of tested durations.

Population clock models are often supported by the growing evidence for the existence of so-called *time cells* that were recently found in various brain areas: hippocampus in rodents [229, 284], prefrontal cortex in non-human primates [363] and rodents [59], the posterior parietal cortex in rodents [152] and non-human primates [86], cerebellum in rodents [154], striatum in rodents [246], and entorhinal cortex in rodents [157]. However, the presence of time cells in a specific area of the rodent or primate brain does not directly indicate the existence of such cells in the human neuronal system. It was previously demonstrated that the hippocampus, a region consisting of time cells in the rodent model [229, 284], was not proven to be an efficient timing mechanism across various duration ranges in non-human primate research [310]. In humans, the time-tuning property of neuronal populations was recently presented in the inferior parietal lobule [153].

1.4.3 Ramping models and decision-making

Population clocks are supported by research that indicates the coincidence of two activities: the time-keeping neuronal activity and the activity that manages the action to which this timekeeping is related [80]. However, building a widely-sketched model of behaviour is difficult. Although perception and decision-making are two interleaved cognitive processes, their models are often developed separately. The next set of models assumes that the mechanism of temporal perception strongly informs decision-making.

Evidence accumulation models ('EAM' [301], for review, see [117]) show that the decision process can be explained by a set of parameters: evidence accumulation rate, response caution, and non-decision time [41, 177]. All these parameters can be manipulated by internal and external factors, affecting the characteristics of behavioural reaction times. For example, a study of non-human primates showed that neurons in the lateral intraparietal area encode evidence accumulation and slow down the drift of activity when the anticipated stimulus is uncertain [184].

In 1981, Carpenter defined the decision process as a result of an action

procrastination, extended in time to accumulate enough evidence to support one of the decision options. The length of this procrastination could be called latency. The Linear Approach to Threshold with Ergodic Rate ('LATER' [63, 272]) proposed to analyse the *reciprocal* of response latency, that is, the Gaussian distribution. This transformation allows a logarithmic relationship to be drawn between the prior probability of an event and the average latency of a response to that event. In this way, behaviour becomes an indirect measure of the brain's representation of the expectation of the event [64, 280] in a conceptually simple way [398].

However, the simplicity of the LATER model, based on a small number of modifiable parameters, narrowed the range of its applications. Contrary to drift-diffusion models ('DDM' [301]). DDM, although complex, assumes more degrees of freedom [243]. It allows modelling a two-choice behaviour (a Wald model assuming correct or incorrect response) or a one-choice behaviour (a shifted Wald model assuming mostly correct responses). Similarly to the LATER model, the evidence accumulation about the incoming signal occurs at a *drift rate* and continues until a *threshold*, which, when reached, evokes the response. The latency of a response consists of decision time and non-decision time. The drift rate and the threshold modulate the former, while the latter models the influence of non-decision processes (encoding process, pre-attention, motor preparation [177]). Response caution can be modelled by changing the threshold value [42], while the rate of the drift itself can describe decision difficulty [258] (for review, see [303]). Finally, it was also hypothesized that top-down processes could control the onset of drift [357]. An optimisation could occur to avoid performance errors when the accumulation started too early or to avoid the loss of valid information when it started too late. Indeed, such optimisation could be crucial to maintain good performance in an environment with a changing temporal context and a varying amount of perceptual noise [125].

DDM was recently updated to the opponent Poisson-based theory of interval timing. It claims that the drift is built from the sum of excitatory and inhibitory neuronal spikes, forming a linear ramp-like activity [21, 337]. The

uncertainty or noise in the system comes from the postsynaptic potential variability, modelled as a Poisson process. Ramping neurons decrease or increase their activity to perform time-keeping of a range of different durations. This is different from the population clock hypothesis because population clocks consider the linear activity of neurons only as a group, while the activity of each neuron is non-linear (for review, see [97]).

An inverse Gaussian distribution describes the latency of motor responses assumed by DDM. By applying the model, Simen et al. were able to confirm a set of properties of interval timing using data from both decision and timing tasks in various perceptual modalities (see [337] for details). The results suggest that DDM could serve as a unified theory of decision-making and timing, implemented via neuronal spike activity.

1.5 Temporal expectation

When the task is to compare two durations and decide which is the shortest, the temporal character of this challenge is evident. However, when a mission is to make great coffee, a good sense of the time passing between the beginning and the end of brewing is just a tool to achieve a goal. The implicit usage of elapsed time (*implicit timing* [295]) allows us to find the optimal moment to *act*. This act is a result of decision making, with our attention directed towards a future goal (*future-oriented attending* [25]) and with an informed prediction about the optimal moment for reaction (*anticipation of events in time* [173]). These processes are often hidden under the umbrella term: *temporal expectation* [79, 373, 270].

The temporal expectation is a set of beliefs and predictions about the timing of a future event used to optimise perceptual or motor performance [185, 103]. High levels of preparation are effortful and cannot be held for a long time [274, 175], so temporal expectation helps to highlight the intervals of justified vigilance [377]. Due to this process, the response to an expected event usually has shorter latency and greater accuracy [400, 267, 212].

1.5.1 What is uncertainty?

Expecting something to happen is inevitably bound with some uncertainty. This uncertainty could be represented by the question, "Is something going to happen?". This is called *discrete uncertainty* or uncertainty about the occurrence of events ($P_o < 1$, where P_o is the probability of event occurrence [273, 365]). This term also exists in the literature as *unexpected* or *irreducible uncertainty* [401], as it entails events that go beyond what can be expected from the surroundings (e.g., the coffee pot suddenly disappearing). This uncertainty is not reducible by the process of statistical learning. However, if we are sure that there will be an event to respond to ($P_o = 1$ [383, 332, 280]) but we just do not know exactly when, then a *continuous uncertainty* about stimulus temporal characteristics appears [128, 188]. It could also be called *expected* or *reducible uncertainty* [278], as its source lies in the predictable unreliability of the surrounding status quo (e.g., the changing temperature in the room influences the coffee brewing time). Similarly, expected spatial uncertainty would be related to an event that would surely occur but at an unknown location. Crucially, this type of uncertainty can be reduced by acquiring knowledge about the extent to which an event's unreliability occurs.

1.5.2 A priori information versus a posteriori representation

Many possible distributions can describe the occurrence of an event in time. If an event can appear at one of a few different time points with equal probability, its occurrence can be described with a uniform distribution [91, 166, 356]. If an event appears with some temporal variability but its probability strongly decreases or increases with time, then it is defined by the anti-exponential [143] and exponential distribution [142], respectively. Finally, if an event appears at a certain time point most of the time but may be too early or too late from time to time, it can be described by the Gaussian distribution [366, 155, 156].

However, the actual probability distribution (*a priori probability* [368]; the *probability density function* or 'PDF' [142]) that describes the occurrence of the

event may not be the exact information that our brain processes. The process of deriving temporal information from the environment via repeated exposure, as well as the imperfection of our perceptual apparatus to estimate time, re-shapes the objective probability distribution [285]. Only this re-shaped probability (*a posteriori probability*) is then used to tune temporal expectation and movement [173, 332, 53, 88]. Now, we will take a look at the possible models of this transformation.

1.5.3 Versions of the hazard rate

Temporal expectancy can be expressed by calculating a *hazard rate function* ('HR'). The HR describes the change in the probability that an event will occur, given that it has not yet occurred [173, 269, 220]. For example, if during an implicit temporal foreperiod task, a 'go' signal appears according to a certain probability distribution of the foreperiod, then the classic HR can be described using a formula:

$$HR_{clas}(t) = \frac{f(t)}{1-C(t)}$$

where 't' describes time points in a trial $t = 1...T$, 'f' is the probability distribution of the foreperiod, and 'C' is the cumulative probability distribution [155]. This idea can be easily depicted using the uniform foreperiod probability distribution. For example, FP distribution can be constructed from three different durations or critical moments: 600 ms, 1000 ms, and 1400 ms. At the beginning of the trial, the HR of the 'go' signal appearing at the first critical moment (600 ms) is 0.33. Once the 600 ms point is reached and no 'go' signal appears, the HR at each incoming critical moment (1000 ms and 1400 ms) increases to 0.5. Finally, when the 'go' signal does not also appear at the 1000 ms point, the HR at the last critical moment reaches a maximum (HR = 1). This form of the hazard rate was also called *ageing* [368].

However, the HR function becomes more complex when different distributions are used in the task [214]. If the hazard rate is a good explanation for

the shape of temporal expectancy in a given task, then the latency of response to the 'go' signal should be correlated with it. Higher values of the classic HR function would indicate the existence of a higher preparatory state of the perceptual and/or motor system.

Some researchers proposed additional modifications to the HR function that could improve its fit to the response data:

- *mirrored* HR ('HR_{mir}'): a linear transformation, mirroring the HR variable around its mean [173, 53];
- *reciprocal* HR ('HR_{rec}'): a non-linear transformation that implicates a diminution of low probability events (resulting in relatively longer latencies) and an amplification of high probability events (leading to relatively shorter latencies). It was proposed that the HR_{rec} better describes the engagement of attention during the time of the foreperiod [143, 142];
- *temporally blurred* or *subjective* HR ('tb-HR'): solves the problem of classical HR not representing the scalar property. The subjective HR was created by *blurring* the f(t) with a Gaussian kernel. The standard deviation (σ) of that kernel is proportional to the elapsed time: $\sigma = kt$, where k is the Weber fraction [173, 53, 143, 142];
- *probabilistically blurred* HR ('pb-HR'): was also created by blurring the f(t) with a Gaussian kernel, but σ of that kernel scales according to the PDF of the event's occurrence instead of changing in proportion to elapsed time [280].

Several studies confirmed that the hazard rate modulates the behavioural response under temporally uncertain conditions. HR influenced processing speed [383] and reaction time [267, 368]. Furthermore, some electrophysiological results from non-human primates indicated that the activity of the substantia nigra pars compacta [283] and the lateral intraparietal area [173] is modulated by the *tb*-HR. Human studies suggested that the classic HR could influence the activity of the supplementary motor area [155, 191, 88]. Neu-

roimaging also tracked the influence of the *tb*-HR on the BOLD signal in the visual and visuomotor regions [53].

However, the hypothesis poses a few challenges. Firstly, HR computation requires many intermediate steps: PDF calculation, cumulative density function ('CDF') calculation, the transformation from the CDF to the survival function, and the division of the PDF by the survival function [220, 143]. Therefore, its complexity and proneness to errors could make it ineffective in natural environments. At the same time, it must be noted that how the brain calculates HR is still an open question. Secondly, it was shown that the introduction of reward uncertainty makes HR unfit to explain obtained behavioural results [343]. Third, the HR hypothesis does not take into account the influence of previous foreperiods on the current response. Therefore, it fails to explain the sequential FP effect, which is present in implicit timing tasks [214]. The HR function also cannot differentiate between the constant foreperiod task and the variable foreperiod task with exponential FP distribution. Although the HR function derived from these two distributions is the same, the behavioural results differ. The constant foreperiod task results in an increasing latency-FP slope, while the exponential distribution of FP produces a flat latency-FP relationship [214].

In fact, upon closer examination, the classic hazard rate is the PDF divided by the survival function [220], making the PDF a major factor in the development of the measure. Therefore, it is possible that, when looking for the ways in which the brain encodes temporal expectation, we should turn to something much more straightforward.

1.5.4 Probability density function and its blurring

The hazard rate can be complex for the brain to implement. Therefore, a new proposition is to build an *a posteriori* temporal expectation by deriving it directly from the *a priori* temporal distribution. This proposition assumes that temporal expectation will take the form of the *reciprocal PDF* [143, 142]:

$PDF_{rec} = \frac{1}{PDF}$.

For example, if in the variable foreperiod task, subjects are asked to respond to a 'go' signal after the Gaussian FP distribution, the latency of executed movement should be U-shaped. Further, it was proposed that the PDF_{rec} can be considered in one of three versions:

- original: no blurring is applied to the function;
- temporally blurred ('tb-PDF_{rec}'): also called subjective, the variance of the Gaussian uncertainty kernel increases linearly with the elapsed time;
- probabilistically blurred ('pb-PDF_{rec}'): the kernel's variance depends on the probability distribution of events across time.

This proposal was supplemented with the simple foreperiod test including a fixed number of catch trials (P_o = 0.91). Subjects were required to make a key-press response after the arrival of auditory, visual, or somatosensory 'go' signals. FP duration was derived from the exponential or anti-exponential function, and information about the used distribution was given to subjects implicitly [143]. The Gaussian and uniform distributions were also tested in the subsequent publication, and the percentage of catch trials varied (P_o = {0.6, 0.8, 1} [142]). To summarise, the latency data were fitted to the following set of functions: HR_{mir}, HR_{rec}, PDF_{mir}, and PDF_{rec}. All four functions could be of the original (non-blurred), temporally blurred (tb-), or probabilistically blurred (pb-) form. The results confirmed that the PDF_{rec} outperforms the PDF_{mir} and better fits to the multimodal sensory data than any of the HR versions [143, 142]. This was true for the tasks with a fixed [143] and varied number of catch trials [142]. Finally, the results indicated that probabilistically blurred functions outperformed the temporally blurred models [143, 142].

However, it is worth mentioning that neither experiment included any reward. At the same time, the HR's proficiency in explaining the latency

results was previously shown to depend on the probability of the reward assumed by the task [343, 173, 332, 88].

1.5.5 Single- and dual-process models

Another approach to temporal expectation was proposed by Los et al. and called the *trace conditioning model* [216]. According to the hypothesis, subjects build a mental representation of all critical moments that occur during the FP. This occurs through implicit or explicit learning of the history of FP duration. Each critical moment has a specific conditioned *strength* based on the amount of time the 'go' signal actually occurred at that time. The strength is defined by the balance between neuronal inhibition and activation. If the 'go' signal appeared at the critical moment 'n', this critical moment was *reinforced* in the memory. If the 'go' signal did not appear, the critical moment 'n' strength was *extinct*. The critical moments with the highest strengths would evoke the shortest response latencies. This would happen as a previously inhibited motor system would become activated based on the memory trace attached to that critical moment. The constant inhibition of the motor system during the FP is crucial for the prevention of premature responses [380, 113, 213].

Importantly, the asymmetry of the sequence effect can be explained by the fact that the strength differs for critical moments that occur before and after the imperative moment. Specifically, only if the current FP (FP_n) is shorter than the previous FP (FP_{n-1}) is the strength in trial n reduced by inhibition related to the n-1 trial.

The major goal of the hypothesis was to explain the asymmetry of the sequential effect (also called the *short-term effect*) by the same mechanism that explains the latency-FP effect (*long-term effect*). Hence, this model was labelled as a *single-process model*. Some experimental results confirmed its assumptions [345], but others highlighted that trace conditioning only explains the latency-FP effect under specific experimental conditions [377, 375].

In response, Vallesi et al. proposed a *dual-process model* [377], in which the asymmetrical sequential effect and the latency-FP effect result from differ-

ent mechanisms [374]. First, the latency-FP effect relies on the non-automatic monitoring process based on changing the HR of the 'go' signal onset [267]. Second, sequential effects result from a more automatic, arousal-related process, highly affected by the trial history. Finally, the asymmetry of the sequential effect borrows from both automatic and non-automatic mechanisms [377].

1.5.6 Multiple Trace Theory of Temporal Preparation

The trace conditioning model was soon updated to the Multiple Trace Theory of Temporal Preparation ('MTP' [214]). In this hypothesis, each critical moment was associated with the accumulated strength of neuronal inhibition and activation (also called the *AI-ratio*) stored in a single memory trace. The memory trace included all the attended details related to the WS and the 'go' signal that occurred within a trial. In this way, the WS could be regarded as a retrieval cue that evoked all the memory traces accumulated in previous trials. The newer the memory trace, the more *weighted* or valuable it is to the process. If the trace is not activated, that is, if the given critical moment was not recently related to the arrival of the 'go' signal, its weight could decay over time [353].

MTP assumes that the long-term effects rely on frequencies of distinctive memory traces caused by the prior FP distribution and the short-term effects on the different weights of the memory traces caused by exposition history. Authors proposed to solve the 'single- versus dual-process' problem in favour of the former by assuming that a given experimental variable could selectively influence the strength and weight of the memory traces without assuming that both these properties result from different mechanisms.

The formalisation of MTP ('fMTP' [318]) assumes that the MTP mechanism is realised by time cells. Time cells that encode time points in agreement with the scalar property [164, 229] could communicate with the motor brain regions. This communication, implemented by Hebbian associations, could be a basis for creating the memory traces assumed by the MTP. The

fMTP was further tested on datasets of various existing temporal experiments [368, 216, 266, 217, 344]. It was also compared with the hazard models [318]. According to the authors, only the dataset collected using the Gaussian FP distribution, re-fitted from the study of Trillenberg et al. [368], presented a better fit to the classical HR compared to the fMTP with the HR component ('$fMTP_{hz}$' [318]). Therefore, it was concluded that the fMTP provides a working unified model of temporal preparation that explains a wide range of temporal expectation-related phenomena.

1.6 Ramp-like activity in the brain

Studies measuring event-related potentials ('ERP') report modulation of neural activity before the arrival of the 'go' signal, often attributed to increased *readiness*. One of the ERP components sensitive to these preparatory processes is the *contingent negative variation* ('CNV'). This slow negative electrical wave occurs late in the ERP pattern that is evoked by the warning signal. Its offset latency depends on the duration of the WS. Early findings indicated that CNV amplitude is highest towards the end of to-be-timed intervals, predominantly in motor-related areas [387, 227].

Recent studies have shown that the CNV signal originates from the supplementary motor area ('SMA') and the pre-SMA (e.g., [155], for review, see [83, 192]). It should be noted that both structures are part of the supplementary motor cortex ('SMC' [262]), along with the frontal eye fields ('FEF') that manage the monitoring and inhibition of saccades [351, 350] (for review, see [24]).

1.6.1 The CNV function

The function of the CNV signal is difficult to establish and has been frequently debated over the last twenty years. Early hypotheses proposed that the CNV indexed the accumulation of neuronal spikes from the SMA [225], essentially playing the role of the accumulator module in the pacemaker-

counter model [227, 54, 370, 291] and scalar timing (for review, see [72]). However, later findings that broadened the functional characteristics of the CNV signal repeatedly challenged this view.

An early study by Friedman et al. [124] revealed that the amplitude of the CNV component depends on the predictability of the auditory event. The study included a 'certain' experimental condition in which subjects were explicitly informed about the type of sound incoming. In the 'uncertain' condition, subjects guessed the type of sound based on implicit knowledge about the current block of trials. The CNV was more negative in the 'uncertain' condition compared to the 'certain' condition. The results indicated that the ramping of the CNV can be influenced by factors other than merely the length of the number of theoretical pulses collected by the accumulator before the 'go' stimulus [370]. Further, Kóbor and his team [195] designed a four-choice reaction time task, where predictable and unpredictable streams of targets were presented to subjects. Similarly, the CNV amplitude that built up before the target presentation was more negative for unpredictable streams. Therefore, attention allocation was proposed as the function of the CNV signal. As the unpredictability of the target structure requires more attentional resources to be put into the response, a centrally located CNV could represent the accumulation of the resources necessary for motor planning (for review, see [248, 192]).

Setting up for the motor response is not the only purpose of the CNV ramping activity. Mento et al. [247] presented subjects with the passive oddball task, where no motor response to the 'go' signal was expected. In this task, the delay period between the WS and 'go' signals was varied, but subjects were not informed about the underlying structure of this variability (implicit timing task). The results revealed the existence of the passive CNV signal originating in the SMA, which, again, reached the maximum negativity peak around the expected arrival of the 'go' signal. As the task did not require a response, the function of the CNV in this study was to represent the accumulation of temporal expectancy that is independent of motor programming.

In explicit temporal bisection [265] and implicit choice response tasks [295], the negative peak of the CNV recorded from the fronto-central electrodes was detected at the target duration, which was the base for further decision-making. The CNV was also shown to depend on the trial history. Wiener et al. observed that on a trial-by-trial basis, more negative amplitudes of the CNV followed the longer duration trials and durations that were previously repeated [394]. Similarly, in temporal reproduction tasks, the fronto-central CNV was more negative for trials that followed adaptation to shorter intervals [209] or trials that belonged to a generally shorter-range context [91]. Those findings indicate that the CNV is dependent on prior experience and could reflect shifts in the memory used for anticipation and temporal decisions [189] rather than reflecting the activity of the absolute accumulator module [71].

The group of Boehm et al. proposed an interesting discrimination task [42]. Subjects were asked to observe a cloud of pseudo-randomly moving dots and decide, as fast as possible or as accurately as possible, whether a cloud as a whole moves to the left or to the right. The recording from the FCz electrode demonstrated that more negative CNV amplitudes predicted shorter movement latency. The authors concluded that the CNV could generally represent the level of cognitive readiness to process information. Similar results obtained previously by Wascher et al. (choice response task [390]) were interpreted as a representation of visual attention allocation.

In the family of foreperiod-like tasks, CNV activity is also widely observed. When temporal information about the duration of the incoming FP was implicit, a CNV, recorded from the central and posterior midline electrodes, was shown to reflect the a posteriori probability of the occurrence of the 'go' signal, well described by the hazard rate [368]. When the task included an informative temporal cue, indicating the duration of the incoming FP, or non-informative cue, the fronto-central CNV was more negative for informative cues [215]. Similarly to the work of Boehm et al. [42] and Waschet et al. [390], these results could further indicate that the CNV is sensitive to explicit cues that could justify the increased level of cognitive readiness to

process incoming information.

The results mentioned above contribute to the broader picture of the functionality of the CNV, compared to the early hypotheses related to the pacemaker-counter model [227, 291]. This early work placed the CNV signal as a direct representation of the passage of time with a dedicated neuronal source. According to the updated view, the CNV activity can index both the cognitive and motor preparation processes [136]. Especially in temporal tasks, the CNV is strongly associated with the perceptual and motor aspects of the higher-order functions required to maintain temporal processing [189], with preparation and anticipation being the cornerstones of this process [84]. Depending on the task specification and the effector of the planned movement (a hand or an eye), multiple brain areas were shown to contribute to the global CNV signal [381] (for review, see [192, 189]).

1.6.2 SMA as a source of the CNV

The SMA was proposed as a region responsible for the connections between motor programming [5, 6] and cognitive control systems [13, 12]. This places the SMA as a decision-making centre that inhibits inappropriate responses [338, 255, 5]. The SMA is also responsible for decision trade-offs in the context of increased spatial impulsivity [292, 65]. The activity of the pre-SMA was shown to increase when the perceptual demands of a temporal discrimination task were increased ([83] but see [3] for the contradictory results in non-human primates).

On the other hand, in motor timing tasks, the activation of the SMA was dependent on the task context. The SMA was activated alongside the basal ganglia when the representation of the timed interval was specified internally [129]. The basal ganglia were activated alone for the externally specified representations of the time interval [83]. The ramping activity of the SMA region was also manipulated by changing the hazard function of the foreperiod duration [155, 53]. However, it should be noted that, depending on the task at hand, this SMA activation could be accompanied by a collection of task-

dependent regions that contribute to the ramping activity [53].

Recent findings propose that the CNV is a result of the synchronisation of multifunctional groups of time-keeping neurons (motor cells, relative and absolute timing cells, and time accumulator cells; for review, see [248, 192]. All of these cells are characterised by specific ramping activity and could contribute to the overall shape of the scalp CNV [248]. In this way, the CNV could represent the optimization process of neuronal excitability during the event anticipation [285]. Within this framework, more negative amplitudes would represent a stronger disinhibition of the CNV source regions [189] and different oscillation tempos would be used to encode representations of different time ranges [192]. This view of the CNV functionality would be closer to intrinsic timing systems such as population clocks [57, 285]. According to this model, various recurrent neural networks create a multidimensional space from which the neural population clock emerges naturally. It was demonstrated that the systems discussed could be trained to output a linear ramp similar to the pattern of the CNV [252]. It must be stressed, however, that presented associations between CNV ramping activity and the suggested optimization of neuronal excitability are based on correlational evidence.

1.7 Oculomotor system - an unique effector

Saccades are fast gaze-orienting eye movements occurring between fixation periods when the visual axis is immobile [133, 232]. They could be described as 'first respondent' motor reactions, as they usually precede hand movement or a re-direction of the person's gait. Saccades are performed to direct the fovea that processes fine details of a visual object towards the most informative parts [277, 232]. In order to initiate a saccade, some information about the object of interest is gathered by peripheral vision. This information is processed by various higher-order cortical areas, which decide whether the target is worth reacting to [63, 28, 141, 39, 161]. If the decision was made to initiate a movement, the latency of the saccade is a crucial marker of decision complexity (*oculomotor procrastination* [63]). After the saccade ends, the

fixation re-occurs and the system can gather the maximum amount of information about a given object [398, 347, 211]. This information can be used to influence future decisions.

Oculomotor responses are strongly dependent on the temporal predictability of the incoming event. The expectation of an event with a predictable onset time is related to the inhibition of saccadic behaviour just before its arrival [94, 355]. Furthermore, since this inhibition can also be observed before non-visual targets [18, 1], it is hypothesised that oculomotor inhibition could be used as a non-specific marker of temporal expectation (for review, see [81]).

Therefore, when a saccade is directed towards a specific object, it reveals not only the spatial information about its location but also the latency-encoded information about the complexity of the decision process that leads to a movement.

1.7.1 Neuronal basis of saccadic behaviour

This section will discuss the brain regions and muscles that cause saccadic eye movements. The approximate localisation of involved brain structures is presented in Fig. 1.1A, whereas the simplified functional diagram of the neuronal pathways engaged in the saccade execution is shown in Fig. 1.1B. Different neuronal pathways that inform future saccadic movement converge towards the *superior colliculus* ('SC' [168]). Based on its function, the SC can be divided into two parts. First, the *superficial* SC ('SCs') receives input from the *retina* and the *visual cortex* ('VC'). Its function is simply to integrate visual information. Second, the *intermediate* SC ('SCi') integrates motor signals from different sensory modalities and uses cognitive information to influence saccade-related decisions. The SCi receives input from the *supplementary eye fields* ('SEF') and the *frontal eye fields* ('FEF'). This information transfer can take two forms: direct excitatory input, which defines the direction of the saccade, and indirect inhibitory input through the *basal ganglia* ('BG' [183]), which controls saccade onset through inhibition [159, 28].

The mediation of the BG over the SC occurs through the activity of its two

nuclei: the *substantia nigra pars reticulata* ('SNr') and *caudate nucleus* ('CD'). In general, the SNr sends the inhibitory information to the SCi. However, when the CD receives input from the FEF, it can disinhibit the SNr and lead to the excitation of the iSC [159]. Finally, the intermediate SC can also be modulated by the activity of the *lateral intraparietal area* ('LIP'). The function of the LIP is to determine whether the visual target is behaviourally relevant [28, 141, 39, 161]. The LIP was shown to receive information related to the task even before the FEF or SEF [335]. The SC is also involved in the information transfer between the retina and the VC [48], mediated by the visual part of the *thalamus* [315].

The sum of SC activity is further transferred to the *burst neurons* ('BN') in the *midbrain* and *brainstem* (for review, see [323]). The BNs control the transition between periods of fixation and saccades. The bursts are then sent to the *extraocular muscles* ('EOM'), which finally perform the saccadic movement. Interestingly, the BNs can receive direct input from the FEF, which not only chooses the direction for a saccade by selecting the appropriate target but also suppresses distractors [78, 74]. Furthermore, some results indicate that the FEF can be an evaluator of movement history used to optimise future behaviour [357]. The *cerebellum vermis* is another region that transfers the signal from the SC to the BNs. It plays a role in error-based learning [108] and saccade adaptation [361, 325]. Finally, the BN are strongly influenced by the activity of the *omnipause neurons* ('OPN') located in the *raphe interpositus nucleus* ('RIP' [162]). The OPNs are always active, except when a saccade is executed [277, 313], and their role is to prevent the onset of ill-planned movements.

1.7.2 Measuring saccadic behaviour

Saccades can be described using various movement-related measures, such as the *amplitude* of a singular saccade (in degrees), *maximum velocity* (also called *peak velocity*, further abbreviated 'V_{max}'; in degrees per second) or saccade *latency* (in milliseconds; see Fig. 1.2A for details) [232].

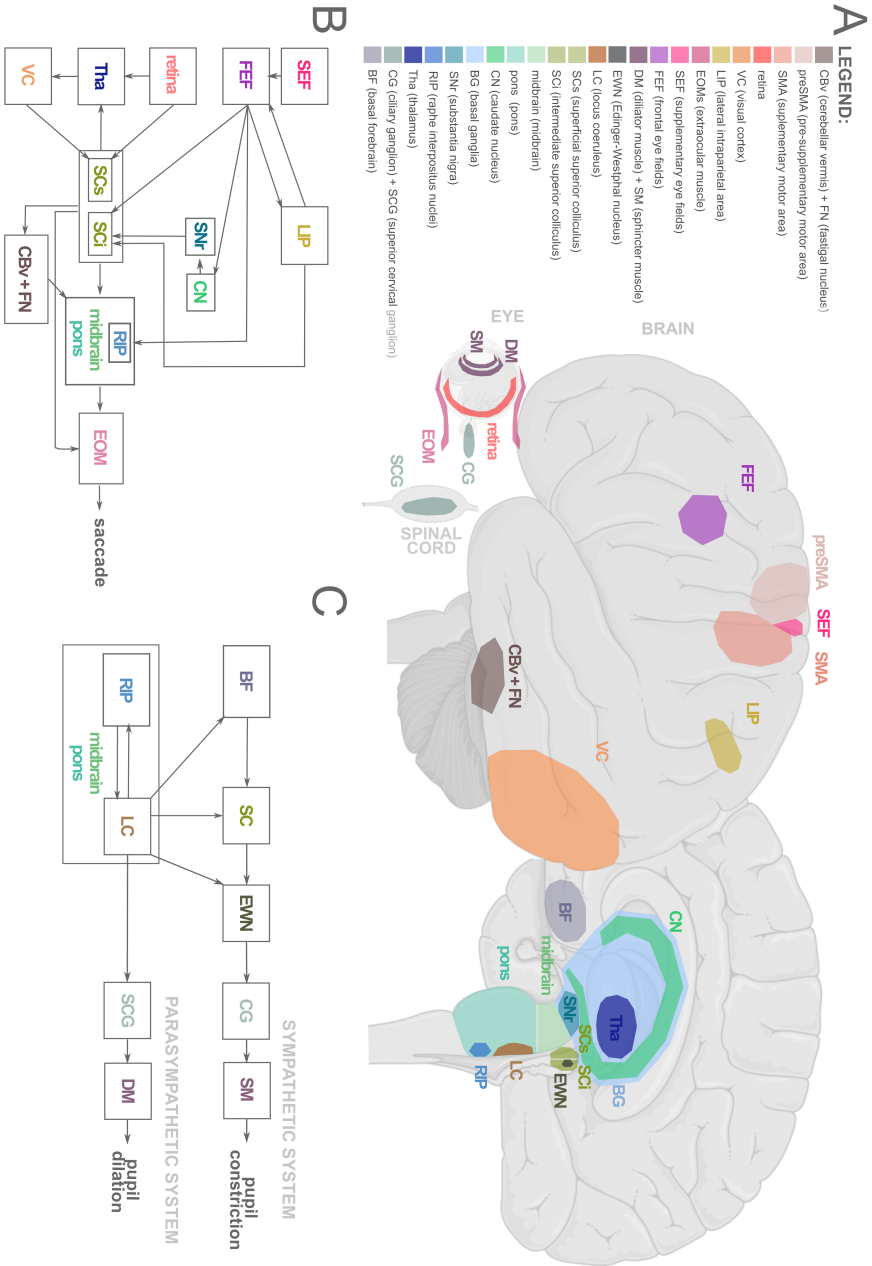

Fig. 1.1 Neuronal pathways that control the oculomotor system. (A) Approximated localisation of the brain regions and eye muscles (*coloured shapes*). **(B)** Major known neuronal pathways and muscles involved in making a saccadic movement. *Arrows* represent the main direction of the information transfer. *Outlines* represent specific regions. **(C)** Major known neuronal pathways and muscles involved in forming a pupillary response.

It is well-known that mean and maximum velocity increase with the relative amplitude of a saccade, a function known as the *main sequence* [19, 306]. However, saccadic V_{max} could also reflect the cognitive processes related to anticipated and perceived events. Non-human primate research indicates that arousal, elevated by the possibility of reward, can increase saccadic velocity [354, 183, 69, 362, 327]. This reward effect present in humans [250] can also be modulated by individual motivation [257]. V_{max} is defined by the maximal firing rates of the BN during saccadic movement [127, 104, 341, 115]. Therefore, it was hypothesised that the level of neuronal excitation presented by the BN could be a result of arousal changes related to the current or anticipated perceptual situation [259]. Munoz and Everling proposed that this neuronal modulation could originate directly from the FEF, and the SC mediated by the cerebellum. Saccadic eye movements result from a sequence of acceleration and deceleration of the eyeball executed by the extraocular muscles. The works of Goossens et al. [139, 140] introduced the *dynamic vector summation model* where the SC overlooks each eye movement via a series of *mini-vectors* that can be modulated instantaneously as the movement progresses. Electrophysiological data from non-human primates recently supported this hypothesis [339]. Finally, it was also experimentally shown that the OPN can change the speed of the saccades [253]. In addition to the reward incentive, the eye's V_{max} can be modulated by the difficulty of the visual task [104], target valuation [306] or luminance-related changes in pupil size [389].

The latency of the saccade, also called saccadic reaction time, describes the delay between the arrival of the visual stimulus and the start of the eyeball movement (see Fig. 1.2A for details). Similarly to velocity, it can be influenced by the reward incentive, with shorter latencies evoked in response to rewarded targets [183, 69, 362, 36, 250]. Latencies are also modulated by target probability, with shorter ones being evoked by predictable targets [250]. Consequently, saccadic behaviour can be successfully described using ramping models of decision-making such as LATER [63, 272] or DDM [301, 337].

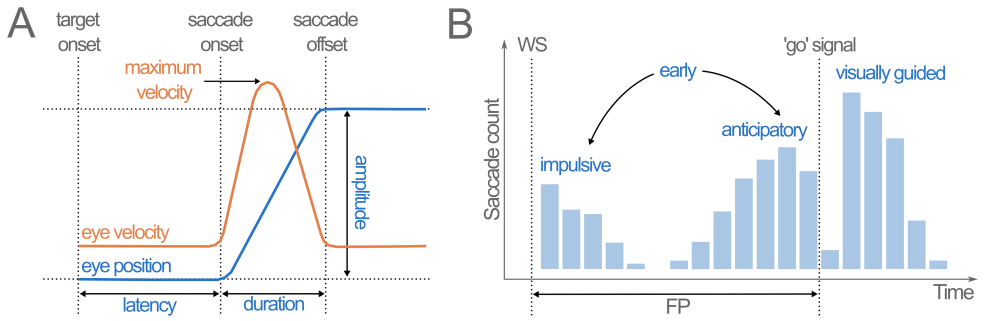

Fig. 1.2 Types of saccades and saccadic parameters in the current project. **(A)** Schematic representation of saccadic parameters derived from the velocity (*orange traces*) and the eye's position (*blue traces*). **(B)** Schematic distribution of different types of saccades. Early impulsive saccades occur just after the WS offset. Early anticipatory saccades are evoked by the anticipation of the onset time of the 'go' signal. Finally, the visually guided saccades are evoked by the 'go' signal. *Blue bars* representing the saccade count are included for illustrative purposes.

1.7.3 Saccades and impulsivity

Saccadic movements can be divided into different categories depending on their timing and origin. The execution of a *voluntary* saccade is based on cognitive decision-making. For example, when we decide to move our sight away from the painting that we have just inspected to let our eyes freely explore another part of the exhibition room. A *visually guided* saccade ('VG', see Fig. 1.2B) is performed when the visual target appears in the periphery of vision and guides our sight towards itself (a *prosaccade*) or when an aversive stimulus appears close to our fixation point and forces us to turn our eyes elsewhere (an *antisaccade* [106]). Average latency of visually guided saccades is approximately 200 - 250 ms, while V_{max} can range from 100 to 700 °/s [232].

Upon a closer look at the neuronal basis of the saccadic movement, we can see that the system is kept under persistent inhibitive control. Burst neurons that send motor commands to the extraocular muscles around the eyeball are constantly inhibited by the OPN, except when the saccade occurs [277, 313].

If this inhibitory system was malfunctioning or overridden by another influence [251, 294] (e.g., influenced by the activity of the FEF [350] or the LIP [28, 348]), it could lead to increased saccadic intrusions [281]. This hypothesis was strengthened by the recently published results, linking the single-trial neural dynamics in the LIP area to decision-making processes modelled by DDM [346]. Uninstructed saccades could blur the vision of a currently observed object or disrupt the temporal anticipation of the oculomotor system. This disrupting behaviour will be further described as *oculomotor impulsivity* [166], a possible sign of impaired inhibitory control [105, 112, 204, 58]. Studies suggest that the uninstructed saccade should not be treated simply as an error response. Uninstructed saccades could provide valuable information about the state of inhibitory control in the oculomotor system [166, 102].

In itself, impulsivity is a complex concept that arises from reduced inhibitory control [118, 24, 386]. Its cognitive aspects can be observed as impaired decision-making (e.g., the tendency to gamble). Its motor aspects can be observed, for example, in nervous ticks or premature reactions [231, 150, 186]. Diagnostically, this type of behaviour is usually assessed using self-administered questionnaires such as the Barratt Impulsiveness Scale [27, 286]. However, this method has its downsides. First, subjectively assessed measures are often variable, as they succumb to the influence of subjects' mood or personal bias. Indeed, it can be difficult for subjects to objectively assess their own behaviour. Secondly, questions or statements in the self-assessed questionnaires can be difficult to understand. Consequently, there is a need for reliable behavioural measures of impulsivity [24]. Attempts have already been made to evaluate the motor consequences of increased impulsivity using oculomotor responses [166, 102, 9]. Those will be described in the following subsections.

1.8 Psycho-sensory pupillary response

The basic function of a pupil is to optimise vision in different environments. First, it can modify the amount of light that reaches the retina (*pupil light re-*

sponse). Further, pupils can control the precision of vision for far and near objects (*pupil near response*). Most importantly for this work, pupillary responses can reflect the arousal-related changes or the amount of mental effort put into a given task (*psycho-sensory pupil response* or 'PPR') [238]. Pre-stimulus pupillary response, recorded in anticipation of the incoming event could reflect modulations of attention, aka *attentional readiness* [235]. The pupil's tonic or phasic activity is usually measured by its *dilation*, averaged between both eyes and relative to baseline [232, 238].

The approximate localisation of the structures involved in the pupillary response is presented in Fig. 1.1A. The simplified functional diagram of the neuronal pathways involved in the pupillary response is shown in Fig. 1.1C. Changes in pupil size are mechanically caused by the sphincter muscle ('SM') and the dilator muscle ('DM') located in the eye's iris. The SM, driven by the parasympathetic part of the nervous system, is responsible for pupil constriction, while, coherently with its name, the sympathetically operated DM causes the pupil to dilate [70, 238].

1.8.1 Neuronal mechanism and the function of PPR

So far, the research has indicated that the PPR response could be altered by the following neuromodulatory agents: the basal forebrain ('BF') through cholinergic transportation ('ACh' [304]); the midbrain and the SC through dopamine ('DA' [98, 388]); the RN via serotonin signaling ('5-HT' [68]); and by the LC through norepinephrine ('NE' [15, 49, 98, 179, 304], for review, see [349, 147]).

It was hypothesised that the phasic PPR could represent the moment of change in the internally generated predictions of the incoming stimuli [264, 98, 99]. Arousal, represented by changing levels of pupil dilation, could reflect the extent to which the incoming event fits already existing predictions about the environment (*stimulus-related surprise*). If an event fits the internally built expectations, arousal and pupil dilation remain low. However, if newly acquired information contradicts the existing model, the high

arousal increases dilation. Consequently, increased pupillary dilation indicates the need for the actualisation of expectations [278, 403, 187, 202, 296]. The above-mentioned changes in the pupillary response are detected even when predictions about the environment are made unconsciously [4]. This expectation-updating system was nuanced by suggesting that the BF-ACh pathway could transfer information about expected changes in the environment (or *expected uncertainty* [96]) while unexpected modulations (*unexpected uncertainty* [193]) were maintained by the LC-NE signalling [401, 196] (for review, see [35]). Finally, this activation of the LC-NE pathway was also associated with enhanced exploratory behaviour. In turn, the exploratory behaviour was shown to result from a sudden, unexpected change in the environment [15, 176].

Another body of research has linked the arousal-related pupil response with increased task difficulty related to decision-making [371, 308, 131], the amount of information held in the working memory [181], or the complexity of processes for which this information is used [378].

Finally, a growing set of results linked pupil dilation to time-related processes. Changes in pupil size could reflect adaptation of the decision strategy dependent on the implicitly learned temporal structure of the task [203]. Pupils were also responsive to the increasing temporal expectation related to incoming events [296, 261, 395, 46]. Crucially, the group of Akdoğan et al. [2] tested pupil dilation levels during a visual discrimination task with variable foreperiod and catch trials. It was demonstrated that the rate of pupil dilation was dependent on the expected timing of the incoming event, with the steeper progression of dilation for imminent events.

1.9 Temporal expectation interacting with spatial uncertainty

1.9.1 Spatial uncertainty as surprise

The word '*uncertainty*' can be associated with '*surprise*' [170]. In this context, surprise is not used to describe an emotion or a startling response [116].

Instead, surprise describes a quantity of error related to a given prediction [296, 170, 307]. Significant space was already dedicated to discussing the differences between the 'uncertainty' and 'surprise' terms in different theories [219, 170].

In this work, *Shannon's surprise* will be used [331]. This form of stimulus-bound surprise is expressed in bits and describes the amount of information given to an observer when an event occurs (so-called *information gain*). It relies on the assumption that each occurrence allows us to learn something about the implicit characteristics of a given event. Shannon's surprise can be used when these characteristics can take one of a few nominal states (e.g., a future event can appear in the left, central, or right box) [331]. When few possible spatial locations can contain the future event, the surprise ('S') related to its arrival can be computed as the negative logarithm of the probability that a visual target will appear at a given position, using the following formula:

$$S = log_2(\frac{1}{P_o})$$

where P_o is the probability of an event at a given position. Similarly to event timing, knowing the exact location of the event can be beneficial to its encoding and processing [23]. This facilitation occurs because the observer's attention shifts to the expected location even before the event appears [22, 290]. Oculomotor responses are particularly suitable to test the effects of spatial uncertainty on anticipation [138, 66].

1.9.2 Spatio-temporal information

Although spatial and temporal uncertainties can be separated in laboratory settings, they often co-occur in natural environments. Consequently, a question can be posed: Are these types of uncertainty affecting eye movements differently, or is there a common neuronal and functional mechanism responsible for encoding the combined uncertainty? Some hypotheses claim that the uncertainty of various types (also called *canonical uncertainty*) is jointly en-

coded in neuronal populations (*summary statistics*, see [16] for an overview). An opposing view assumes that the uncertain aspect of an event is bound to its representation. That is, an uncertainty about the location of a future object will be represented and processed in a different area than its timing variability.

Some research indicated that when spatial and temporal cues related to future events are available together, an additive effect of both can be observed on performance. This is true for the target discrimination [249, 309], temporal orienting [107, 82], and visual search tasks [326]. These observations challenge the hypothesis of separate attentional mechanisms working for spatial and temporal information [82, 230, 126, 393]. Finally, a spatio-temporal neurophysiological model was proposed, suggesting that the link between spatial and temporal processing originates in the retinotopic receptive fields. Those receptive fields were shown to be spatially specific but synchronised in a time-specific way [270].

1.10 Previously published research on the topic

Previous research has already studied oculomotor behaviour in a temporal context. The set of tasks designed by Ameqrane et al. and tested on healthy human subjects [9] was followed by the work of Hsu et al. [166] and Degos et al. [102], where the results of the healthy control group were compared with the oculomotor data collected from a cohort of the Major Depressive Disorder ('MDD') and Parkinson's disease ('PD') patients, respectively. Although in the current work, I will mainly refer to the results of the control groups, the insights related to PD and MDD groups will be included in the last chapter.

Ameqrane et al. [9] tested the influence of temporal uncertainty on oculomotor responses in the absence of spatial uncertainty. In the implicit variant of the experiment, four FP durations were presented to subjects (400, 900, 1400, and 1900 ms), either randomly chosen for each trial with the same probability (*implicit variable FP task*) or randomly chosen for a whole block

of trials (*implicit blocked FP task*; see Fig. 1.3 for details). In the explicit variant of the task, the same durations were randomly assigned to each trial, but the chosen FP duration was cued at the beginning of the trial (*explicit variable FP task*). In the blocked FP task, results demonstrated that the latency of saccades was increasing with FP duration (see Fig. 1.3 for details), which is consistent with the fixed foreperiod effect, widely observed in manual reaction time tasks [33, 376, 216]. In the variable version of the implicit task, the latency of saccades decreased with increasing foreperiod duration (see Fig. 1.3 for details), which confirms the existence of the variable foreperiod effect [216, 366, 217, 368] in the oculomotor domain. This was also true when the duration of the FP was explicitly cued. Interestingly, however, in implicit and explicit variable FP tasks, the variance of saccadic responses decreased as FP duration increased. This result opposes the scalar property of variance previously observed in manual tasks of explicit [270, 83] and implicit contexts (the perceptual timing task [293] similar to [9]). Interestingly, previous research suggested that the oculomotor system could not obey the scalar property [280].

Furthermore, a special version of the explicit variable task was created, where the duration of the FP was cued to subjects but the 'go' signal did not appear at the end in a predetermined proportion of trials (probe or *catch trials*). Interestingly, another type of saccade was observed during the explicit procedure with catch trials. Those saccades were executed during the FP, but their latency was very close to the cued 'go' signal timing. It suggests that subjects presented with explicit information about the possible timing of the 'go' signal use it to generate fast responses. Sometimes, a so-called anticipatory saccade can occur when their anticipation was too early [182]. The existence of anticipatory saccades was demonstrated in both non-human primate [254, 9] and human research [200, 290]. We suggest that this type of saccade provides an insight into subjects' expectation process that cannot be obtained only from stimulus-evoked responses [9, 290, 289, 10].

Another type of saccade initiated during the foreperiod was observed in the work of Hsu et al. [166]. Those saccades occurred mainly just after the

warning signal offset and were defined as 'premature'. In this work, they will be defined as *impulsive saccades* as they probably originate from impaired inhibitory control of the eye [112, 204, 58, 102]. In the experiment of Hsu et al., a form of spatial uncertainty was introduced to the task, where the 'go' signal could appear in one of the four boxes at the top of the screen. No previous indication of the location of the future signal was given to subjects. Therefore, this task includes 'maximal spatial uncertainty' (see Fig. 1.3 for details). However, similarly to the situation where there was no spatial uncertainty [9], the variable foreperiod effect was also observed.

Finally, the research of Degos et al. [102] showed that both types of saccades observed during the foreperiod can occur in one task. Here, the duration of the variable FP was explicitly cued to subjects (see Fig. 1.3 for details). Visual inspection of saccade latency distributions during the FP demonstrated the existence of two modes. The 1^{st} mode describes a transient increase in the number of early saccades after the offset of the WS. Those are the *impulsive* saccades. The 2^{nd} mode shows a gradual increase in the probability of the occurrence of a saccade as time elapsed during the foreperiod. Those are the *anticipatory* saccades. To capture the entirety of the bimodal structure of the distribution, in the present thesis work, all saccades that occurred after the offset of the WS but before the arrival of the 'go' signal (impulsive and anticipatory) will be referred to as *early* saccades (see Fig. 1.2B for details).

In Degos et al. [102], the number of impulsive saccades decreased in the explicit timing task compared to the implicit task. In contrast, changing from an implicit to an explicit task increased the number of anticipatory saccades. This strengthens previous observations and indicates that impulsive and anticipatory saccades occur due to two separate mechanisms [9, 166]. If information about the predictable 'go' signal timing changes only the number of anticipatory saccades but not impulsive ones, then the former must be guided by a cognitive processing of information. Anticipatory saccades could be driven by neuronal activity in the SC and modulated by the SNr with the participation of inhibition from the OPN. On the other hand, impulsive saccades could simply be an effect of the impaired SC-SNr-OPN pathway [102].

1.11 Overview of the project

This project aimed to further study characteristics of the oculomotor response in the context of temporal uncertainty. Most studies on temporal perception and anticipation use manual operant responses, such as a key press or a hand movement. However, when an object appears in the surroundings, the subjects' first reaction is usually to gaze towards that occurrence before reaching for or moving away from it. Furthermore, eye movements are very susceptible to changes in inhibitory control. Therefore, saccades can be used to investigate how temporal uncertainty bound to an incoming event influences human impulsivity. Using saccadic eye movements as a tool for the screening of neurodegenerative diseases could provide valuable insight into the impulsivity-related characteristics of these impairments. Existing temporal perception and anticipation studies, reviewed in Chapter 1, demonstrate that various factors such as the implicit and explicit nature of temporal information, the presence of spatial and temporal cueing, and the shape of the temporal distribution could influence the decision process leading to the motor reaction.

Recently, it was proposed that expected and unexpected uncertainty could independently influence behaviour [142]. In the present thesis, the main focus will be on expected uncertainty related to the timing and location of a visual target. Related research suggested certain patterns that describe early and visually guided saccades in different types of foreperiod tasks [9, 166, 102] (see Fig. 1.3 for details). Based on those results, Chapters 2 to 4 will describe experimental studies designed to test human oculomotor responses under different forms of spatial and temporal uncertainties. The number and distribution of early saccades, and the pupillary traces recorded during the anticipation period will be presented, along with measurements of saccadic latency and maximum velocity.

In Chapter 2, two experiments demonstrated the influence of spatial uncertainty on oculomotor responses. In the work of Hsu et al. [166], only maximal spatial uncertainty was investigated. Here, four spatial uncertainty

levels were introduced. Experiment 1 presents the influence of spatial uncertainty on oculomotor responses using a foreperiod task with an explicit spatial cue and without temporal uncertainty (see Fig. 1.3 for details). Then, in Experiment 2, an *implicit foreperiod variability* differing over the course of *blocks* of trials was introduced to test the joint influence of temporal and spatial uncertainties on behaviour. The choice of the foreperiod duration used in the current experiment (400, 900, 1400, and 1900 ms) was motivated by related research [9, 166] (see Fig. 1.3 for details).

Chapter 3 further tests the hypothesis that the representation of spatial and temporal uncertainties could interact using *explicit spatio-temporal cues*. In that experiment, temporal uncertainty was informed with a cue about the variability of the FP distribution used in a given trial (see Fig. 1.3 for details).

In Chapter 4, a variable foreperiod paradigm was used to test the influence of the implicit temporal uncertainty on eye movements. Furthermore, this approach allowed to test existing theories of temporal expectation with saccadic eye movements, instead of a manual reaction time task. Crucially, the Gaussian-shaped foreperiod distribution is a little closer to everyday life situations where the uncertain timing of an incoming event is usually centred around a specific value with a given level of variability (see Fig. 1.3 for details). Furthermore, electrophysiological recordings made during the same experiment are presented to explore possible neuronal markers of the implicit anticipation process.

Finally, Chapter 5 discusses results to address the question of how spatial and temporal uncertainties shape the oculomotor responses in a healthy human population.

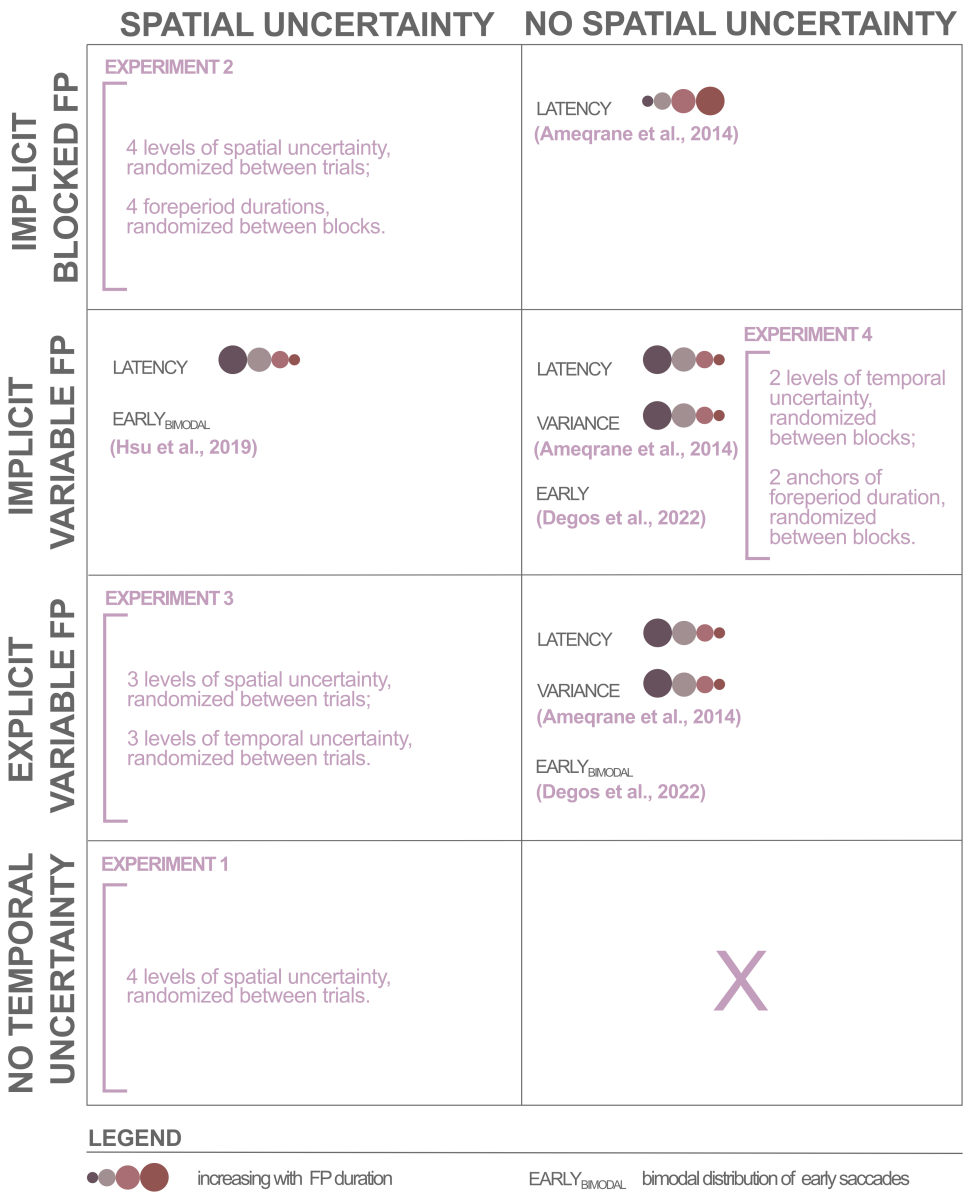

Fig. 1.3 Summary of related research and the current project. Each experiment is presented in one of two *columns* based on the role of spatial uncertainty in the design. *Rows* indicate the type of FP task used in the given design. Cells include a short summary of experimental designs (*in pink*). *Coloured pictograms* are described in the legend. See also: [9, 166, 102].

2

Chapter 2

2.1 Introduction

PREDICTION of future events is essential for a successful optimisation of behaviour [125, 358, 399]. However, each event is related to some spatial and/or temporal uncertainty that must be estimated in the decision process [219]. It has been suggested that acetylcholine involved in pupil size control [244] could signal uncertainty processing [401, 360]. Therefore, the pupillary response is commonly used as a behavioural measure of the subjective impact of uncertainty on sensory and decision processes [131, 187, 4, 296, 202] (for review, see [403]). The size of the pupil was shown to reflect changes in both temporal and spatial expectations [2, 296, 202].

Uncertainty also plays a major role in gaze shifting [163, 300, 52] and could 'capture' oculomotor behaviour [137]. If surprise partly determines oculomotor behaviour, it remains to be established how this phenomenon affects different types of eye movements. Indeed, eye movements occur either in reaction to a stimulus in the environment and are *visually guided* ('VG') or *early*, occurring before the target appears [201, 166]. In Chapter 2, two experiments will demonstrate the influence of spatial uncertainty on oculomotor responses.

Specifically, the analysis will test the likely logarithmic relationship between the VG saccade latency and spatial uncertainty, also called the Hicks law ('HL' [158, 167], for review, see [297]). In Hick's original experiment, human subjects had to associate a key on a keyboard with the spatial position of

a visual target. This task required the association between a set of stimuli and responses. Hick's law states that increasing the number of response alternatives (uncertainty) will cause a logarithmic increase in reaction time. HL can be interpreted as a measure of information transfer in Shannon's sense. In order to test Hick's law, spatial uncertainty will be quantified using *Shannon's surprise* [331] and expressed in bits. Hick's law has been repeatedly observed in different sensorimotor modalities. So far, evidence suggests that VG saccades obey HL if a cued target is chosen among several alternatives [205]. However, it is not observed if saccades are simply visually guided [194].

In Experiment 1, only the level of spatial uncertainty will be manipulated. The future position of the target will be provided by a cue that creates a prior expectation but with a certain amount of spatial 'surprise'. The delay between the warning and 'go' signals (also called foreperiod or 'FP') will be constant throughout the experiment (see Fig. 1.3 for details). In Experiment 2, an implicit temporal uncertainty will be introduced using a variable foreperiod differing over the course of trial blocks (see Fig. 1.3 for details). Both experiments will test the impact of spatial surprise on the parameters of VG saccades after the 'go' signal and the number of early saccadic responses and pupillary changes during the foreperiod. Additionally, Experiment 2 will demonstrate how the relationship between oculomotor responses and spatial surprise established in Experiment 1 is changed by introducing some form of temporal uncertainty.

The first part of the chapter describes the results of Experiment 1. It consists of a paper published in Scientific Research in 2022, adjusted to the structure of the thesis. The official citation of the work is as follows:

Drazyk, D., & Missal, M. (2022). The oculomotor signature of expected surprise. *Scientific Reports*, *12*, Article 2543.

The second part of Chapter 2 consists of a manuscript that will be submitted for publication in The Journal of Neuroscience, adjusted to the structure of the thesis.

2.2 Experiment 1: Methods

2.2.1 Subjects and Ethics

Thirty-six subjects participated in the present study. One subject was excluded due to extensive noise in oculomotor recordings, and one subject was excluded due to the misunderstanding of the task. The final sample used in the analysis included 34 subjects (24 women; *mean* $\pm$ *SD*, age 24.5 $\pm$ 4.2 years). Subjects were between 18 and 65 years old, had no known neurological or psychiatric diseases, did not take illegal psychoactive substances at least one day prior to the experiment, and had corrected to normal vision, if necessary. Each subject was informed about the aim of the study, signed an informed consent document regarding procedures, and was informed about the possibility of withdrawing from the experiment at any time without consequences. The study was carried out according to the Declaration of Helsinki guidelines and approved by the local Ethics Committee of the Université catholique de Louvain under number B403201733677 (Belgium).

2.2.2 Experimental procedure

The present study is an oculomotor variant of the constant foreperiod task [267] with a spatial cue. Each trial started with a white fixation box with a cross (5.7 × 4.3° of visual angle) appearing at the bottom of the screen for 500 ms (see Fig. 2.1). Next, a cue was presented above the fixation box for 2000 ms. The cue consisted of four cued boxes (referred to as 'CB'; dark or bright; 5.7 × 4.3° of visual angle each). The centre of each cue box was at an approximate distance of 17° of visual angle from the centre of the fixation box. Subjects were asked to maintain gaze fixation on the fixation box before, during, and after the cue presentation. Next, four empty test boxes (referred to as 'TB'; 5.7 × 4.3° of visual angle each) were displayed on the top of the screen for 1000 ms at the same positions as the CBs. The warning signal ('WS', red square) was shortly displayed in the fixation box for 50 ms. After a constant FP of 1900 ms, the 'go' signal (eccentric red square) was displayed

in one of the TBs for 50 ms. Subjects were instructed to maintain their gaze on the fixation cross during the FP and then make a visually guided saccade towards the 'go' signal as fast as possible. Each trial ended with an inter-trial interval ('ITI') of a randomised duration (2250 $\pm$ 250 ms).

This task can clearly separate the expected uncertainty encoding period (cue presentation) from the response preparation period (foreperiod). Indeed, the cue indicated the different levels of spatial uncertainty about the future target position. If the cue consisted of one marked box (n = 1), the probability of the target appearing in that box at the end of the foreperiod was P(TB_1) = 1 (no uncertainty). Note that for P(TB_1) = 1, the actual box being marked could be randomly assigned to one of four different possibilities on the screen. If two boxes were marked (n = 2), the target could later appear in either one of them with the same probability P(TB_2) = 0.5. The group of two cued boxes could occupy three different positions on the screen (left, as in Fig. 2.1, middle or right). If three boxes were marked, the probability for each box to be occupied by the future target decreased to P(TB_3) = 0.33. The group of three boxes could appear mainly on either the left or right side of the screen. Finally, if four boxes were marked, the probability of each box to be occupied by the future target was P(TB_4) = 0.25. In summary:

$$P(TB_n) = \begin{cases} 1.00, & \text{if n = 1} \\ 0.50, & \text{if n = 2} \\ 0.33, & \text{if n = 3} \\ 0.25, & \text{if n = 4} \end{cases}$$

where: TB_n, target appearing in one of n boxes; n, number of marked boxes, n $\in$ {1, 2, 3, 4}. The value of expected surprise (expected spatial uncertainty; *in bits*) bounded to each experimental condition (TB_n) can be calculated using Shannon's formula:

$$SU_n = -log_2 P(TB_n)$$

which is a negative base 2 logarithm of the probability of the target appear-

ing on one of the marked boxes P(TB_n). For example, in the TB_1 condition, $SU_1 = 0$ did not indicate any surprise about the outcome, and subjects were precisely informed about the box that would be occupied by the future 'go' signal. The oculomotor preparation was maximal. The surprise for each condition was: $SU_1 = 0$, $SU_2 = 1$, $SU_3 = 1.58$ and $SU_4 = 2$. Two different versions of the experiment were tested. For half of the subjects, the CBs were represented as filled white squares (bright cue). For the other half, the open square CBs were used (dark cue, see Fig. 2.1). The edges of the bright and dark CBs were blurred to minimise the pop-up effect of a cue appearing at the top of the screen and to facilitate maintaining the gaze on the fixation box. Each experiment consisted of 160 trials divided into four blocks. The presentation of spatial cues was randomised within the experiment, with each spatial cue presented 40 times.

2.2.3 Data collection and preprocessing

Eye movements and pupil size were recorded binocularly at 500 Hz using an infrared eye tracking system (EyeLink1000, desktop mount, SR Research, Ontario, Canada) with an average spatial accuracy of 0.25° of visual angle and a pupil size resolution of 0.2% of diameter. The eye tracker was calibrated at the beginning of each data collection session and re-calibrated every 30 trials after the subjects' rest break. Subjects were sitting at a distance of 80 cm from the high-resolution screen (size: 54 × 30 cm, 1920 × 1080 pixels, VPixx Technologies, Canada), displaying stimuli at 60 Hz. Stimuli display and eye movement recordings were created using Experimental Builder (SR Research).

After the experiment, artefact rejection was performed with DataViewer (SR Research, Ontario, Canada) to exclude oculomotor recordings of poor quality. Trials with frequent blinking, discontinuous recording, or drift of calibration were excluded from further analysis. Artefact rejection amounted to only 4% of all trials. The remaining pool of trials was searched by the saccade detection algorithm using amplitude (> 1°), velocity (> 22°/s), and

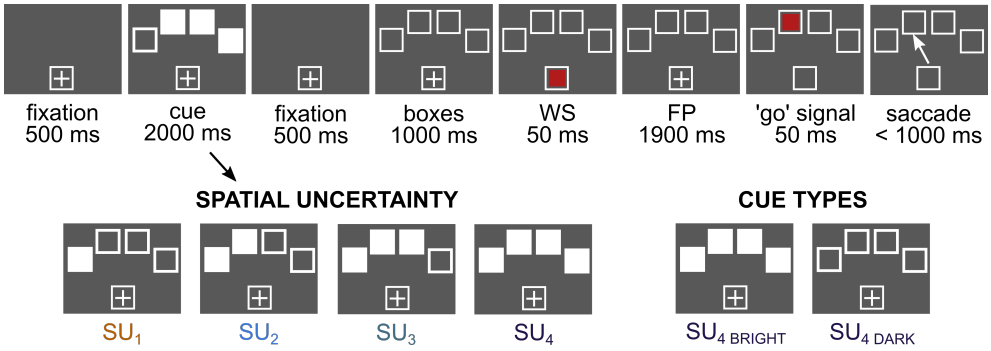

Fig. 2.1 Schematic representation of the design in Experiment 1. Timeline of visual events on the screen in front of the subject. The experiment started with the *fixation cross* presented at the bottom of the screen. Next, during the cue interval, while maintaining gaze on the fixation cross, subjects were presented with a spatial cue (*cue boxes* or 'CB') on top of the screen. Subjects were randomly divided into two equal groups. For the first group, the CBs were *filled white squares* ('bright' cue type), and for the other group, the *open white squares* ('dark' cue type). CBs indicated the amount of expected uncertainty bound to the target's future position (SU_1, SU_2, SU_3, or SU_4). Subjects were then presented with four *empty test boxes* ('TB'), followed by the warning signal ('WS', the first *red square*) briefly presented in the bottom box. The extinction of the WS initiated a 1900 ms foreperiod ('FP'). Then, the 'go' signal (the second *red square*) was briefly presented in one of four TBs. Subjects were asked to maintain their gaze on the fixation cross during the FP and then make a visually guided saccade towards the 'go' signal as quickly as possible.

acceleration ($> 3800°/s^2$) criteria. Saccades occurring after the extinction of the WS and up to 100 ms after the 'go' signal onset will be referred to as *early* saccades. The early saccades were detected in 5.5% of all trials remaining after artefact rejection. Saccades with a latency superior to or equal to 100 ms after the appearance of the 'go' signal will be termed *visually guided* saccades ('VG'). The VG saccades with a latency > 1000 ms, executed after an early saccade or landing in the incorrect target box, were not considered for further analysis. The final pool of the trials with the VG saccades amounted to 87% of all trials remaining after artefact rejection.

The trials that remained after the artefact rejection were also used to anal-

yse the pupillary response during the foreperiod. First steps of the analysis were performed using DataViewer (SR Research, Ontario, Canada). The pupillary responses of the left and right eyes were averaged on a trial-by-trial basis to improve the stability of the signal. Pupil size during blinks was estimated using a linear interpolation within the window of 100 ms before the starting point and 100 ms after the end of a blink. The pupil diameter during the FP was then averaged in 50-ms bins and further processed in *R* (version 4.4.2) using the *PupillometryR* package [121, 120]. Saccades can be a source of pupillometry artefacts [238]. Therefore, trials that included any early saccade executed during the FP were excluded from the pupil data analysis. The pupil traces were filtered using the median filter and baselined to 200 ms before data segment onset. Finally, pupil traces were normalised using the z-score [239].

2.2.4 Statistical analysis

To avoid the pupillary response being affected by the VG saccades, the statistical analysis of the pupil size was performed only at the longest possible interval that did not include the 'go' signal onset time (further referred to as the *analysis interval*). In this experiment, the analysis interval was equal to FP length (0 - 1900 ms after the WS offset).

The statistical analysis of multidimensional data is often associated with the multiple comparison problem. The cluster-based permutation test ('CBPT') is a popular data-driven approach that solves the multiple comparison problem [234]. In this method, a statistical test was first calculated at the sample level. Then, the statistics were summed up on the channel-time level to form a cluster. For each CBPT, 1000 permutations were then executed to create a null distribution of the statistic. Then the cluster statistics value was compared with the null distribution (α = 0.05 for thresholding). To test for possible differences in pupillary response in different levels of spatial uncertainty, pupil traces were subjected to CBPT in R using the *permutes* package [385] and ANOVA F statistics. The CBPT results include information about the time in-

terval associated with the detected effect. However, contrary to widespread use, CBPT is not tailored to support claims about the precise location of the effects [319]. Therefore, in the next analytic step, pupillary data within the proposed time interval was averaged on a trial-by-trial basis for each subject and modelled using linear mixed-effects model analysis ('LMM').

Pupil size averaged from the window indicated by the CBPT, the number of early saccades, and the maximum velocity ('V_{max}') and latencies of the VG saccades were subjected to the LMM analysis in R using the *lme4* package [31, 30]. Each linear mixed-effects model used in the manuscript can be explained by the general equation:

$$Y_{is} = \beta_0 + \beta_1 X_{is} + S_{0s} + \epsilon_{is}$$

where Y_{is} is the outcome for the s-th subject in the i-th trial, X_{is} is the fixed effect for the s-th subject in the i-th trial, β_0 is the intercept parameter, β_1 is the slope parameter of the fixed effect, S_{0s} is the random intercept effect for subjects and ϵ_{is} is the corresponding residual error. First, to choose the best random effects structure, a 'full' model (including all assumed variables) was fitted to data using the restricted maximum likelihood method ('REML' [26, 340]). The different random structures of the compared full models were expressed using the 'rs' suffix and the number: 'full.rs1' describes the random intercept structure model that includes the id of the subject as an intercept ('1 | subject'); 'full.rs2' denotes the model with the random slope structure ('1 + SU | id'). The best random structure was chosen based on the lowest Bayes Information Criterion ('BIC' [43]). For the results of model selection, see Tab. S2.1 in the Supplementary Materials.

Continuous outcomes (VG saccade latencies, VG saccade V_{max}, and pupil size) were fitted using the Gaussian model with a chosen random structure. The main effects of each model were estimated using Type III ANOVA with Satterthwaite's method. The count of early saccades was fitted using the Poisson distribution within the Generalised Linear Mixed Models ('GLMM') framework. If a large number of zeros in the measure was observed, a zero-

inflated Poisson model was implemented using *glmmTMB* package [51, 50]. The main effects of Poisson models were estimated using Type II Wald χ^2 tests. The coefficients obtained from the GLMM analysis were transformed to Incidence Rate Ratios ('IRR') describing how much more likely is the occurrence of an event in one group compared to another.

Pairwise comparisons for each dependent variable were calculated using the R package *emmeans* [208]. Diagnostics of each of the presented models were evaluated to ensure the quality of convergence and conformity with the assumptions. The quality of the model was assessed with the QQplot and residuals (R package *performance* [223, 221]; R package *DHARMa* [151]). The significance level assumed in the present study was $\alpha = 0.01$.

Finally, we tested the possibility that early saccade distribution was multimodal. A mixture of 'k' Gaussian components was fitted to the distribution of early saccades, using the expectation-maximization algorithm (*normalmixEM* function, R package *mixtools* [38, 37], maximal number of iterations: 1000). The k number ranged from 2 to 5 between mixtures (models *mix.2*, . . . , *mix.5*). The number of components that best fitted the data was determined by selecting the mixture with the lowest log-likelihood value ('LL'). The time point where the components intersected was then identified and further used to classify early saccades.

2.3 Experiment 1: Results

2.3.1 Spatial uncertainty alters saccadic latency and maximum velocity

In the Introduction, we hypothesised that an internal representation of spatial uncertainty ('SU') could alter the preparation of visually guided saccades. Increasing uncertainty could also increase movement latency and/or kinematics. To test these hypotheses, a linear mixed-effects analysis of the saccadic parameters was performed.

First, a random intercept model was created to test the latency in differ-

ent SU contexts. Spatial uncertainty significantly modulated the latency of VG saccades (F[3, 4454.52] = 75.46, $p < 2.22 \times 10^{-16}$). Pairwise comparisons showed that saccades with the shortest latency were evoked in SU_1 (*mean* $\pm$ *SD*, 216.0 $\pm$ 63.9 ms) compared to the SU_2 (229.8 $\pm$ 62.9 ms, $p = 4.36 \times 10^{-8}$), SU_3 (241.6 $\pm$ 68.0 ms, $p = 4.36 \times 10^{-8}$) and SU_4 conditions (244.5 $\pm$ 68.2 ms, $p = 4.36 \times 10^{-8}$). The SU_2 evoked shorter latency compared to the SU_3 ($p = 3.50 \times 10^{-6}$) and SU_4 conditions ($p = 4.49 \times 10^{-8}$), but the comparison between the SU_3 and SU_4 conditions was not significant (p = 0.535; see Fig. 2.2A).

In order to test whether saccadic V_{max} followed the same trend, an analogous random intercept model was created. Spatial uncertainty significantly modulated the V_{max} of the VG saccades (F[3, 4473.42] = 20.81, $p = 2.18 \times 10^{-13}$). Pairwise comparisons showed the highest V_{max} in SU_1 (*mean* $\pm$ *SD*, 399.9 $\pm$ 100.8°/s) compared to the SU_2 (384.9 $\pm$ 89.9°/s, $p = 1.58 \times 10^{-8}$), SU_3 (385.2 $\pm$ 89.6°/s, $p = 1.25 \times 10^{-9}$), and SU_4 conditions (383.7 $\pm$ 90.1°/s, $p = 4.04 \times 10^{-12}$). No significant differences were detected between the SU_2 and SU_3 conditions (p = 0.979), the SU_2 and SU_4 conditions (p = 0.606), and the SU_3 and SU_4 conditions (p = 0.837; see Fig. 2.2B).

2.3.2 A larger pupil dilation in the "no spatial uncertainty" context

Observation of pupil size as a function of time during the foreperiod suggests that pupil dynamics up to 500 ms after the WS offset was probably related to luminance changes only (see Fig. 2.2C). Therefore, a cluster-based permutation analysis ('CBPT') was performed on pupillary data in the 500 - 1900 ms window. A significant modulation of pupil size by spatial uncertainty was found ($F_{mass} = 434.42$, $p_{mass} = 9.99 \times 10^{-4}$, interval 550-1900 ms). To confirm the effect, the pupillary response from the 550-1900 ms interval was therefore averaged on a trial-by-trial basis and included as an outcome of the random intercept model. Spatial uncertainty significantly altered pupil size within the 550 - 1900 ms interval (F[3, 5151.15] = 4.73, p = 0.003). Specifically, pairwise comparisons showed that pupil size was larger in SU_1 (*mean* $\pm$ *SD z-score value*; 0.20 $\pm$ 1.51) compared to the SU_2 (0.02 $\pm$ 1.54, p = 0.012) and

SU_4 conditions (0.00 $\pm$ 1.55, p = 0.004). The difference was less pronounced between the SU_1 and SU_3 conditions (0.04 $\pm$ 1.60, p = 0.038; see Fig. 2.2D).

2.3.3 The bimodal structure of early oculomotor behaviour under spatial uncertainty

Saccades initiated during the foreperiod and up to 100 ms after the onset of the 'go' signal are defined as 'early'. Figure 2.3A shows the latency distribution of early saccades. From the mixture models fitting between 1 and 5 Gaussian functions, the *mix.2* model assuming the bimodal distribution of early saccades fitted the data best (*mix.2* LL = -1084.77; *mix.3* LL = -1067.75; *mix.4* LL = -1046.97; *mix.5* LL = -1059.33). The latency threshold used to separate early saccades into two modes was established at the crossing point between the two Gaussian components (1000 ms). Latencies below the threshold were assigned to 1^{st} mode (N = 88, μ = 364.9 ms, σ = 232.4), while the latencies surpassing the threshold were assigned to 2^{nd} mode (N = 199, μ = 1702.1 ms, σ = 243.8, see Fig. 2.3A). 1^{st} mode describes a transient increase in the number of early saccades after the offset of the WS. 2^{nd} mode shows a gradual increase in the probability of the occurrence of an early saccade as time elapsed during the foreperiod, with the mean of the distribution approaching FP length. This behaviour was particularly salient in the SU_1 condition (see Fig. 2.3B). As SU increased, the number of early saccades decreased strongly, and the bimodal pattern could only be conjectured.

A GLMM was performed to quantitatively compare the number of early responses for different SUs. Spatial uncertainty significantly reduced the number of early saccades during the foreperiod ($\chi^2[3] = 133.79$, $p < 2.22 \times 10^{-16}$). Pairwise comparisons showed that the occurrence of early saccades was more likely in SU_1 condition compared to the SU_2 condition ($IRR \pm SE$, 3.9 ± 0.7, $p = 2.37 \times 10^{-13}$), more likely in SU_1 condition compared to the SU_3 condition (5.5 ± 1.3, $p = 8.57 \times 10^{-13}$), and more likely in SU_1 condition compared to the SU_4 condition (5.8 ± 1.2, $p = 3.78 \times 10^{-14}$).

The same analysis was then repeated for early saccades belonging to 1^{st}

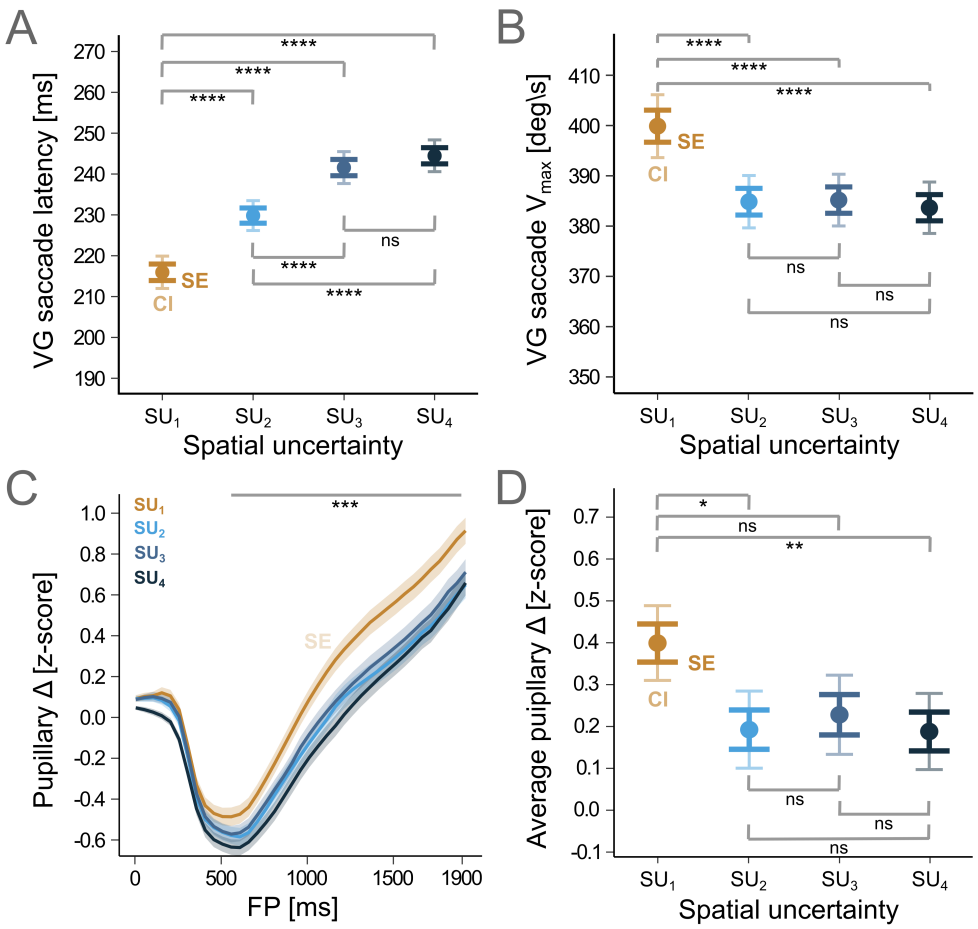

Fig. 2.2 Oculomotor results of Experiment 1. (A) Mean latency of VG saccades (*dots*) for each SU context with SE and CI (*whiskers*). *Horizontal grey lines* indicate post-hoc LMM significance between SU levels (* $p \leq 0.05$, ** $p \leq 0.01$, *** $p \leq 0.001$, **** $p \leq 0.0001$, ns - not significant). **(B)** Mean V_{max} of VG saccades for each SU context. **(C)** Time course of pupil size during the FP. Time 'zero' on the X-axis indicates the extinction of the warning stimulus. *Coloured lines* indicate the baseline-corrected and z-scored mean pupil size in different SU levels with SE (*coloured ribbons*). *Horizontal grey lines* indicate clusters of differences between SU levels and p-values obtained with the CBPT. **(D)** Mean pupil size (*dots*) for each SU context in the 800 - 1900 ms time window with SE and 95%CI (*whiskers*). *Horizontal grey lines* indicate post-hoc LMM significance between SU levels.

and 2^{nd} modes, separately. First, spatial uncertainty significantly reduced the number of 1^{st} mode saccades during the foreperiod (χ^2[3] = 24.87, p = 1.65 $\times$ 10^{-5}). The occurrence of 1^{st} mode saccades was more likely in SU_1 condition compared to the SU_2 condition ($IRR \pm SE$, 2.4 $\pm$ 0.7, p = 0.01), more likely in SU_1 condition compared to the SU_3 condition (4.3 $\pm$ 1.5, p = 2.00 $\times$ 10^{-4}), and more likely in SU_1 condition compared to the SU_4 condition (2.4 $\pm$ 0.7, p = 0.01, see Fig. 2.3C).

Similarly, the effect of spatial uncertainty on the number of 2^{nd} mode saccades was also demonstrated (χ^2[3] = 156.34, p < 2.22 $\times$ 10^{-16}). 2^{nd} mode saccades were more likely in SU_1 condition compared to the SU_2 condition ($IRR \pm SE$, 5.1 $\pm$ 1.1, p = 6.33 $\times$ 10^{-14}), more likely in SU_1 condition compared to the SU_3 condition (7.3 $\pm$ 1.8, p = 5.14 $\times$ 10^{-14}), and more likely in SU_1 condition compared to the SU_4 condition (10.7 $\pm$ 3.1, p = 4.95 $\times$ 10^{-14}, see Fig. 2.3D).

2.3.4 Latency of visually guided saccades driven by information gain

The observation that visually guided saccadic latencies increased with spatial uncertainty suggested that a particular instantiation of Hick's law ('HL' [158]) could be observed:

Model HL: $latency_i \sim \beta_0 + \beta_1 SU_i$

with: $latency_i$, average saccadic latency in the i-th trial; β_0, intercept of the model; β_1 slope; SU_i, spatial uncertainty expressed in bits (*Shannon's surprise*) for the i-th trial. A significant regression was found between Shannon's surprise and the latency values (ANOVA, F[1,134] = 13.47, p = 3.49 $\times$ 10^{-4}) with an R^2 of 0.085. The latency of the VG saccades increased by 25.06 ms for each unit of spatial surprise (see Fig. 2.4A).

Further, we tested whether a Poisson counting model could predict saccadic latencies [85, 337, 336]. This model uses a random walk to represent a

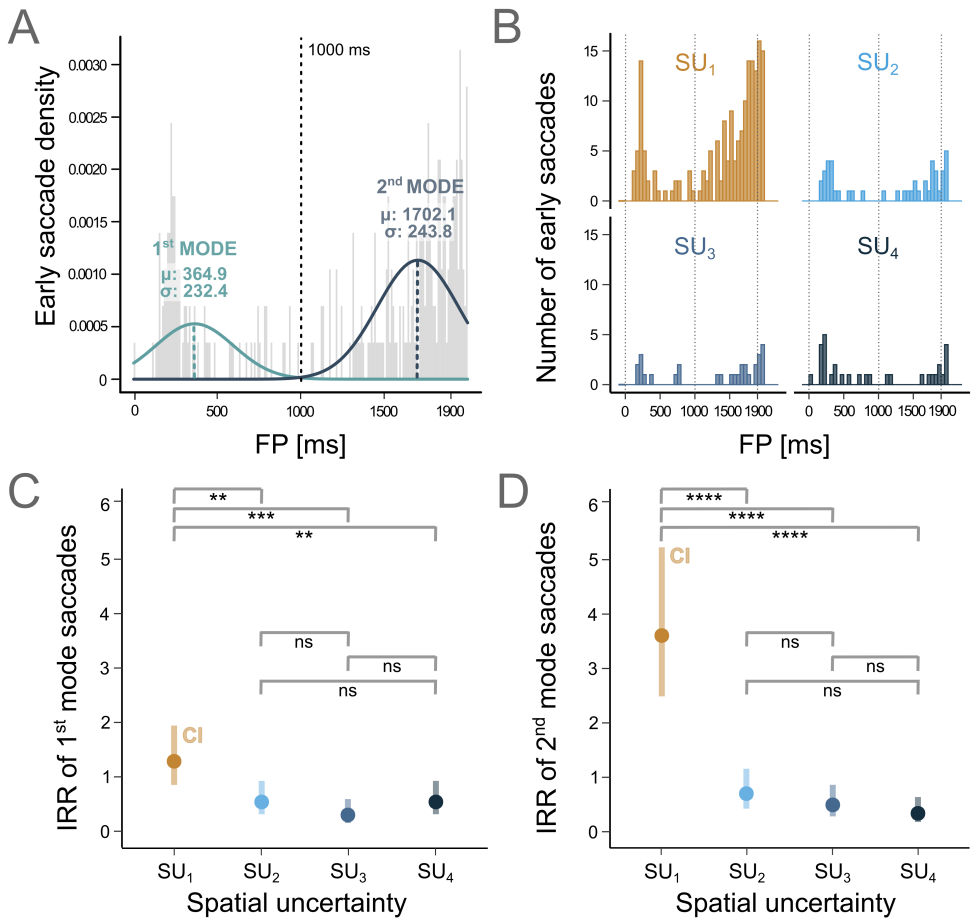

Fig. 2.3 Early saccades in Experiment 1. (A) Latency distribution of early saccades (*grey bars*) and mixture models (*coloured density plots*) for each experimental block. Time 'zero' on the X-axis indicates the onset of the FP. A bimodal distribution best describes the data. The *black dashed lines* show the transition between modes and the threshold value for saccade classification (1000 ms). Labels describe mean (μ, *coloured dashed lines*) and standard deviation (σ) of each mode. **(B)** Latency distributions of early saccades for different SUs. The bimodal distribution of latencies was observed for all SUs. **(C)** The Incidence Rate Ratio ('IRR') of 1^{st} mode saccades during the FP (*coloured dots*) with CI (*whiskers*). *Horizontal grey lines* indicate the level of GLMM statistical significance between SU levels (** $p \leq 0.01$, *** $p \leq 0.001$, **** $p \leq 0.0001$, ns - not significant). **(D)** The IRR of 2^{nd} mode saccades during the FP.

hypothetical decision signal that builds up to a threshold and leads to a saccade. Each sample could be considered as a unit of evidence approaching the decision boundary. The samples were drawn from an exponential distribution and counted using a Poisson counting model. The accumulation average rate determines how quickly the decision threshold could be crossed.

Two variants of the model were tested: in the 'R_V/T_C' model, the rate of evidence accumulation 'R' was variable and could encode the different SUs tested. In this case, an arbitrary fixed threshold 'T' was selected (see Fig. 2.4D); in the 'R_C/T_V' model, the rate of evidence accumulation was constant, but the decision threshold could vary to encode SU (see Fig. 2.4E). The R_V/T_C model was fitted by simulating the latencies of each SU condition separately with a threshold fixed at 10 units of accumulated evidence and an accumulation rate varying between 30 and 80 evidence units/s. Then, each fit was compared to the average saccadic latency corresponding to each condition. The residual sum of squares ('RSS') between the simulated and observed data was then calculated and compared for all fits. Figure 2.4B shows that the RSS plotted as a function of the accumulation rate was U-shaped and reached a minimum at 51, 48, 45, and 45 units/s for the SU_1, SU_2, SU_3, and SU_4 conditions, respectively. The rate of evidence accumulation was, therefore, different for each tested SU. The average saccadic latencies for the R_C/T_V model were simulated with a constant accumulation rate of 60 units/s and a range of possible threshold values from 1 to 50 units. Figure 2.4C shows that the RSS for each fit plotted against the corresponding threshold value created an exponential function. This model produced larger RSS values than the R_V/T_C model and provided an unrealistic fit of the latency data since it did not properly differentiate the influence of SUs on saccadic latencies (except for the SU_1 condition).

2.4 Interim discussion

In the present chapter, a simple oculomotor task was developed in which subjects were cued about the level of spatial uncertainty related to the location of

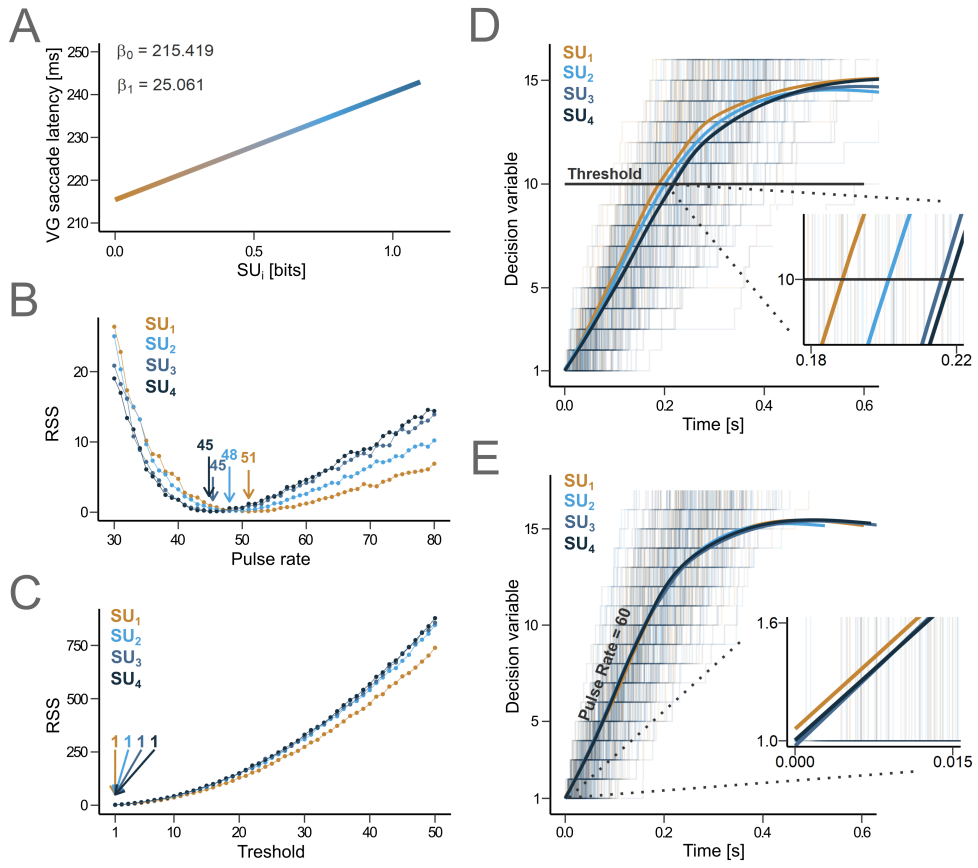

Fig. 2.4 Modelling the latency of VG saccades in Experiment 1. (A) Fit of the Hick's model to the latency of VG saccades. Predicted latency plotted as a function of the logarithm of the number of choices. **(B)** Residual sum of squares ('RSS') of the comparison between the empirical data and the R_V / T_C predictions. The plot was U-shaped with a variable minimum between SU levels. **(C)** RSS of the comparison between the empirical data and the R_C / T_V predictions. The RSS plot was exponentially shaped with an arbitrary fixed minimum, identical in all SU levels. **(D)** R_V / T_C model. Fifty simulation trials (*light traces*) per condition are displayed with the mean path for every condition (*dark lines*). The *horizontal line* indicates the constant threshold. **(E)** R_C / T_V model.

an incoming 'go' signal. Experiment 1 manipulated only the level of spatial uncertainty. The duration of the foreperiod preceding the arrival of the 'go' signal was constant throughout the experiment.

In Experiment 1, the latency of visually guided saccades logarithmically increased with the amount of spatial surprise (see Fig. 2.4A), following Hick's law ('HL' [158, 167], for review, see [297]). So far, evidence suggests that VG saccades obey HL if there is a choice of a cued target amongst several alternatives [205], but it is not observed if saccades are simply visually guided [194]. We found that HL robustly fitted the relationship between the average latency of VG saccades and spatial surprise. This observation was unexpected, given that there was only one choice for the final response (the single visual 'go' signal). Simply cueing surprise could have induced HL in saccadic latencies. Therefore, we suggest that HL could be observed even if there is no complex stimulus-response mapping but just expected (cued) surprise in memory. We suggest that attentional competition between the potential saccadic goals could lead to HL in VG saccades. Spatial theories of attention suggest that attention could be oriented towards a saccade goal before movement onset. If several potential target positions are present simultaneously, then attention could be allocated in parallel to these different saccade goals [137, 22]. Therefore, in Experiment 1 reported here, when the 'go' signal appeared but before movement initiation, the non-selected attentional goals could compete for attentional resources and should be suppressed. This process could take more time if there are more potential goals (increasing cued surprise) leading to an increasing saccadic latency and HL.

The maximal velocity ('V_{max}') of VG saccades did not follow the same increasing trend found for latencies (see Fig. 2.2B). In the oculomotor domain, saccadic eye movements V_{max} is considered as a reliable indicator of arousal (for review, see [104, 106]). In agreement with this view, the strong influence of the absence of spatial uncertainty on eye velocity was shown in the current study (SU_1 condition). We suggest that the 'no spatial uncertainty' condition favoured anticipation due to an increased arousal level in the absence of uncertainty. In contrast, the abrupt decrease in early responses observed for

higher uncertainty values (SU_2, SU_3, SU_4 conditions) could be a consequence of a "do not bet on the unknown" strategy that reduces exploration [287]. Indeed, not knowing precisely what could happen could activate behavioural inhibition [14]. In the present study, the SU_2, SU_3, and SU_4 conditions were associated with uncertainty, while in the SU_1 condition, the 'go' signal position was fully determined. V_{max} did not differentiate between the remaining levels of spatial uncertainty (SU_2, SU_3, SU_4 conditions). Different results for latency and V_{max} suggest that those measures could result from the work of different neuronal mechanisms.

Besides the saccades resulting from the arrival of the 'go' signal, also the early responses occurring during the foreperiod were tested. Interestingly, the latency distribution of early saccades was bimodal (see Fig. 2.3A). We suggest that 1^{st} mode of this distribution consisted of *impulsive* saccades that were evoked simply by the extinction of the WS. Around the middle of the FP, when nothing was expected to happen on the screen, early saccades were scarce. Finally, in 2^{nd} mode the number of early saccades increased as time elapsed during the FP, reaching the maximum around FP duration. This suggests an increasing temporal expectation of the 'go' signal, perhaps due to an increasing hazard rate of target onset [171]. Therefore, we argue that the bimodality of the early saccade structure illustrates an important distinction between types of saccades executed during the foreperiod. While 1^{st} mode impulsive saccades may, to a large extent, result from reduced inhibitory control, 2^{nd} mode could represent truly intentional early responses driven by expectation - the *anticipatory* saccades.

The number of early saccades was alleviated in the situation of no spatial uncertainty (SU_1 condition, 0 bits, see Fig. 2.3B). Global motor inhibition resulting from introducing any level of spatial uncertainty (SU_2, SU_3, SU_4 conditions) could result in a reduced probability of early responses. This reduction was shown for 1^{st} and 2^{nd} mode early saccades, which could suggest a strong top-down inhibitory process (see Fig. 2.3C and Fig. 2.3D).

An increase in arousal was also visible in the pupillary response. The

strongest dilation was observed when no spatial uncertainty was cued to subjects (see the SU_1 condition in Fig. 2.2C). This finding is in agreement with previously published observations about pupil size and uncertainty [131, 187, 4, 296, 202] (for review, see [403]). This experiment showed no gradual increase in pupil size with spatial uncertainty, suggesting that the SU_1 condition specifically increased arousal. The stronger impact of SU_1 could also be since the 'no spatial uncertainty' condition was globally less frequent than the uncertain conditions considered together (SU_1 condition, P = 0.25; {SU_2, SU_3, SU_4}, P = 0.75). Therefore, it cannot yet be excluded that arousal was related to the probability density of the low uncertainty event.

Recently, a relationship between the pupil size and saccadic V_{max} was found [389, 70]. A subcortical mechanism involving the superior colliculus ('SC') could explain this relationship given its role in determining saccade metrics and pupil size (for review, see [388, 389]).

One standard way to model decision processes in psychology is a random walk to a threshold. This approach has encountered enormous success in modelling multiple-choice tasks when there is a progressive accumulation of sensory evidence [337, 302]. In the present study, there was no sensory evidence accumulation during the FP and only one choice. Therefore, we used a single threshold Poisson counting model that suggests that uncertainty could be encoded by the rate of rise of a decision signal (R_V / T_C model, see Fig. 2.4B and Fig. 2.4C). This simple model predicted observed saccadic latencies with a variance accounted for (R^2) of 0.09, which was higher than if a fixed threshold with a variable rate was postulated (R_C / T_V model). The observation that the R_V / T_C model yields HL is not in agreement with previous modelling studies of HL, where a criterion adjustment was found to be more likely [205, 372]. This difference could also be explained by the fact that there was no choice among several alternatives in the experimental design used here. In a context of cued surprise, HL could be observed even in a simple reaction time experiment with a single stimulus-response alternative. We dissociated surprise from complex stimulus-response mappings and nonetheless found HL [95].

In summary, Experiment 1 suggests two different processes involved in saccade preparation in an uncertain context: one related to arousal that does not obey HL (pupil size, V_{max}, and early saccade occurrence) and the other related to cognitive information processing that obeys HL. We suggest that the arousal-related process could be partly determined by SC activity, whereas the second process could explicitly encode surprise and be cortically controlled.

The second part of the chapter will report on Experiment 2. Here cued spatial uncertainty was also used, but this time FP durations could vary between blocks of trials, taking one of four different durations (400, 900, 1400 or 1900 ms). Experiment 2 will demonstrate how the relationship between oculomotor responses and spatial uncertainty established in Experiment 1 is changed by introducing some form of temporal uncertainty. Chosen FP durations will allow the comparison of obtained results with previously published studies [9, 166, 102].

2.5 Experiment 2: Methods

2.5.1 Subjects and Ethics

Twenty-seven subjects participated in the present study. Two subjects were excluded due to extensive noise in oculomotor recordings. The final sample used in the analysis included 25 subjects (18 women; *mean* $\pm$ *SD*, age 24.2 $\pm$ 3.7 years). Subjects were between 18 and 65 years old, had no known neurological or psychiatric diseases, did not take illegal psychoactive substances at least one day prior to the experiment, and had corrected to normal vision, if necessary. Each subject was informed about the aim of the study, signed an informed consent document regarding procedures, and was informed about the possibility of withdrawing from the experiment at any time without consequences. The study was carried out according to the Declaration of Helsinki guidelines and approved by the local Ethics Committee of the Université catholique de Louvain under number B403201733677 (Belgium).

2.5.2 Experimental procedure

The design of the experiment was the same as in Experiment 1, with the exceptions listed below. Firstly, only the bright type of cue was used. The cue boxes ('CB') were represented by filled white squares (see Fig. 2.5). Secondly, a variable blocked foreperiod was introduced. FP could take one of the four durations within each of the four blocks (each block including 120 trials): 400, 900, 1400, or 1900 ms. The order of blocks was randomised between subjects. Each spatial cue (SU_1, SU_2, SU_3, SU_4) was randomly presented to the subject 30 times in each block, with 120 trials per cue.

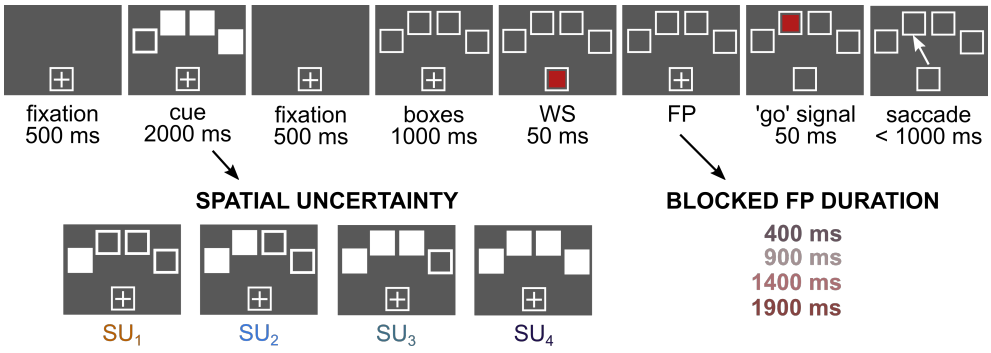

Fig. 2.5 Schematic representation of the design in Experiment 2. Timeline of visual events on the screen in front of the subject. The experiment started with the *fixation cross* presented at the bottom of the screen. Next, during the cue interval, while maintaining gaze on the fixation cross, subjects were presented with a spatial cue (cue boxes or 'CB') on top of the screen. CBs indicated the amount of expected uncertainty bound to the future position of the target (SU_1, SU_2, SU_3, or SU_4). Next, four *empty test boxes* ('TB') were presented to subjects, followed by the warning signal ('WS', the first *red square*) briefly presented in the bottom box. The extinction of the WS initiated a foreperiod ('FP'). In a given block of trials, the FP could take one of four durations (400 ms, 900 ms, 1400 ms, 1900 ms). Then, the 'go' signal (the second *red square*) was briefly presented in one of four TBs. Subjects were asked to maintain their gaze on the fixation cross during the FP and then make a visually guided saccade towards the 'go' signal as quickly as possible.

2.5.3 Data collection and preprocessing

Data collection and preprocessing procedures matched those described in Experiment 1. Only 15% of all the recorded trials were excluded in the artefact rejection procedure. Early saccades were detected in 10% of all trials that remained after rejection. Visually guided saccades ('VG') used in the final analysis were detected in 78% of the trials remaining after rejection.

2.5.4 Statistical analysis

Firstly, to compare pupillary response to spatial uncertainty context in Experiment 1 and Experiment 2, only data collected during the 1900 ms FP block were used in the first part of the analysis. For this comparison, the analysis interval was equal to FP duration (0 - 1900 ms after the WS offset). Secondly, to illustrate the effect of FP duration on the pupillary response, the following pairs of comparisons were planned: 900 ms - 1400 ms, 900 ms - 1900 ms, and 1400 ms - 1900 ms. The shortest duration of 400 ms was excluded from the comparison, as it is too short for a proper development of the psycho-sensory pupillary response ('PPR', see [238]). For chosen comparisons, the analysis interval was equal to 0 - 900 ms after the WS offset, as the 900 ms represents the shortest possible FP duration without the appearance of the 'go' signal for those pairs.

The remaining statistical methods used match the ones described in Experiment 1, with the exceptions listed below. As in Experiment 1, pupil size, averaged from the window indicated by the CBPT, the number of early saccades, the maximum velocity of the VG saccade ('V_{max}'), and its latencies were subjected to LMM analysis. In this experiment, the models used the following predictors: 'FP' - the duration of the FP in the given block; 'SU' - the level of expected spatial uncertainty. The following labelling of models was used: the 'full' prefix indicated the model with all predictors. Models that included only one predictor were labelled using its name. For example, 'SU.rs1' denotes the model with SU as the only predictor and the random intercept structure. The choice of random structures was based on the BIC values de-

tailed in Table S2.2 and Table S2.6 of the Supplementary Materials. BIC was first calculated from models of different random effect structures, calculated using a REML method. Further, since more than one variable could influence the outcomes in this experiment, the best data-predicting model was chosen by re-fitting all comparable models using a maximum likelihood method ('ML'). Then, re-calculated BIC values were compared.

Finally, a mixture model analysis was used to test the multimodality of early saccade distribution. However, as FP duration changed between experimental blocks, the mixture analysis was conducted on early saccade distribution from each block, separately.

2.6 Experiment 2: Results

2.6.1 Saccadic latency and velocity are differently affected by variable FP

Experiment 1 indicated that increasing spatial uncertainty alters visually guided saccadic latency and V_{max}. To test whether this effect is present in the variable foreperiod task, LMM analyses were performed with FP duration as a covariate.

As in Experiment 1, spatial uncertainty significantly modulated the latency of saccades (*SU.rs3* model, F[3, 7497.43] = 40.95, p < 2.22×10^{-1}; see Tab.S2.3). Pairwise comparisons showed that saccades had a shorter latency in SU_1 condition (*mean* $\pm$ *SD*, 207.4 $\pm$ 49.6 ms) compared to the SU_2 (210.9 $\pm$ 50.7 ms, p = 1.60×10^{-6}), SU_3 (215.9 $\pm$ 51.5 ms, p = 3.20×10^{-14}), and SU_4 conditions (217.0 $\pm$ 53.4 ms, p = 4.22×10^{-14}). The SU_2 condition evoked shorter latency compared to the SU_3 (p = 1.28 × 10-3) and SU_4 conditions (p = 6.31×10^{-7}), but the comparison between the SU_3 and SU_4 conditions was not significant (p = 0.361; see Fig. 2.6A).

Further, FP duration also modified the latency of VG saccades (*FP.rs3* model, F[1, 23.52] = 24.88, p = 4.51×10^{-5}; see Tab.S2.3). The latency of VG saccades increased with FP duration (β = 0.017 $\pm$ 0.003). To better illustrate

the effect, the difference in VG saccade latency between the 400 ms and 900 ms FP block was approximately 10 ms (see Fig. 2.6B). However, no interaction between spatial uncertainty and FP duration was found for the latency of VG saccades (*full.rs3* model, p = 0.540; see Tab.S2.3).

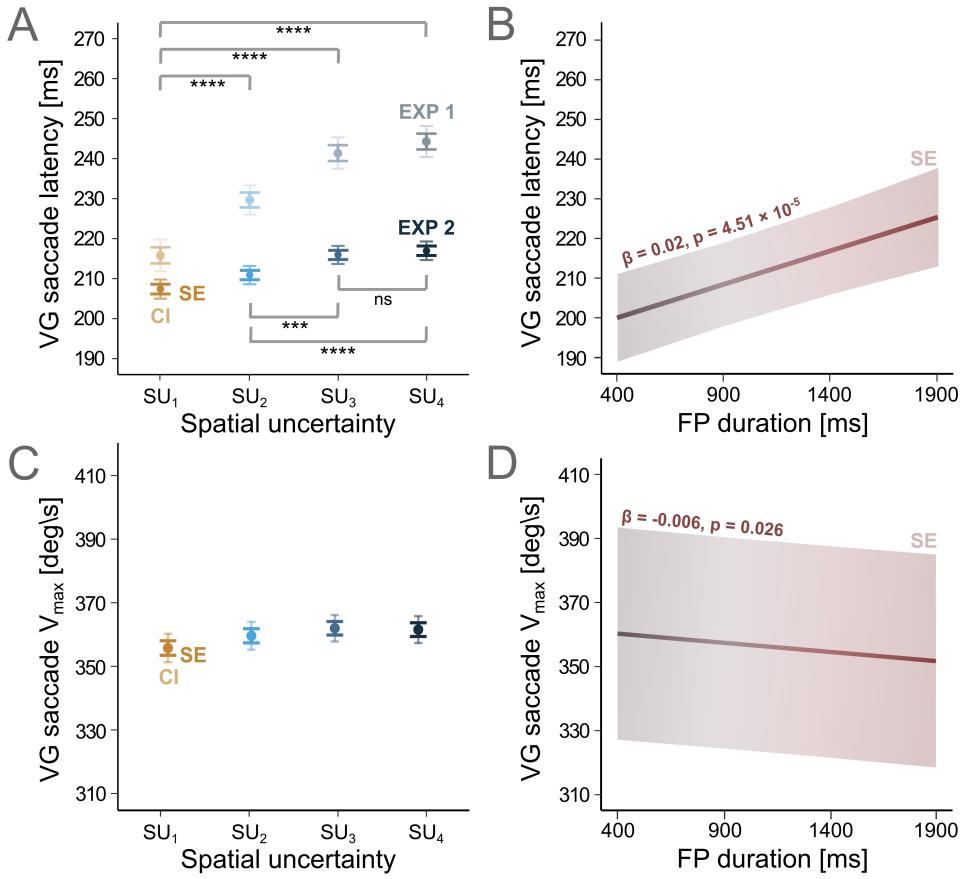

Fig. 2.6 Latency and V_{max} of VG saccades in Experiment 2. (A) Mean latency of VG saccades (*dots*, *EXP 2*) for each SU with SE and 95%CI (*whiskers*). *Horizontal grey lines* indicate post-hoc LMM significance between SU levels (**** $p \leq 0.0001$). Corresponding results of Experiment 1 added for a comparison (*EXP 1*). **(B)** Latency of visually guided saccades plotted against FP duration (LMM, *coloured regression line*) with SE (*coloured ribbon*). **(C)** Mean V_{max} of visually guided saccades for each SU level. **(D)** V_{max} of visually guided saccades plotted against FP duration.

Next, to check whether saccadic latency obeys HL when a variable blocked foreperiod was introduced in the task, a regression analysis identical to the one included in the analysis of Experiment 1 was performed. Spatial uncertainty was again expressed in bits as Shannon's surprise [331]. However, no significant regression was found between Shannon's surprise and the latency values (ANOVA, p = 0.051).

A corresponding LMM analysis was performed to test whether saccadic V_{max} was modulated by spatial uncertainty and FP duration. Results indicated a weak effect of spatial uncertainty on V_{max} (*SU.rs3* model, F[3, 7673.47] = 3.161, p = 0.024; see Tab.S2.4). However, pairwise comparisons showed that there was a significant difference only between SU_1 ($mean \pm SD$, 355.8 $\pm$ 93.2 ms) and the SU_2 condition (359.6 $\pm$ 97.9 ms, p = 0.018; see Fig. 2.6C). Further, FP duration only marginally modified the V_{max} of VG saccades (*FP.rs3* model, F[1, 23.94] = 5.60, p = 0.026; see Tab.S2.4). The V_{max} of VG saccades decreased with FP duration (β = 0.006 $\pm$ 0.002). The difference in V_{max} between the 400 ms and 900 ms FP block was approximately 6°/s (see Fig. 2.6D). Finally, there was no interaction between spatial uncertainty and the duration of the FP on maximum velocity (*full.rs3* model, p = 0.890; see Tab.S2.4).

2.6.2 Pupil dilation covaries with foreperiod duration

To test the influence of spatial uncertainty on the pupillary response and to compare it with the results of Experiment 1, only the block of the longest possible FP (1900 ms) was included in the first part of the analysis. Observation of pupil size as a function of time during the foreperiod suggests that pupil dynamics up to 500 ms after the WS offset was probably related to luminance changes only (see Fig. 2.7A). CBPT was conducted on the pupillary traces in the 500 - 1900 ms window, but no significant pupil size modulation by spatial uncertainty was found.

Further, to test the possible influence of FP duration on the pupillary response (900 ms - 1400 ms and 900 ms - 1900 ms pairs), the window of 500 - 900 ms was chosen for the CBPT. Comparisons including 400-ms FP were

excluded from the analysis as 400 ms duration is too short to develop a PPR. A significant effect of FP duration was observed in the 500 - 900 ms window (CBPT, F_{mass} = 273.35, p_{mass} = 9.99 $\times$ 10^{-4}, see Fig. 2.7B). Therefore, the pupillary response was averaged within the chosen window for each subject and trial. Then, a LMM was performed on the averaged data. The duration of the foreperiod significantly modulated pupil size (F[3, 5362.33] = 9.10, p = 1.14 $\times$ 10^{-4}). Specifically, pairwise comparisons showed that pupil size was larger in the 900 ms duration block (*mean* $\pm$ *SD z-score value*; -0.11 $\pm$ 0.43) compared to the 1900 ms block (-0.17 $\pm$ 0.42, p = 3.09 $\times$ 10^{-4}). Furthermore, pupil size in the 1400 ms block (-0.12 $\pm$ 0.40) was larger than in the 1900 ms block (p = 0.002). The comparison between the 900 and 1400 ms blocks was not significant (p = 0.923; see Fig. 2.7C).

2.6.3 The differential influence of foreperiod duration and spatial uncertainty on early saccades.

Figure 2.8A shows the latency distribution of early saccades for each FP duration, separately. A set of mixture models with different k, ranging between 1 and 5 was fitted to the early saccade distribution of each FP duration. For all FP durations, the *mix.2* model assuming the bimodal distribution of early saccades fitted the data best (see Tab.S2.5 for details). The latency threshold used to separate early saccades into two modes was established at the crossing point between the two Gaussian components and was the same for all FP durations (375 ms). Based on that threshold, early saccades were assigned to 1^{st} (N = 349) and 2^{nd} modes (N = 760, see Fig. 2.8B).

It was previously shown that 2^{nd} mode saccades were more likely to occur as time elapsed during the FP. In the current study, a visual assessment of the parameters of mixture components indicate that both the mean and the standard deviation of 2^{nd} mode increases with increasing FP duration (see Fig. 2.8B). This increase is also demonstrated by comparing the trial-by-trial latencies of early saccades in 1^{st} and 2^{nd} mode plotted against the increasing FP length. Results showed an interaction of early saccade mode and FP du-

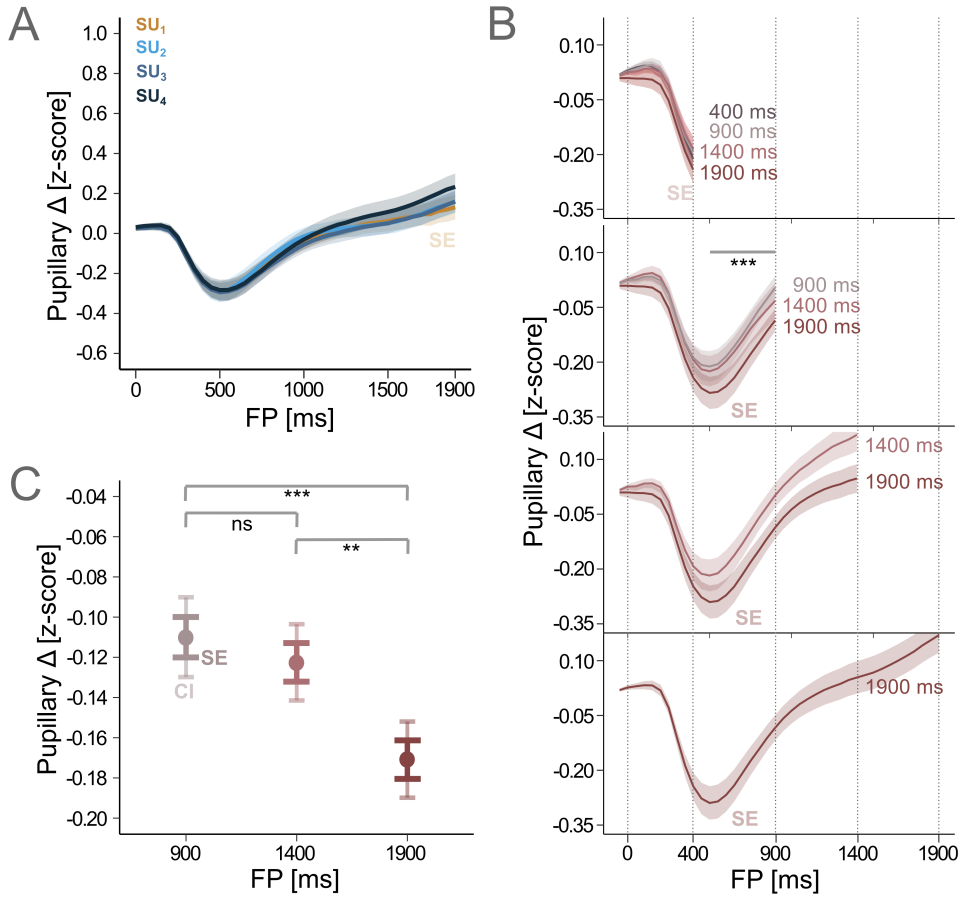

Fig. 2.7 Pupillary response in Experiment 2. (A) Time course of pupil size during the FP. Time 'zero' on the X-axis indicates the extinction of the warning signal. *Coloured lines* indicate baseline-corrected mean pupil size in different SU levels with SE (*coloured ribbons*). **(B)** *Coloured lines* indicate baseline-corrected and z-scored mean pupil size in different FP durations. *Horizontal grey lines* indicate clusters of differences between durations, together with p-values obtained with the CBPT (** $p \leq 0.01$, *** $p \leq 0.001$, ns - not significant). **(C)** Mean pupil size (*dots*) for 900 ms, 1400 ms, and 1900 ms conditions in the time window of 500 - 900 ms with SE and 95%CI (*whiskers*). *Horizontal grey lines* indicate post-hoc LMM significance between durations.

ration on early saccade latency (LMM, model *full.rs1*, F[1, 1031.98] = 366.28, $p < \times 10^{-16}$, see Tab.S2.7). Post-hoc analysis indicated that only the latency

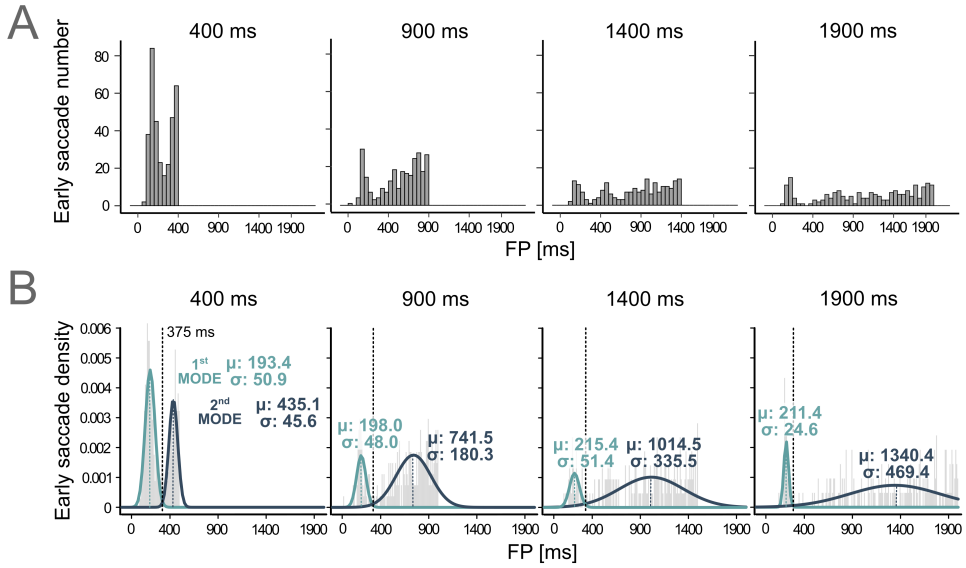

Fig. 2.8 Latency distribution of early saccades in Experiment 2. (A) Latency distributions of early saccades (*grey bars*) for each FP duration. Time 'zero' on the X-axis indicates the onset of the FP. **(B)** Latency distribution of early saccades. Mixture models (*coloured density plots*) added for each experimental block. A bimodal distribution best describes the data. The *black dashed lines* show the transition between modes and the threshold value for saccade classification (375 ms, the same for all four FP blocks). Labels describe mean (μ, *coloured dashed lines*) and standard deviation (σ) of each mode.

of 2^{nd} mode saccades increased with FP duration ($\beta = 0.61 \pm 0.02$, $p < 2.22 \times 10^{-16}$,see Fig. 2.9A). The latency of 1^{st} mode saccades were not changed by FP length ($p = 0.365$).

Next, the duration of the foreperiod also significantly modulated the standard deviation of early saccade latency, but only for 2^{nd} mode saccades. Results showed an interaction between mode of early saccades and FP duration on latency SD (LM, $F[1] = 34.68$, $p = 4.82 \times 10^{-8}$, see Tab.S2.8). The standard deviation of 2^{nd} mode saccade latency increased with FP duration ($\beta = 0.17 \pm 0.02$, $p = 1.36 \times 10^{-13}$, see Fig. 2.9B). The SD of 1^{st} mode of saccadic latencies was not modulated by FP length ($p = 0.466$).

At the same time the absolute number of 2^{nd} mode saccades did not systematically increase with FP duration. GLMM results indicated an interaction effect between mode of early saccades and FP duration on saccade number (model *full.rs4*, χ^2[1] = 11.67, p = 6.34 $\times$ 10^{-4}, see Tab.S2.9). Only the Incidence Rate Ratio ('IRR') of 1^{st} mode saccades decreased with FP duration (β = -0.001 $\pm$ 0.0003, p = 4.82 $\times$ 10^{-4}). It can be inferred that the occurrence of 1^{st} mode saccades was approximately 1.5 times more probable in a 400-ms FP compared to the 900-ms FP block (see Fig. 2.9C). The rate of occurrence of 2^{nd} mode saccades was not modified by FP length (p = 0.612).

The V_{max} of saccades was 21.2 $\pm$ 7.5°/s higher in 2^{nd} mode (model *mode.rs1*, F[1, 1015.27] = 8.04, p = 0.005, see Tab.S2.10) and an interaction effect between mode and FP duration was detected (model *full.rs1*, F[1, 1015.91] = 6.94, p = 0.009). Only the V_{max} of 2nd mode saccades was decreasing with increasing FP duration (β = -0.02 $\pm$ 0.01, p = 0.027, see Fig. 2.9D).

Further, the amplitude of 1^{st} and 2^{nd} mode saccades was different (model *mode.rs1*, F[1, 1013.92] = 18.95, p = 1.48 $\times$ 10^{-4}, see Tab.S2.11). The amplitude of 2^{nd} mode saccades was on average 0.8 $\pm$ 0.2° higher than the amplitude of 1^{st} mode saccades. However, no interaction between mode and FP duration was detected (model *full.rs1*, p = 0.112).

A GLMM was performed to compare the number of early saccades for different SUs, including mode of saccadic latencies as a covariate. Spatial uncertainty (*SU.rs2* model, χ^2[3] = 435.44, p < 2.22 $\times$ 10^{-16}) significantly influenced the IRR of early saccades. Pairwise comparisons showed that the occurrence of early saccades was more likely in SU_1 compared to the SU_2 condition (*IRR* $\pm$ *SE*, 3.5 $\pm$ 0.3, p < 2.22 $\times$ 10^{-16}), more likely in SU_1 compared to the SU_3 condition (3.5 $\pm$ 0.3, p < 2.22 $\times$ 10^{-16}), and more likely in SU_1 compared to the SU_4 condition (4.5 $\pm$ 0.5, p < 2.22 $\times$ 10^{-16}). However, there was no interaction between spatial uncertainty and mode of early saccades (*full.rs2* model, p = 480; see Tab.S2.12)

The V_{max} of early saccades was influenced by the spatial uncertainty (*SU.rs1* model, F[3, 1014.36] = 3.42, p = 0.017). Pairwise comparisons showed that the

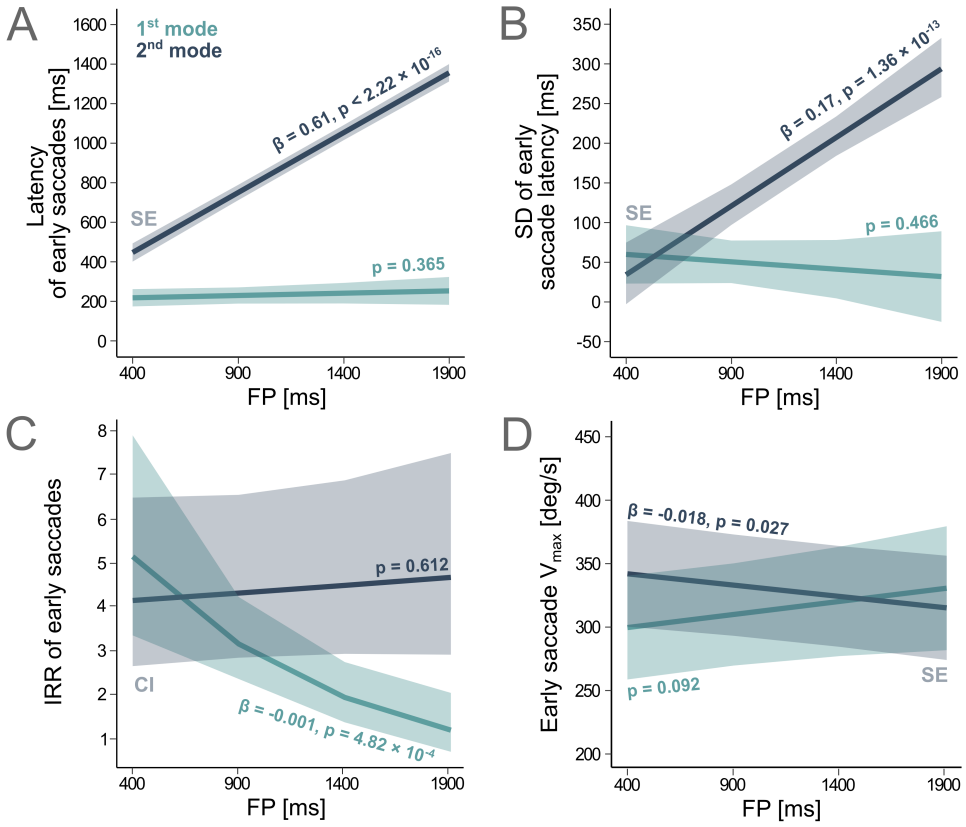

Fig. 2.9 The characteristics of early saccades in Experiment 2. (A) Latency of 1^{st} and 2^{nd} mode saccades plotted against FP duration. *Coloured lines* describe post-hoc LMM fits with SE (*ribbons*). **(B)** SD of 1^{st} and 2^{nd} mode saccade latencies plotted against FP duration (*coloured line*) with SE (*coloured ribbon*). **(C)** Incidence Rate Ratio ('IRR') of 1^{st} and 2^{nd} mode saccades plotted against FP duration. *Coloured lines* describe post-hoc GLMM fits with CI (*ribbons*). **(D)** V_{max} of 1^{st} and 2^{nd} mode saccades plotted against FP duration.

V_{max} of early saccades was 34.0 $\pm$ 10.6°/s higher in SU_1 compared to the SU_3 condition (p = 0.008). No interaction between spatial uncertainty and modality was found for the V_{max} of early saccades (*full.rs1* model, p = 0.150, see Tab.S2.13).

The amplitude of early saccades was also influenced by the spatial uncertainty (*SU.rs1* model, F[3, 1015.08] = 37.81, p < 2.22 $\times$ 10^{-16}). Pairwise com-

parisons showed that the amplitude of early saccades was 1.5 $\pm$ 0.2° higher in SU_1 compared to the SU_2 condition (p = 1.33 $\times$ 10^{-9}), 2.4 $\pm$ 0.3° higher in SU_1 compared to the SU_3 condition (p < 2.22 $\times$ 10^{-16}), and 1.5 $\pm$ 0.3° higher in SU_1 compared to the SU_4 condition (p = 8.16 $\times$ 10^{-7}). No interaction between spatial uncertainty and modality was found for amplitude of early saccades (*full.rs1* model, p = 0.147, see Tab.S2.14).

2.7 Discussion

The results of Experiment 1 suggested that, under spatial uncertainty, the oculomotor response could be influenced by two processes: an arousal-related one (pupil size, V_{max}, and early saccade occurrence) and a cognitive-related one (VG saccade latency). How did blocked temporal variability influence the relationship between oculomotor responses and spatial uncertainty?

In Experiment 2, no interaction of spatial uncertainty with FP duration was reported for the latency of VG saccades. Shortest latencies were observed for shortest FPs (400 ms, see Fig. 2.6B). This result is in agreement with the *fixed foreperiod effect*, where movement latency increases with FP duration [33, 376, 216]. Crucially, however, the results of Experiment 2 demonstrated that saccadic latency did not obey HL. This could indicate that introducing blocked foreperiod variability could disrupt the relationship between cued spatial uncertainty and the latency of movements. If the hypothesis of attention allocation could explain the logarithmic increase of latency with increasing surprise, introducing temporal variability could disrupt this distribution of attentional resources.

Interestingly, introducing implicit temporal uncertainty between blocks of trials removed the effect of spatial uncertainty from V_{max} (see Fig. 2.6C) and pupillary results (see Fig. 2.7A). It could be hypothesised that due to a more variable anticipation time, the SU_1 condition was no longer favoured by arousal. However, an interesting effect of FP duration was observed for pupil size.

upil dilation was higher for shorter FPs (see Fig. 2.7B and Fig. 2.7C). Given that pupil dilation controls the amount of light that enters the eye and, therefore, the sensitivity of the visual system to detect stimuli [238], a stronger pupil dilation in expectation of an event that is quickly approaching would be optimal. This is also in agreement with Akdoğan et al. [2], who showed that pupil dilates earlier when the attended target is expected sooner.

Mixture models were applied to the latency distribution of early saccades also in Experiment 2. To provide a clear view of the mixture components, whose structure could be time-dependent, the analysis was conducted for each FP length, separately. Results indicated that a bimodal distribution early responses was present for all FP durations. Although the mean latency of 1^{st} mode saccades was similar across FP durations, the latency of 2^{nd} mode saccades increased with the elongation of the FP (see Fig. 2.9A). The standard deviation of 2^{nd} mixture component also increased with FP duration (see Fig. 2.9B). This illustrates that the rate of occurrence of 2^{nd} mode saccades gradually increased towards the time the expected 'go' stimulus and further confirms the *anticipatory* character of those saccades. It may also indicate that the precision of anticipation decreases with the duration of the FP, which could suggest that anticipatory saccades may obey the *scalar property of variance*. Interestingly, the absolute amount of anticipatory saccades was not gradually increasing as the length of the FP increased (see Fig. 2.9C). The fact that a prolonged waiting time does not simply lead to more anticipatory attempts could further suggest that a cognitive strategy plays a role in the deployment of 2^{nd} mode saccades. Further, 2^{nd} mode responses have generally a larger amplitude and V_{max} compared to 1^{st} mode saccades. Unlike for 1^{st} mode, the V_{max} and latency parameters of 2^{nd} mode responses were altered by FP duration.

Results indicate that 1^{st} mode saccades were more frequent in the shorter FP condition (400 ms, see Fig. 2.9C). The quickly approaching arrival of the 'go' signal could induce hasty movements and increase the occurrence of *impulsive* saccades. Finally, the effect of spatial uncertainty on the number of 1^{st} and 2^{nd} mode early responses was also observed in Experiment 2. As in Ex-

periment 1, most saccades were detected for the condition where there was no spatial uncertainty (SU_1 condition).

In summary, introducing a changing foreperiod duration between blocks could have altered the allocation of attention. In Experiment 2, HL was not observed on the latency of VG saccades. Temporal variability of the foreperiod could alter the arousal-related effects in the oculomotor system. In both cases, the condition of 'no spatial uncertainty' was no longer preferred. Interestingly, in variable foreperiods the pupillary response could reflect the temporally bound preparation of the visual system for the 'go' signal.

3

Chapter 3

3.1 Introduction

SENSORIMOTOR and cognitive preparation for an incoming event is based on prior information about regularities in a given context [358, 241]. Previous research tested the influence of spatial [23, 138, 66] and temporal uncertainty [368, 366, 355] on prediction, separately. However, perceptual events in everyday life are associated with combined expected spatial and temporal uncertainties. Producing optimal behavioural responses could mean we have to simultaneously manage more than one type of uncertainty related to the incoming event [16]. Various sources of uncertainties could also be merged and jointly affect behavioural responses (*combined* uncertainty). The expectation could then be conceptualised as narrowing down the spatio-temporal probability space of the future event [352].

In a visual discrimination experiment, an improved behavioural performance due to temporal expectation was observed only in conditions where the future location of the target was known and, therefore, totally predictable [309]. In contrast, a more recent reaction time experiment did not show behavioural effects related to the combination of spatial attention and contextual temporal expectation [356]. In this chapter, we hypothesise that two types of uncertainty, spatial and temporal, could interact and have a different impact during oculomotor preparation and saccade execution.

Given that the influence of elapsed time on motor preparation during the FP occurs without subjects being informed about the temporal aspect of the

task, it could be qualified as being implicit in most foreperiod studies [9]. However, explicit visual cues could also be used to provide prior information about the duration of the FP and to allow optimal allocation of attention to the timing of the future event [102, 82, 144, 268, 311].

In Chapter 3, spatio-temporal uncertainty about the future 'go' signal will be explicitly cued to subjects. A cue will provide the likely future position of the target and a range of temporal variability related to the 'go' signal onset time. The experiment will test the impact of both types of uncertainty on oculomotor and pupil responses.

The following chapter describes the results of Experiment 3 and consists of a paper published in Scientific Reports in 2024, adjusted to the structure of the thesis. The official citation of the work is:

Boutachkourt, A., Drazyk, D., & Missal, M. (2024). Gazing into spatiotemporal 'known unknowns': The influence of uncertainty on pupil size and saccadic eye movements. *Scientific Reports*, *14*, Article 17509.

3.2 Methods

3.2.1 Subjects and Ethics

This study was conducted at the Université catholique de Louvain, Belgium. Subjects were volunteers (18 - 65 years old) who had no known neurological or psychiatric diseases, did not take illegal psychoactive substances at least one day prior to the experiment, and had corrected to normal vision, if necessary. Thirty subjects (16 women, *mean* $\pm$ *SD*, age 24.6 $\pm$ 8.1 years) provided their informed written consent and participated in this study. Each subject was informed about the aim of the study and the possibility of withdrawing from the experiment at any time without consequences. All procedures were carried out according to the Declaration of Helsinki guidelines and approved by the Ethics Committee of the Université catholique de Louvain under number B403201733677 (Belgium).

3.2.2 Experimental procedure

The present study is an oculomotor variant of the variable foreperiod task [267] with spatial and temporal cues. Each trial started with the appearance of a fixation dot at the bottom of the screen for 500 ms (see Fig. 3.1A). Next, two types of cue appeared on the screen. A spatial cue consisted of three empty *cue circles* regularly spaced from the left to the right side of the screen. Each circle's circumference could appear either red or white. If one circle was red, the future position of the 'go' signal was certain, and, therefore, there was no spatial uncertainty (condition 'SU_1', see Fig. 3.1A). If two circles were red, the future 'go' signal could appear at one of these two positions with the same probability (increased spatial uncertainty, 'SU_2'). Finally, when all three circles were red, spatial uncertainty was maximal ('SU_3'). A temporal cue consisted of a *star-like shape* located at the bottom of the screen at the place of the fixation dot. The star shape could have one of three different numbers of branches. A star with 3 branches indicated that the 'go' signal could appear after 1525 ms (23.33% of trials marked by this star), 1600 ms (53.33% of trials), or 1675 ms (23.33% of trials; see Fig. 3.1B). This distribution assumed that the FP would last on average 1600 ± 75 ms (*mean* $\pm$ *SD*) and defined a context of minimal temporal uncertainty (condition 'TU_1'; kurtosis = 2.14; referred to as *leptokurtic*). The five-arm star cued a wider FP distribution: the 'go' signal could appear after 1250 ms (25.55% of trials marked by this star), 1600 ms (48.88% of trials), or after 1950 ms (25.55% of trials; 1600 ± 350 ms; condition 'TU_2'; kurtosis = 1.96; *mesokurtic*). Finally, the nine-arm star shape indicated a flatter distribution: the 'go' signal could occur after 975 ms (32.22% of trials marked by this star), 1600 ms (35.55% of trials), or after 2225 ms (32.22% of trials, 1600 ± 625 ms; condition 'TU_3'; kurtosis = 1.55; *platykurtic*). Temporal uncertainty increased as: $TU_1 \rightarrow TU_2 \rightarrow TU_3$.

In summary, the increasing kurtosis of the distribution was cued to subjects with an increasing number of branches of the star shape. Increasing the kurtosis of the 'go' signal distribution increased temporal uncertainty. During each trial, subjects were asked to keep their gaze on the star shape while

memorising the position of the red circles in the periphery. After 2000 ms, all circles turned white, and the temporal cue was replaced with a fixation dot for 500 ms. Next, a warning signal ('WS', a smiling face) appeared on top of the fixation dot for 50 ms. The disappearance of the WS marked the beginning of the foreperiod ('FP'). At the end of the FP, the 'go' signal (the same smiling face) appeared in one of the circles that were previously labelled red. The subjects' task was to make a saccadic eye movement towards the 'go' signal as quickly as possible. If saccadic latency was less than 400 ms, subjects received positive feedback (a score point, indicated by the '+ 1' text on the screen; see Fig. 3.1A).

The experiment consisted of nine unique spatial and temporal uncertainty pairings (3 TU levels $\times$ 3 SU levels). Each pairing was repeated 30 times in randomised order. Therefore, the test phase of the experiment consisted of a total of 270 trials distributed between 9 blocks of equal length. After each block, a short rest period was interleaved, and eye-tracker calibration was performed. In order to maintain the motivation of subjects during the experiment, a score point was granted for each saccade directed towards the smiley and executed quickly enough. Furthermore, in 25% of the randomly chosen trials, the 'go' signal did not appear at the end of the FP (referred to as *catch trials*). Catch trails were used to maintain a high level of attention for subjects. Subjects could still obtain a score point in catch trials by making a saccade towards any placer with a latency < 400 ms.

The experimental session started with a set of training blocks. The first stage consisted of 6 trials that familiarised subjects with the three spatial uncertainty conditions (SU_1, SU_2, and SU_3). During this training stage, FP duration was kept constant (1600 ms). The second stage consisted of 150 trials divided into three blocks, each block with one temporal cue. Only one red circle (SU_1 condition) was presented, and subjects focused on forming a mapping between the star shape and the kurtosis of FP distribution. Finally, the last stage consisted of 9 trials, with all cue pairings presented randomly in different trials. A verbal explanation of the meaning of each cue preceded each step of the training procedure. Subjects were informed that the red cir-

cles provided information about the future location of the 'go' signal and that the star shapes carried information about the expected timing of the 'go' signal. No explanation was provided about the exact shape of the distributions, and subjects were not informed about the presence of catch trials.

3.2.3 Data collection and preprocessing

Data collection and preprocessing procedures matched the description for Experiment 1. Only 9.5% of all recorded trials were excluded during the artefact rejection procedure. The early saccades were detected in 13% of all trials that remained after rejection. The VG saccades used in the final analysis were detected in 54% of the trials that remained after rejection. The low number of trials with a VG saccade is caused by the fact that the catch trials must have been excluded from the final analysis.

3.2.4 Statistical analysis

The statistical methods used in the analysis match those described in Experiment 2, with the exceptions listed below.

To compare pupillary response at different levels of spatial and temporal uncertainty, the analysis interval of 0 - 975 ms after the WS offset was chosen. This was the longest possible interval without the 'go' signal in all conditions (see Fig. 3.1B).

As in Experiment 1, pupil size, averaged from the window indicated by the CBPT, the number of early saccades, the maximum velocity of the VG saccade ('V_{max}'), and its latencies were subjected to mixed models analysis. In this experiment, the models used the following predictors: 'TU' - the level of expected temporal uncertainty; 'SU' - the level of expected spatial uncertainty. The following labelling of models was used: the 'full' prefix indicated the model with a maximal fixed effect structure. Models that included only one predictor were labelled using the name of the predictor used (e.g., 'SU'). For example, 'SU.rs1' denotes the model with SU as the only predictor and the

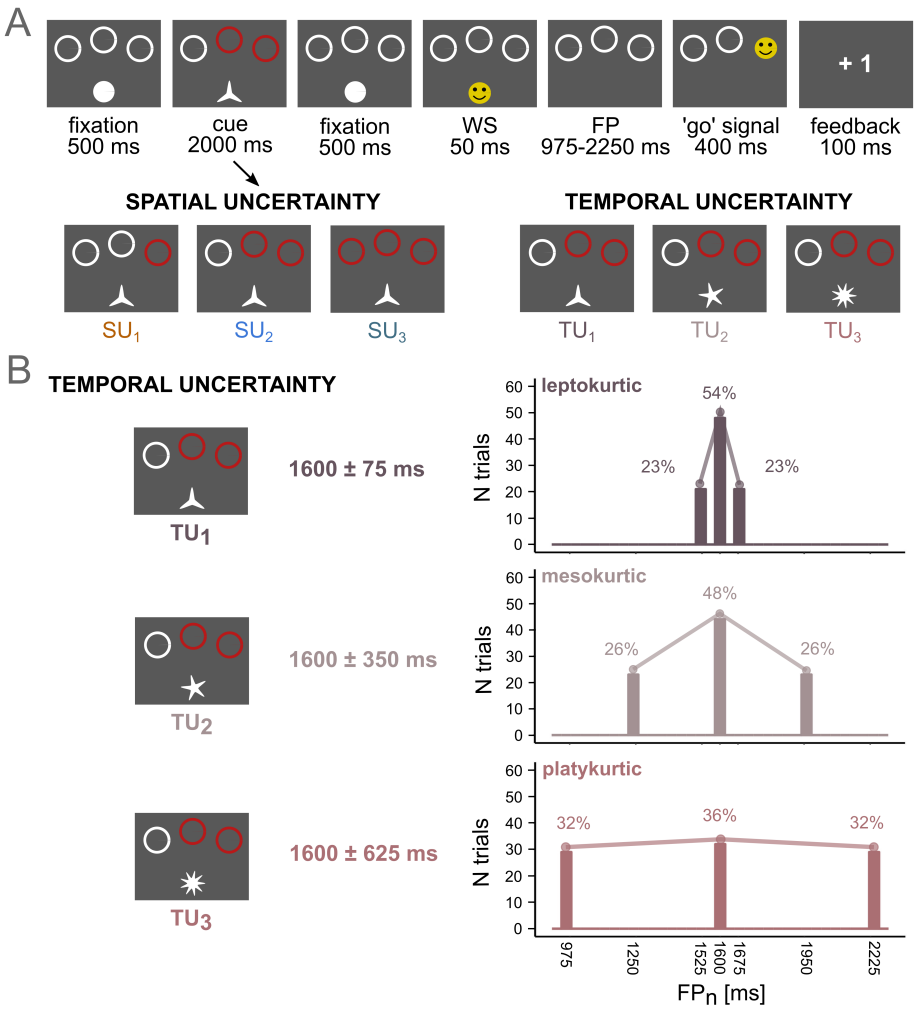

Fig. 3.1 Schematic representation of the design in Experiment 3. (A) First, subjects must gaze at a *fixation dot* at the bottom of the screen. Then they were asked to maintain their gaze on the *star shape* (temporal cue) while memorising the position of the *red circles* (spatial cue). Next, a warning signal ('WS', *smiley face*) was briefly displayed on the screen for 50 ms, starting the foreperiod ('FP'). At the end of the FP, the 'go' signal (*smiley face*) appeared at one of the cued positions for 50 ms. Subjects were asked to make a saccade towards the second smiley as quickly as possible. If the saccade was fast (< 400 ms), subjects received positive feedback ('+ 1'). **(B)** Foreperiod distributions of three temporal uncertainty levels. The *three-arm star* ('TU_1', leptokurtic) indicated that the temporal uncertainty of the 'go' signal was low. The *five-arm star* ('TU_2', mesokurtic) indicated higher temporal uncertainty, whereas the *nine-arm star* ('TU_3', platykurtic) indicated maximal temporal uncertainty.

random intercept structure. Full models with different random structures were chosen using the REML method and the BIC values. For the results of model selection, see Tab. S3.1 in the Supplementary Materials.

The LMM models used a Gaussian distribution to model the outcome. As the distribution for the latency data excluding catch trials was right-skewed, the saccadic latencies were logarithmically transformed before fitting (see Tab. S3.1 in the Supplementary Materials section).

Finally, the bimodality of the early saccade distribution was tested. However, as FP duration changed between the conditions of the temporal uncertainty in Experiment 3, the mixture analysis was conducted on the early saccade distribution from each TU condition, separately.

3.3 Results

3.3.1 Saccadic latency but not velocity is affected by temporal uncertainty

After the appearance of the 'go' signal, subjects were required to make a saccadic eye movement towards its spatial position as quickly as possible. To test the influence of different levels of spatial ('SU') and temporal uncertainty ('TU') on saccadic latency, the LMM was applied. Despite the main effects of SU and TU, no interaction between the spatial and temporal uncertainties was found ($p = 0.865$; see *full.rs1* model in Tab. S3.2). This indicates that each type of uncertainty had an independent effect on the measured outcome. Spatial uncertainty strongly influenced saccadic latency ($F[2, 4155.10] = 89.69$, $p < 2.22 \times 10^{-16}$; see *full.rs1* model in Tab. S3.2). Pairwise comparisons showed that latency increased significantly between the SU_1 (*mean* $\pm$ *SD*, 196.4 ± 50.8 ms) and SU_2 conditions (209.6 ± 53.1 ms, $p = 2.96 \times 10^{-14}$), the SU_1 and SU_3 conditions (219.2 ± 55.2 ms, $p < 2.22 \times 10^{-16}$), and the SU_2 and SU_3 conditions ($p = 1.99 \times 10^{-6}$; see Fig. 3.2A).

The results also showed a main effect of temporal uncertainty on saccadic latency ($F[2, 4154.43] = 74.20$, $p < 2.22 \times 10^{-16}$; see *full.rs1* model in Tab. S3.2).

Pairwise comparisons indicated that the latency of saccades increased significantly between the TU_1 (*mean* $\pm$ *SD*, 200.2 $\pm$ 49.1 ms) and TU_3 conditions (221.8 $\pm$ 57.9 ms, $p < 2.22 \times 10^{-16}$), as well as between the TU_2 (204.4 $\pm$ 52.1 ms) and TU_3 conditions ($p = 2.38 \times 10^{-14}$; see Fig. 3.2B). Increasing temporal uncertainty generally increased the latency of responses, but the effect was not detected between the TU_1 and TU_2 conditions (p = 0.174).

Similarly, the V_{max} of the eye during the saccade towards the 'go' signal was modelled. Saccadic V_{max} decreased together with increasing spatial uncertainty ($F[2, 4093.53] = 15.72$, $p = 1.59 \times 10^{-7}$; see model *SU.rs1* in Tab. S3.3). Pairwise comparisons showed that V_{max} decreased significantly between the SU_1 (*mean* $\pm$ *SD*, 381.8 $\pm$ 80.7°/s) and SU_3 conditions (370.0 $\pm$ 87.4°/s, $p = 6.84 \times 10^{-8}$), as well as between the SU_2 (376.9 $\pm$ 89.3°/s) and SU_3 conditions (p = 0.004). Further, there was no effect of temporal uncertainty (model *TU.rs1*, p = 0.479). Finally, no interaction between the spatial and temporal uncertainties was found (model *full.rs1*, p = 0.458; see Tab. S3.3). The V_{max} of the VG saccades was the largest when no spatial uncertainty was introduced (SU_1; see Fig. 3.2C) but remained independent of temporal uncertainty (see Fig. 3.2D).

3.3.2 Only temporal uncertainty modulates pupil size during the foreperiod

The influence of temporal and spatial uncertainty on pupil size during the foreperiod was also tested. Figure 3.3A depicts the impact of spatial uncertainty, and Fig. 3.3B presents the influence of temporal uncertainty on the pupillary response. In both cases, the time course of pupil size suggests that the pupil dynamics during the first 500 ms were probably related to changes in luminance caused by the offset of the WS [238]. This 0 - 500 ms interval was therefore excluded from the CBPT analysis. A modulation of pupil size by spatial uncertainty was detected in the 500 - 950 ms range ($F_{mass} = 117.20$; $p_{mass} = 9.99 \times 10^{-4}$; see Fig. 3.3A). Therefore, data from that interval were averaged on a trial-by-trial basis. The LMM model of the averaged data indicated that the difference in pupil size for different levels of SU was too small

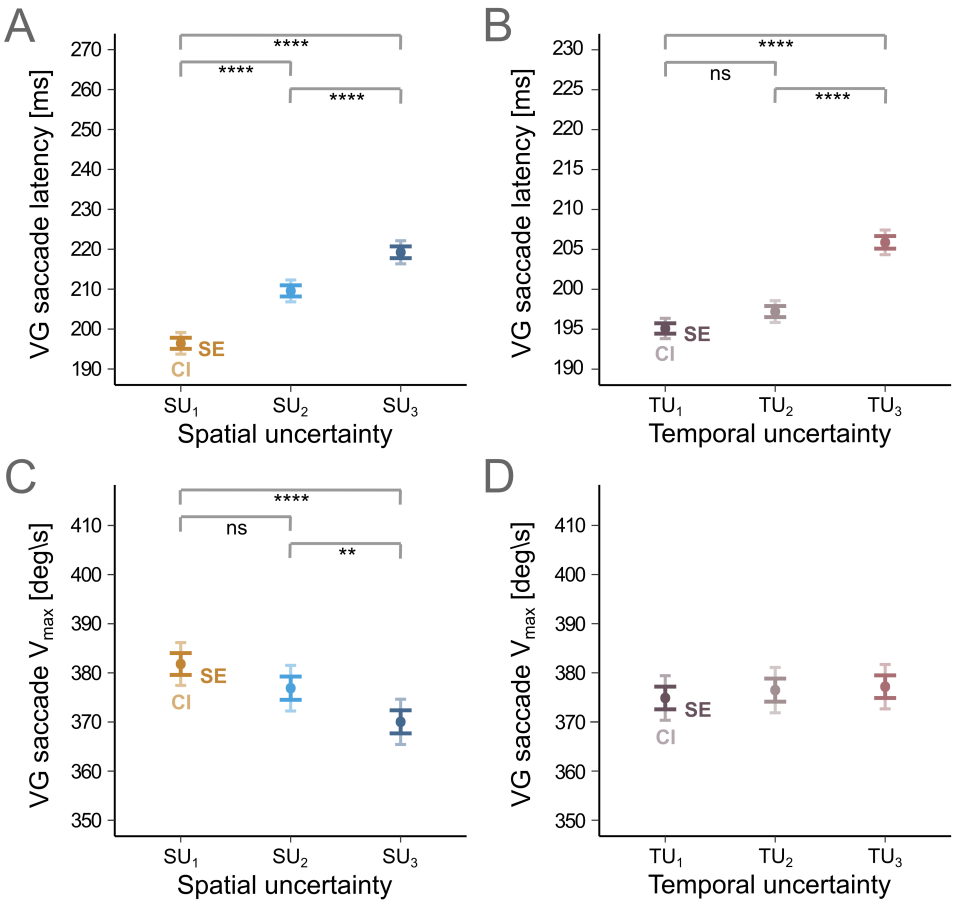

Fig. 3.2 Latency and V_{max} of VG saccades in Experiment 3 (A) Average latency of VG saccades (*dot*) for different levels of spatial uncertainty. *Whiskers* represent SE and 95%CI. *Horizontal grey lines* indicate post-hoc significance between levels (* $p \leq 0.05$, ** $p \leq 0.01$, *** $p \leq 0.001$, **** $p \leq 0.0001$, ns - not significant). **(B)** Average latency of VG saccades for different levels of temporal uncertainty. **(C)** Average V_{max} of the VG saccades for different levels of spatial uncertainty. **(D)** Average V_{max} of the VG saccades for different levels of temporal uncertainty.

to reach statistical significance (p = 0.173).

A significant modulation of pupil size by temporal uncertainty was found during a period from 500 to 950 ms after WS offset (CBPT; $F_{mass} = 361.39$; p_{mass}

= 9.99 $\times$ 10^{-4}; see Fig. 3.3B). Data was then averaged within the chosen time interval on the trial-by-trial basis. The LMM analysis indicated a significant main effect of temporal uncertainty (F[2, 4248.49] = 10.11, p = 4.16 $\times$ 10^{-5}). Pairwise comparisons showed that pupil size was larger in TU_3 (0.00 $\pm$ 0.81) compared to the TU_2 (-0.09 $\pm$ 0.80, p = 0.008) and TU_1 conditions (-0.13 $\pm$ 0.80, p = 3.02 $\times$ 10^{-5}). This indicated that the pupillary response encoded only temporal uncertainty about the future 'go' signal during the FP.

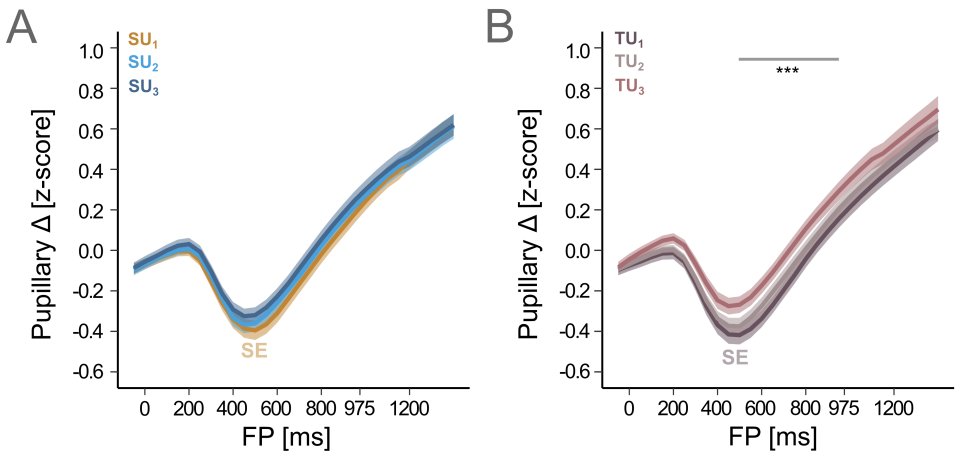

Fig. 3.3 Pupillary response in Experiment 3 (A) Time course of pupil size during the FP. Time 'zero' on the X-axis indicates the extinction of the WS. *Coloured lines* indicate the baseline-corrected and z-scored mean pupil size in different SU levels. The *horizontal grey line* indicates the cluster of significance detected by CBPT (*** p $\leq$ 0.001). **(B)** Time course of pupil size during the FP for different TU levels.

3.3.3 Spatial uncertainty reduces the total number of anticipatory saccades

Early saccades were also observed in the present experiment. A set of mixture models with different k, ranging between 1 and 5 was fitted to the early saccade distribution of each FP duration. For all FP durations, the *mix.2* model assuming the bimodal distribution of early saccades was best fitted to the data (see Tab. S3.4 for details). The latency threshold used to separate early

saccades into two modes was established at the crossing point between the two Gaussian components, different for each TU condition: 975 ms for TU_1; 675 ms for TU_2; 500 ms for TU_3. Based on those thresholds, early saccades detected for each of the TU conditions were assigned to 1^{st} (N = 233) and 2^{nd} modes (N = 860, see Fig. 3.4A). Figure 3.4B shows the latency distribution of early saccades for each TU condition, and for each SU context, separately.

Visual assessment of the parameters of mixture components showed that the mean of 2^{nd} mode was stable across TU conditions, but the SD increased with temporal uncertainty (see Fig. 3.4A). The LMM of the trial-by-trial latencies confirmed the lack of significant differences between TU conditions (p = 0.087). However, the LM results indicated that temporal uncertainty significantly modulated the standard deviation of 2^{nd} mode saccade latency (F[2, 71] = 58.44, p = 9.93×10^{-16}). Pairwise comparisons showed the SD was higher for the TU_1 compared with the TU_2 (p = 0.005), and with the TU_3 condition (p < 2.22×10^{-16}). The significant difference was detected also between TU_2 and TU_3 conditions (p = 2.93×10^{-9}).

In order to quantitatively compare the number of 1^{st} mode responses for different levels of spatial and temporal uncertainty, a GLMM was performed. Results indicated that neither SU (p = 0.484; see *SU.rs1* model in Tab. S3.5) nor TU (p = 0.084; see *TU.rs1* model in Tab. S3.5) did influence the number of 1^{st} mode saccades. There was also no interaction between variables (p = 0.756; see *full.rs1* model in Tab. S3.5).

The same test was performed on the number of 2^{nd} mode saccades. First, results showed the influence of SU on the number of 2^{nd} mode saccades (GLMM, χ^2[2] = 30.90, p = 1.95×10^{-7}; see *SU.rs1* model in Tab. S3.6). The occurrence of 2^{nd} mode saccades was more likely in SU_1 compared to the SU_2 condition ($IRR \pm SE$, 1.3 ± 0.1, p = 6.45×10^{-4}) and more likely in SU_1 compared to the SU_3 condition (1.6 ± 0.1, p = 3.50×10^{-7}). The comparison between SU_2 and SU_3 conditions was not significant (p = 0.223, see Fig. 3.5A).

Secondly, results indicated that TU influenced the number of 2^{nd} mode saccades (GLMM, χ^2[2] = 9.98, p = 0.007; see *TU.rs1* model in Tab. S3.6).

Pairwise comparisons showed that the occurrence of the saccades was less likely in TU_1 compared to the TU_3 condition ($IRR \pm SE$, 0.8 ± 0.1, p = 0.005). However, the comparison between TU_1 and TU_2 conditions (p = 0.107), as well as between TU_2 and TU_3 conditions (p = 0.495) were not significant (see Fig. 3.5B).

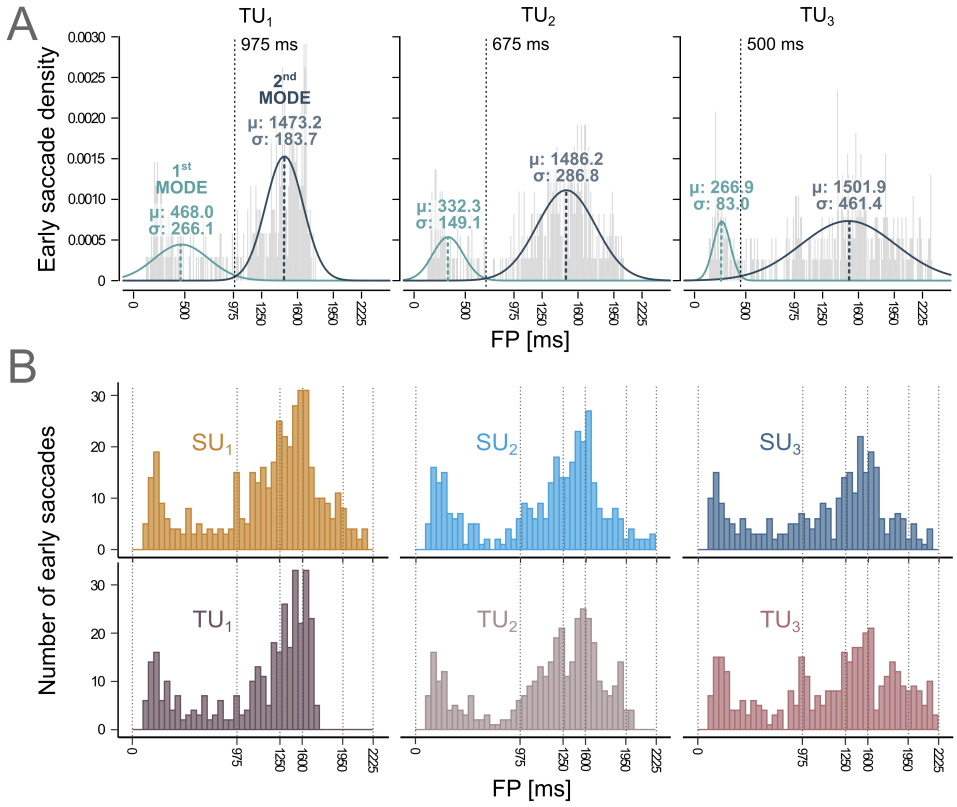

Fig. 3.4 Latency of early saccades in Experiment 3. (A) Latency distribution of early saccades (*grey bars*) and mixture models (*coloured density plots*) added for each TU. Time 'zero' on the X-axis indicates the onset of the FP. A bimodal distribution best describes the data. The *black dashed lines* show the transition between modes and the threshold value for saccade classification (different for each TU level). Labels describe mean (μ, *coloured dashed lines*) and standard deviation (σ) of each mode. **(B)** Latency distributions of early saccades for different SU and TU levels.

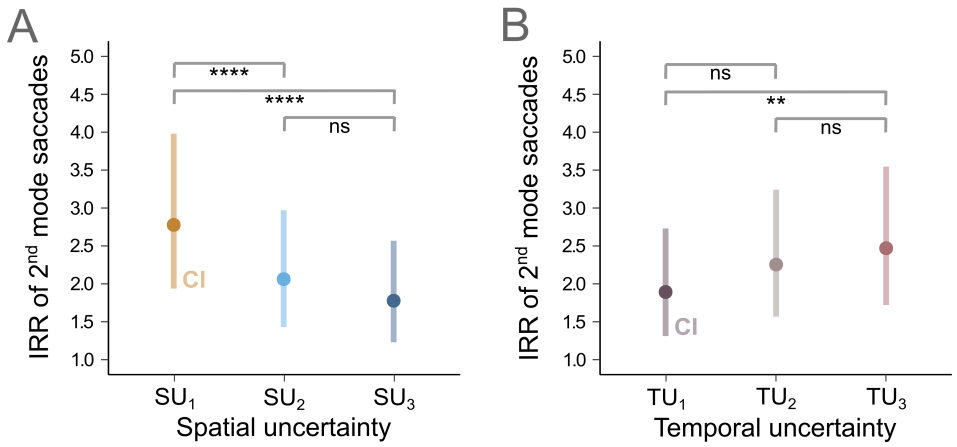

Fig. 3.5 Occurrence of early saccades in Experiment 3. (A) The Incidence Rate Ratio ('IRR') of 2^{nd} mode saccades for each SU level (*coloured dots*) with CI (*whiskers*). *Horizontal grey lines* indicate the level of GLMM statistical significance between SU levels (** $p \leq 0.01$, **** $p \leq 0.0001$, ns - not significant). **(B)** The IRR of 2^{nd} mode saccades for each TU level.

3.4 Discussion

In this chapter, we tested the possibility of the combined influence of cued spatial ('SU') and temporal uncertainty ('TU') on the oculomotor response. We hypothesised that these two types of uncertainty could interact and have a different impact during movement preparation and execution.

We found that during the FP, pupil dilation was significantly modulated only by temporal uncertainty and maximal for the higher level of TU (see Fig. 3.3B). First, this observation suggests that subjects retrieved the association between the star-shaped cue and the probability distribution of the 'go' signal from memory [218]. Secondly, previous studies in decision-making indicated that increased pupil dilation could be evoked by higher cued uncertainty ([320, 131, 96] but see [67]) and higher expected task difficulty [169]. In the current study, greater difficulty in predicting the onset of the 'go' signal could be associated with the TU_3 condition, therefore causing a larger pupil

dilation. Shalev and Nobre also observed an increase in pupil size in anticipation of an event with high temporal variability [330]. It was interpreted as an adaptation of the level of arousal to the experimental context where the duration of inter-stimulus intervals was either fixed or variable.

However, a more parsimonious interpretation would be to suggest that subjects prepare for the earliest possible appearance of the 'go' signal. This interpretation is supported by the results of Experiment 2 and the findings of Akdoğan et al. [2]. Given that pupil dilation controls the amount of light that enters the eye and, therefore, the sensitivity of the visual system to detect stimuli [238], a stronger pupil dilation could be achieved in anticipation of an event that could appear earlier. Indeed, the temporal cue did not provide information about the exact FP duration but only informed about its kurtosis. Given that the TU_3 cue indicated that the 'go' signal could appear as early as 975 ms after WS offset (see Fig. 3.1), a significant increase in pupil size early into the FP could occur.

At the end of the variable foreperiod, the 'go' signal evoked saccadic eye movement. We found that the latency of these VG saccades increased with increasing spatial (see Fig. 3.2A) and temporal uncertainty (see Fig. 3.2B). However, no statistical interaction between the SU and TU was detected. This independence of temporal and spatial expectations is in contrast to what was suggested by Rohenkohl et al. [309]. However, this could be related to the use of a simple reaction time task in the present study [356]. Indeed, the potential spatio-temporal interaction could depend on the task at hand and not occur in simple reaction time tasks [379, 393].

Furthermore, spatial uncertainty (but not temporal uncertainty) affected V_{max} (see Fig. 3.2C and Fig. 3.2D). Saccadic velocity was previously reported to change under the influence of mental fatigue [17], arousal [104, 106], reward [233, 257], intrinsic value [148], and economic utility of the stimulus [329]. Here, we show that it could covariate with spatial but not temporal uncertainty. It could be suggested that during movement execution, temporal information was no longer relevant. Indeed, temporal information could

be crucial when the timing of the movement is being prepared and manifests itself via changes in movement latency. However, there was no constraint to precisely time the saccade to the position where the target was briefly presented. Therefore, temporal information was not relevant to gaze at the final position of the 'go' signal. The position of the 'go' signal could be represented in the premotor map, which is located in the deeper layers of the superior colliculus ('SC'). It has been shown that spatial uncertainty could alter the representation of the saccade goal on this collicular map [29] and that saccadic V_{max} could be modulated by variation of neural activity in the SC [398, 339]. Therefore, we suggest that spatial uncertainty could alter V_{max} by modulating neural activity at the locus of SC activation.

It should also be noted that the lack of the effect of temporal uncertainty on the V_{max} in this experiment could be related to the results from Experiment 2. The presence of a cued spatial uncertainty effect on V_{max} in both experiments is not accompanied by temporal uncertainty modulation. This is true for the variable blocked FP in Experiment 2 and the cued temporal uncertainty in the current experiment.

As different TU levels implied different distributions of FP duration, mixture models were applied to each of the TU conditions, separately. For each TU, the distribution of early saccades latency was bimodal, consisting of 1^{st} mode (*impulsive*) and 2^{nd} mode (*anticipatory*) saccades. The mean of 2^{nd} mixture component remained constant, as was the mean of the distributions used in different temporal uncertainty conditions. However, the standard deviation of 2^{nd} mode increased together with the temporal uncertainty, illustrating the changes in kurtosis of FP duration distribution between conditions (see Fig. 3.1B).

A detailed analysis of the number of 1^{st} mode saccades did not show an effect of spatial or temporal uncertainty. Both those effects were previously observed in Experiment 2. Perhaps, as for pupil size, introducing explicit temporal uncertainty weakened the influence of spatial uncertainty on impulsive saccades. As for the previously reported effect of FP duration, it could

be possible that the shortest FP duration in this task (975 ms, TU_3 condition) was too long to invoke the time pressure, as the 400 ms FP did in Experiment 2. As a consequence, no increased susceptibility to impulsive saccades in the TU_3 condition was demonstrated in the current analysis.

As in both previous experiments, introducing levels of spatial uncertainty (SU_2 and SU_3) lowered the amount of 2^{nd} mode saccades as compared with the no spatial uncertainty condition (SU_1). This could be again related to the increased global motor inhibition evoked by the uncertain location information. Interestingly, also the effect of temporal uncertainty on the absolute amount of the anticipatory saccades was present in this task, however small. Anticipatory saccades were *more* frequent in TU_3 compared to TU_1 conditions. This could not be attributed to the difference in the summed length of the FP in each TU condition, as this was the same for all temporal uncertainty levels (see Fig. 3.1B). The direction of the effect also differs from the spatial uncertainty modulation, as the more temporally uncertain condition evokes more frequent anticipatory saccades. When the most frequent 'go' signal arrival time (1600 ms) has a reduced share in the overall FP distribution (as it is in TU_3 compared to TU_2 and TU_1 conditions, see Fig. 3.1B), more attempts to anticipate the 'go' signal at 1600 ms turns out to be inaccurate.

To sum up, only temporal uncertainty modulated pupil size during target expectation. After the 'go' signal appeared, saccadic latency increased with both uncertainties. However, movement execution was affected only by spatial uncertainty. We suggest that the most relevant information could be prioritized at different steps during the task. Indeed, temporal preparation was more relevant during the FP, and spatial uncertainty had no significant effect. This could explain the discrepancy with the results of Experiment 1, where an influence of spatial uncertainty on pupil dilation was observed in a context without temporal uncertainty. Spatial uncertainty was downplayed during the FP, but the cue could have been stored in working memory. After the appearance of the 'go' signal but before the saccade onset, a lingering temporal expectation and a (now) relevant spatial uncertainty probably added their effects, altering saccadic latency.

4

Chapter 4

4.1 Introduction

SUCCESSFULLY processing temporal uncertainty associated with a future event is essential to prepare an appropriate behavioural response. However, the timing of a movement is affected by at least two sources of uncertainty: the intrinsic temporal stochasticity of the stimulus (referred to as *stimulus-bound* or *objective* uncertainty) and the uncertainty about one's estimation of its timing (*subjective* uncertainty).

Before the 'go' signal, temporal preparation increases and reduces movement latency (e.g., keypress reaction time or eye movement latency). This process could rely on an estimation of the hazard rate ('HR') of the 'go' signal, which is defined as the conditional probability that an event will appear given that it has not yet appeared [267, 220, 368, 269, 382, 383, 155, 366, 318]. Mathematically, the HR increases rapidly during the foreperiod ('FP') and reaches a maximum at the time of the longer 'go' signal. Therefore, movement latency should be shorter when the HR reaches that maximum. The subjective variant of the HR hypothesis further suggests that the inner representation of future events could be 'blurred' [143, 142, 173, 280].

Indeed, estimating the timing of a distant future event is more error-prone (or variable) than estimating a closer one. This could be modelled by convolving the objective probability distribution of the 'go' signal with a variable Gaussian kernel, whose variance linearly increases with elapsed time [173, 283, 155] or equivalent procedure [100]. Subjective uncertainty about

the precise timing of a future event could explain why latency variability increases as the delay between the warning and 'go' signals increases. This phenomenon is probably a particular instantiation of the *scalar property of variance*, which describes how temporal perception becomes more variable as the duration to be estimated becomes longer [134, 128, 392].

An alternative hypothesis to HR suggests that under certain circumstances (e.g., absence of reward), instead of performing a complex computation of HR, the brain could instead use an internal representation of the probability density function ('PDF') of the 'go' signal to plan a motor response. This approach to temporal expectation is called the PDF hypothesis. Where the PDF is maximum (peak value for a symmetrical function), movement latency should be minimum given the higher number of 'go' signals experienced by the subject at that time. Event timings infrequently experienced on the sides of the PDF should evoke longer latencies, and an inverted U distribution of reaction times should be observed [143, 142]. The PDF hypothesis further suggests a form of probabilistic *blurring* where the size of the blurring kernel does not increase linearly with time but is a function of the probability distribution of the 'go' signal. If a Gaussian-shaped distribution of 'go' signal timing is used, then movement timing variability should be minimal around the mean value and increase on both sides of the distribution. Lastly, unlike the HR and the PDF hypotheses, the formalised Multiple Trace Theory of Temporal Preparation ('fMTP') suggests that a representation of 'go' signal timing could emerge by classical associative learning without the need for sophisticated probability computations [214, 318]. In fMTP, a memory trace of previously experienced timings guides future behaviour. For instance, a shorter FP duration during trial 'n-1' than during the current trial 'n' will be associated with a relatively shorter movement latency. This model explicitly represents temporal blurring by a *smearing* factor 'k'. This aspect of fMTP is functionally equivalent to a convolution with a Gaussian kernel.

The neural representation of temporal uncertainty is still largely unknown, but the contingent negative variation ('CNV') could be a candidate EEG potential. The CNV negative amplitude increases around the time of the ex-

pected appearance of an event [295] or towards the end of a previously learned event duration [291, 226]. Therefore, the slope of the CNV was believed to encode elapsed time, reflecting an accumulation of hypothetical clock 'pulses' as the interval to be estimated progressively elapses [291, 114, 275]. However, compelling evidence indicates that the 'ramping' CNV activity probably reflects motor preparation, event anticipation [190, 191, 11, 91], and decision-making processes [42] that are inevitably dependent on the time keeping. These functions could serve the common goal of adjusting the brain excitability to optimally prepare for the processing of information associated with the upcoming event (for review, see [189]). Based on the assumption that the CNV peaks at the expected arrival of the 'go' signal, its amplitude or slope should differentiate between the shorter and longer 'go' signal timings.

Experiment 4 consisted of a simple oculomotor foreperiod task where the timing of the 'go' signal could be constant (condition 'B') or vary according to a Gaussian-shaped distribution (condition 'U'). The aim of Chapter 4 was to present the results from Experiment 4 in light of the above-mentioned hypotheses of temporal blurring, hazard rate, and fMTP. This chapter will, therefore, focus mainly on the results related to the latency of VG saccades.

Chapter 4 consists of a paper published in eNeuro in 2023, adjusted to the structure of the thesis. The official citation of the work is:

Drazyk, D., & Missal, M. (2023). How Does Temporal Blurring Alter Movement Timing? *eNeuro*, *10*(9), Article ENEURO.0496-22.2023.

Results related to the neuronal representation of temporal uncertainty and early saccades were added during the preparation of thesis manuscript.

4.2 Methods

4.2.1 Subjects and Ethics

The present study was conducted at the Université catholique de Louvain. Subjects were volunteers (18 - 65 years old) who had no known neurological

or psychiatric diseases, did not take illegal psychoactive substances at least one day prior to the experiment, and had corrected to normal vision, if necessary. Subjects had corrected to normal vision if necessary. Three subjects were excluded from the study due to an obvious misunderstanding of the task or extensive noise in the oculomotor signal. This resulted in 42 subjects included in the analysis (23 women, *mean* $\pm$ *SD*, age 26.5 $\pm$ 4.3 years). Forty subjects from the original group of volunteers were additionally tested with EEG. One subject was excluded from the study due to the extensive noise in the EEG signal. This resulted in 39 subjects included in the final EEG analysis (age 26.6 $\pm$ 4.4 years, 21 women).

Each subject was informed about the aim of the study, signed an informed consent document regarding procedures, and was informed about the possibility of withdrawing from the experiment at any time without consequences. All procedures were carried out according to the Declaration of Helsinki guidelines and approved by the Ethics Committee of the Université catholique de Louvain under number B403201733677 (Belgium).

4.2.2 Experimental procedure

The present study is an oculomotor variant of the variable foreperiod task [267] with implicit temporal uncertainty. Each trial started with the appearance of two white boxes (3 × 3° visual angle each; see Fig. 4.1A). One box was located in the centre of the screen (central box), and the second was located to the left or the right (eccentric box, eccentricity 9.5° of visual angle from the central box) with the same probability (P = 0.5). These boxes were used to exclude the potentially confounding effects of spatial uncertainty about the future position of the 'go' signal. Subjects were initially required to maintain visual fixation of the central box for 1100 ms. Afterward, an abstract non-informative shape was displayed in the central box for 2000 ms (referred to as the 'pre-FP' interval). This pre-FP interval was introduced to potentially use the same task with an explicit timing cue, however, the idea was discontinued in later research. Next, the warning signal ('WS', first red square;

see Fig. 4.1A) was displayed in the central box for 50 ms. After a variable foreperiod ('FP'), lasting between 1250 and 2750 ms, the 'go' signal (second red square; see Fig. 4.1A) was displayed in the eccentric box for 50 ms. Subjects were instructed to maintain their gaze on the central box during the pre-FP and FP intervals and, then, initiate a visually guided saccade towards the IS as quickly as possible. The trials ended with an inter-trial interval ('ITI') of randomised duration (1050 $\pm$ 400 ms).

In each block of trials, the average duration of the FP was either 1600 ms (short) or 2400 ms (long), collectively referred to as 'anchor'. For each anchor, two blocks of 100 trials each were displayed: first, a block of trials with a constant FP duration referred to as the 'baseline' distribution (referred to as 'B', estimated technical jitter $\approx$ 5 ms); second, a block of trials drawn from a distribution composed of the same anchor durations (1600 or 2400 ms) but with increased temporal uncertainty (referred to as 'U', σ = 120 ms). The rationale for using two different anchor durations was to test the 'temporal blurring' hypothesis. This hypothesis suggests that the variance of temporal estimations should increase with elapsed time (scalar expectancy [134]). The U distributions were obtained by convolving anchors with a Gaussian-shaped distribution (see Fig. 4.1B). Figure 4.1D shows the distributions B and U for short and long anchors and their hazard rate ('HR'). To compute the survival rate, later used in the computation of the HR, the conditional cumulative distribution function ('CDF') was used as defined by Salet et al. [318]. The HR function of the B distribution is composed of a single peak. The HR function of the U distribution has two separated maxima: one local maximum around the anchor value and another for the longer FP (HR = 1).

In summary, there were four different blocks of trials ($mean \pm SD$): B_{short} (anchor = 1600 $\pm$ 5 ms), U_{short} (anchor = 1600 $\pm$ 120 ms), B_{long} (anchor = 2400 $\pm$ 5 ms), and U_{long} (anchor = 2400 $\pm$ 120 ms; see Fig. 4.1D). A block of B trials was always first collected with anchors being either 1600 ms or 2400 ms. This block was followed by the corresponding U block of trials. The sequence was then repeated with the other anchor. As an example, if the anchor in the first B block was 2400 ms (B_{long}), it was followed by a U block

of trials with the same anchor duration (2400 ms or U_{long}). Next, a block of B trials with the other anchor duration (in this example, 1600 ms or B_{short}) was presented, followed by the corresponding U block of trials (1600 ms or U_{short}). This design was used to minimise carry-over effects. Indeed, experiencing U before B would change latencies in response to B that would no longer be a baseline [217, 218, 87]. This carry-over effect could persist even a week after changing the probability distribution of the FP [242]. Pairs of blocks of different anchors were presented in random order, counterbalanced between subjects.

4.2.3 Data collection and preprocessing

Data collection and preprocessing procedures matched those described in Experiment 1. Only 5% of all the recorded trials were excluded during the artefact rejection procedure. The early saccades were detected in 22% of all trials that remained after artefact rejection. The VG saccades used in the final analysis were detected in 73% of the trials that remained after artefact rejection.

Electrophysiological signals were continuously recorded using an ASA-LAB EEG system; Advanced Neuro Technologies, Enschede, The Netherlands) and a 64-channel cap (Waveguard; Advanced Neuro Technologies) with active Ag/AgCl electrodes ordered according to the international 10-20 system. Signal recording was conducted at a 1000 Hz rate and grounded at the forehead ('Fpz' electrode). The continuous EEG recordings were preprocessed using BrainVision Analyzer 2.0 (Brain Products, Gilching) in the following steps. Datasets were downsampled to 500 Hz and filtered using a Butterworth zero-phase filter (2^{nd} order) ranging from 0.1 to 40 Hz. Noisy electrodes were interpolated if needed (spline 4^{th} order interpolation, *mean* $\pm$ *SD electrodes per subject*, 1.5 ± 1.6). Data were then re-referenced to the average of the whole scalp. To highlight blinking artefacts, a new 'VEOG' channel was created using frontal electrodes 'Fp1' and 'Fp2', $VEOG = Fp1 - Fp2$. Then, the blinks were removed from the EEG signal with independent component analysis ('ICA'). Components were detected using the VEOG channel

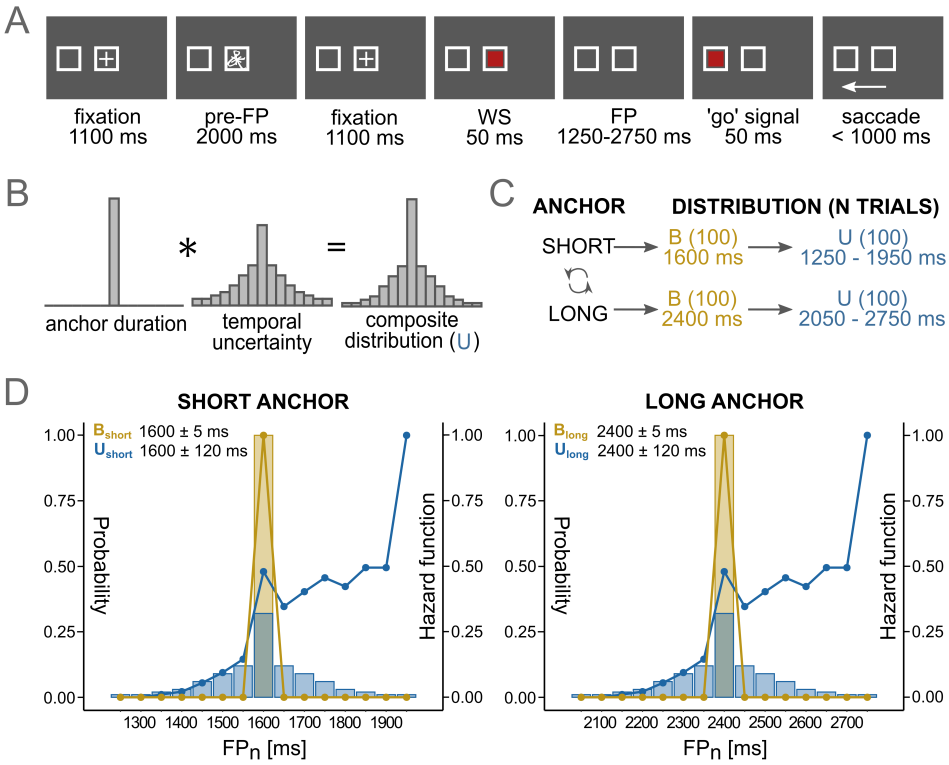

Fig. 4.1 Schematic representation of the design in Experiment 4. (A) First, two *square boxes* appeared with a *fixation cross* in the central one. The location of the eccentric box was randomly assigned to the left or the right of the central one with the same probability. Then, a *non-informative visual stimulus* appeared in the central box for 2000 ms (pre-foreperiod or 'pre-FP' interval), followed by another 1100 ms fixation period. Subsequently, the warning signal ('WS') was briefly presented in the central box (the first *red square*). The appearance of the WS initiated the FP until the 'go' signal appeared in the eccentric box (the second *red square*). The *arrow* illustrates the direction of the correct saccade executed after the 'go' signal appears at the end of the trial. **(B)** The high uncertainty U distribution was a composite obtained by convolving the anchor duration with a Gaussian kernel. **(C)** Data collection started with either the 'short' or 'long' anchor duration (counterbalanced between subjects). For a given anchor duration, two blocks of 100 trials each were collected: first, a baseline condition ('B') consisting of only one duration; second, a block of trials drawn from the uncertain distribution ('U'). The number of trials per condition is included in the round brackets. **(D)** Distributions of short anchors (*left panel*) and long anchors (*right panel*), grouped in 50 ms bins. *Coloured traces* represent the B and U hazard functions.

and removed based on their scalp topography and the time course of the EEG data. The remaining EEG data were further manipulated using MATLAB software (version 2019a) with FieldTrip Toolbox [276]. Data were segmented at 200 ms pre-FP onset to 2750 ms post-FP onset. The 200 ms pre-FP interval was used for the baseline correction. The remaining muscle and technical artefacts were removed using a semi-automatic procedure. Rejected segments included the absolute voltage smaller than 0.5 μV or the voltage fluctuation by more than 200 μV within an interval of 200 ms. This procedure resulted in rejecting 3 $\pm$ 4% trials on average (range between subjects 0 - 19%). The average number of trials remaining per subject was 386.0 $\pm$ 17.2. Further, all trials including a premature saccade were removed from the EEG data. Saccadic activity has been shown to cause significant artefacts in electroencephalographic data, especially on frontal electrodes. Removing trials that included saccades resulted in rejecting 6 $\pm$ 7% trials remaining after artefact rejection (range between subjects 0 - 28%). The average number of trials remaining per subject was 365.2 $\pm$ 34.8.

4.2.4 Statistical analysis

The statistical methods used in this analysis match those described in Experiment 2, with the exceptions described below.

For the pupil size comparison between the B_{short} and U_{short} conditions, the analysis interval was initiated by the offset of the WS and lasted for 1250 ms until the time point of the shortest possible FP duration in the short anchor. Similarly, for the comparison between the B_{long} and U_{long} conditions, the analysis interval was initiated by the offset of the WS and lasted 2050 ms. Next, regarding the early saccades, the bimodality of the saccade distribution was tested using the mixture analysis on each of the anchors, separately.

Further, following the approach of Grabenhorst et al. [143], three instances of the hazard rate function were fitted as potential data predictors:

- the classic HR function ('HR_{clas}'; see Fig. 4.1D) presents a general in-

creasing trend with increasing duration of the FPn, including a local peak around the anchor duration;

- the mirrored HR function ('HR_{mir}') that is HR_{clas} mirrored around its mean. The HR_{mir} shows a general decreasing trend with increasing duration of the FPn, including a local minimum around the anchor duration;
- the reciprocal HR ('HR_{rec}') takes the reciprocal of HR_{clas} ($\frac{1}{HR_{clas}}$). The HR_{rec} presents an abruptly decreasing trend with increasing FP duration, including a negligible local minimum around the anchor duration.

As in Experiment 1, VG saccadic latencies were subjected to LMM analysis. The choice of random structures was based on the BIC values detailed in Table S4.1 of the Supplementary Materials. In this experiment, the models used the following predictors: 'FP_n' - the duration of the foreperiod in the given trial n; 'FP_{n-1}' - the duration of the foreperiod in the previous trial n-1; 'seq' - the difference between the duration of the current and the previously displayed FP (FP_n - FP_{n-1}); 'HR_{clas}'; 'HR_{mir}'; 'HR_{rec}'. The following labelling of models was used: the 'full' prefix indicated the model with a maximal fixed effect structure. Models that included only one predictor were labelled using the name of the predictor used (e.g., 'FP_n'). For example, 'FP_n.rs1' denotes the model with FP_n as the only predictor and the random intercept structure.

Besides the LMM analyses conducted on a trial-by-trial basis, a simple linear model ('LM') was used to test specific predictions of the HR, PDF, and fMTP hypotheses. This time, the dataset was averaged between the subjects and the durations of the FP. Three variants of the HR hypothesis were fitted to the latency data (HR_{clas}, HR_{mir}, HR_{rec}). The classical HR presented the best fit and was included in the Results section. Furthermore, the relationship between the variance of the latency and the FP_n duration was tested using the slope analysis proposed by Ivry and Hazeltine [171] (see also [293, 9]). The slope analysis was used to estimate Weber's fraction k, with the assumption that the variability of the subjective time estimation is a constant fraction of the estimated time. This model also assumes that the total response variance

comes from the timing processes and a time-independent source, modelled by the variable c. Consequently, if saccadic latencies obey Weber's law, then the latency data could be modelled using the following equation:

$$\sigma(latency)^2 = k^2(FP_n)^2 + c$$

where FP_n represents the duration of the foreperiod in the given trial 'n' [9]. As an estimate of effect sizes, adjusted R^2 values are reported [312].

Due to the detection of the non-significant results in the present study, an equivalence test was performed for the analysis of the latency SD between different anchors in the U and B distributions (R package *TOSTER* [199, 197]) and for the influence of the FP_{n-1} on saccadic latency (R package *parameters* [222]). This equivalence test evaluates the hypothesis that the effect size obtained for the non-significant analyses is small enough to be called negligible (see [198] for details). Performing the test requires establishing the smallest effect size of interest ('SESOI') that will create the equivalence bounds ('eqb'). Those should be chosen based on the effect sizes detected in similar experiments from the field. As it was difficult to find a suitable sample of experiments mimicking the current design, the experiment by Tomassini et al. [366], closest to the current task, was chosen as a reference. Reference data included only the control group of Tomassini et al. study. First, the equivalence bounds for the latency SD analysis were calculated based on the critical effect size derived from analyses by Tomassini et al. (eqb = [1.13, 1.13], Cohen's d_z type). The work of Tomassini et al. does not include the analysis of the effect of FP_{n-1} duration on response latency. Therefore, the authors of this manuscript performed the above-mentioned analysis. The resulting equivalence bounds were based on Cohen's f^2 [328] of the calculated model (eqb = [0.09, 0.09] for the short anchor and eqb = [0.02, 0.02] for the long anchor).

The analysis of the CNV amplitude during the FP was conducted excluding trials that included an early, uninstructed saccade. For the comparison between the U_{short} and U_{long} conditions, the analysis interval lasted 1250 ms until the time point of the shortest possible FP duration in the short anchor.

The cluster-based permutation test ('CBPT') from the Fieldtrip Toolbox [276, 234] was used in the current study. First, two-sided dependent t-tests (α = 0.025 for thresholding) were calculated at the sample level. Then, on the channel-time level, the t-values were summed to a cluster. The clusters were constructed using the default cluster formation algorithm and the triangular neighbouring (*ft_prepare_neighbours* function with triangulation method in Fieldtrip Toolbox [276]). This neighbouring method structured all surrounding electrodes as neighbours of a given electrode. Cluster T statistics are created by summing all t-values obtained in a given cluster. For each CBPT, 1000 permutations are executed to create a null distribution of the statistic. Then, the cluster T value is compared with a null distribution (α = 0.05 for thresholding).

Statistically significant differences detected with CBPT were presented using topographic plots. The channels included in the cluster were then averaged into the corresponding Region Of Interest ('ROI') and plotted as event-related potentials ('ERP') for data visualisation. The CBPT results include information about the time interval associated with the detected effect. However, contrary to widespread use, CBPT is not tailored to support claims about the precise location of the effects [319]. Therefore, subject-by-subject amplitudes of the corresponding ROI were averaged within the time window suggested by the CBPT and subjected to a hypothesis-driven analysis. The significant difference within a chosen window was confirmed using a Kruskal-Wallis Rank Sum Test (R package *stats*; version 3.6.2) as the ANOVA assumptions were not met.

Further, trial-by-trial amplitudes of the ROI were averaged within the CBPT time windows and used in the LMM analysis as a covariate of saccadic latency and pupil size together with the corresponding experimental factors. Finally, a number of early saccades were modelled using GLMM. The choice of random structures was based on the BIC values detailed in the Supplementary Materials: Table S4.2 for models of early saccade number, Table S4.3 for models of latency. Models used the following predictors: 'dist' - level of temporal uncertainty related to the duration of the FP in a given trial; 'anchor'

- the mean of FP distribution used in the given trial; 'amp' - the amplitude of the CNV within the given cluster.

4.3 Results

4.3.1 Saccadic latency as a function of FP duration, history, and the HR

To test the influence of the duration of the current foreperiod ('FPn') on saccadic latency in the high uncertainty distributions ('U'), the LMM was applied to short (1600 ms) and long (2400 ms) anchors separately. In the short anchor FP_n*.rs1* model, saccadic latency decreased significantly as a function of the duration of the FP, showing a potential effect of temporal preparation (β = -0.05 $\pm$ 0.008, p = 1.0 $\times$ 10^{-10}). Similarly, for the long anchor FP_n*.rs1* model, saccadic latency moderately decreased as a function of the duration of the FP (β = -0.03 $\pm$ 0.01, p = 9.49 $\times$ 10^{-4}; see Tab. 4.1 for details). The potential of the HR hypothesis to explain observed saccadic latencies was also tested with LMM. For both anchor durations, saccadic latency decreased significantly as a function of the HR_{rec} showing the effect of temporal preparation (model HR_{rec}*.rs1*, short anchor: β = 0.37 $\pm$ 0.06, p = 8.86 $\times$ 10^{-10}; long anchor: β = 0.19 $\pm$ 0.06, p = 0.001; see Tab. 4.2 for details). However, the relationship between the reciprocal HR and the latency had a shallower slope for the U_{long} condition.

The fMTP model suggests that the short-term memory of previously experienced FPs ('FP_{n-1}') could partly determine saccadic latency during the current FP ('FP_n'). Therefore, two possible memory effects were tested. First, the previous FP duration did not affect the saccade latency in the current trial (FP_{n-1}*.rs1* model: short anchor: p = 0.541; long anchor: p = 0.176; see Tab. 4.3 for details). For the equivalence tests related to the relationship between the saccade latency and the FP_{n-1} duration, see Fig. 4.1B in the Supplementary Materials. Second, the sequence variable (difference between the FP_n and FP_{n-1}) was fitted to the latency data. Saccadic latency decreased significantly as a function of sequence for both anchor durations (model *seq.rs1*, short an-

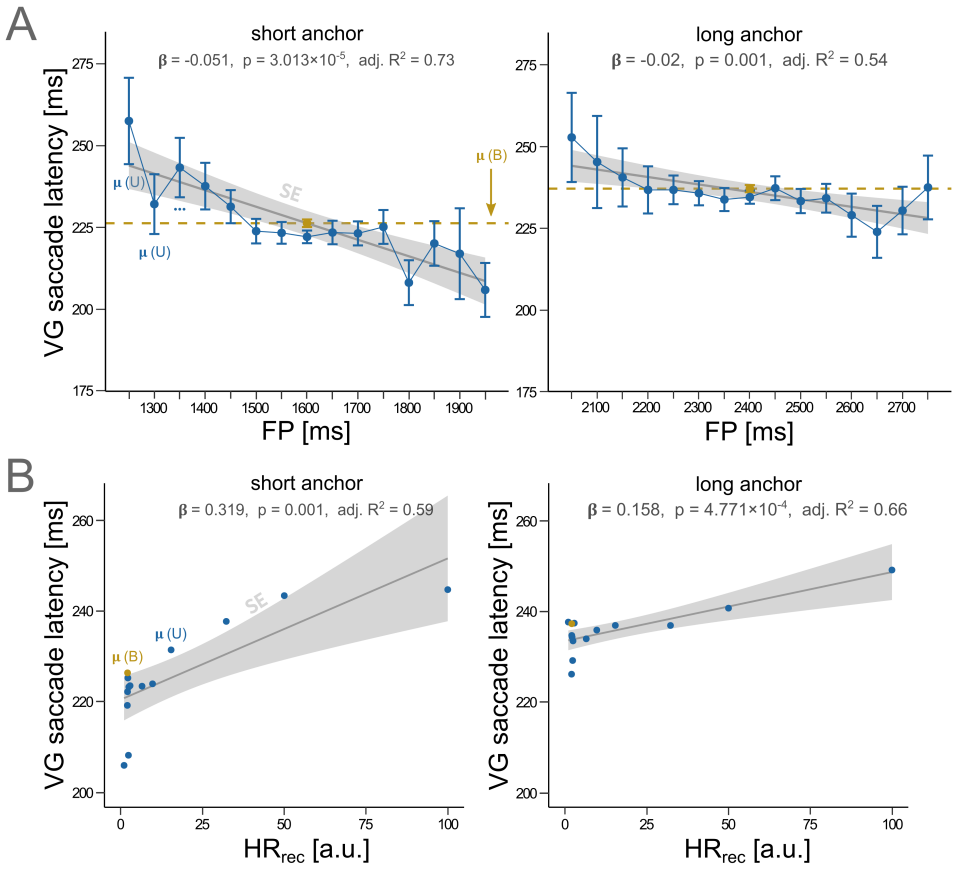

Fig. 4.2 Visually guided saccade latency results of the Experiment 4. (A) Analysis of the saccade latencies as a function of FP duration. Each *dot* shows values for the corresponding bin of the distribution together with its SE (*whiskers*). *Solid grey lines* represent linear regression fits to the U_{short} (*left panel*) and U_{long} (*right panel*) distributions of the FP together with the SE (*grey ribbon*). *Yellow dotted lines* indicate the average latency for the B distributions. **(B)** Average saccade latency as a function of the reciprocal HR (in a.u. - arbitrary units) for the U_{short} (*left panel*) and U_{long} (*right panel*) conditions.

chor: β = -0.03 $\pm$ 0.01, p = 7.01 $\times$ 10^{-7}, long anchor: β = -0.02 $\pm$ 0.01, p = 8.41 $\times$ 10^{-4}; see Tab. 4.4 for details).

In addition to LMM analyses, a simple linear model ('LM') was used to test specific predictions of the HR, PDF, and fMTP models with latencies averaged for all subjects and distinct FP durations. The average saccadic la-

tency decreased with increasing FP duration in the U_{short} (p = 3.01 $\times$ 10^{-5}, adj. R^2 = 0.73; see Fig. 4.2A) and U_{long} conditions (p = 0.001, adj. R^2 = 0.54; see Fig. 4.2A and Tab. 4.5 for details). As expected, these results suggest that temporal preparation increased during the FP. Furthermore, a linear relationship was found between the average latency and the HR_{rec} for the U_{short} (p = 0.001, adj. R^2 = 0.59) and U_{long} condition (p = 4.77 $\times$ 10^{-4}, adj. R^2 = 0.66; see Fig. 4.2B and Tab. 4.5 for details). However, no local minima were observed around the anchor FP durations.

4.3.2 Latency of visually guided saccades violates scalar expectancy

The HR, PDF, and fMTP models all suggest that the SD of timing responses should increase with anchor because of temporal 'blurring' or scalar expectancy. However, in the present study, the SD of saccadic latency for both anchors did not increase (B conditions, t[41] = 0.66, p = 0.511; U conditions, t[41] = 0.06, p = 0.952; see Fig. 4.3A). Furthermore, the SD of latencies was also computed when movements were grouped according to the bins of the U distributions. A slope analysis was performed to test the relationship between the SD of the latency and the duration of the FP in the given trial. The SD of latencies decreased significantly with elapsed time for the U_{long} condition (p = 3.84 $\times$ 10^{-5}, adj. R^2 = 0.72; see Tab. 4.5). However, since the square of the Weber's fraction was negative (k^2 = -42253.76; see Fig. 4.3B), Weber's law was not obeyed and the scalar property was not detected. Instead, the relationship between the SD of the saccadic latency and variants of the hazard rate hypothesis was tested. Unexpectedly, the SD significantly decreased with the HR_{clas} (p = 7.88 $\times$ 10^{-5}, adj. R^2 = 0.75 for short and p = 0.002, adj. R^2 = 0.56 for long anchor; see Tab. 4.5) and therefore presented a better fit than FP_n.

Table 4.1 LMM analysis of the FP_n effects on VG saccade latency.

Dataset	*Model*	*Fixed terms*	$\beta \pm$ SE	*95% CI*	*p value*	*Random terms* σ	
						subject	*resid*
U_{short}	FP_n.rs1	Intercept	307.50 ± 14.29	279.50, 335.47	$< 2.22 \times 10^{-16}$	33.57	51.91
		FP_n	-0.05 ± 0.01	-0.07, -0.04	1.0×10^{-10}		
U_{long}	FP_n.rs1	Intercept	298.04 ± 20.47	257.94, 338.11	$< 2.22 \times 10^{-16}$	34.55	52.32
		FP_n	-0.03 ± 0.01	-0.04, -0.01	9.49×10^{-4}		

CI confidence interval, resid residual, σ SD of the random terms.

Table 4.2 LMM analysis of the HR_{rec} effects on VG saccade latency.

Dataset	*Model*	*Fixed terms*	$\beta \pm$ SE	*95% CI*	*p value*	*Random terms* σ	
						subject	*resid*
HR_{rec}	HR_{rec}.rs1	Intercept	217.92 ± 5.31	207.40, 228.43	$< 2.22 \times 10^{-16}$	33.40	51.95
		HR_{rec}	0.37 ± 0.06	0.25, 0.49	8.86×10^{-10}		
HR_{rec}	HR_{rec}.rs1	Intercept	231.10 ± 5.47	220.27, 241.93	$< 2.22 \times 10^{-16}$	34.50	52.33
		HR_{rec}	0.19 ± 0.06	0.07, 0.31	0.001		

CI confidence interval, resid residual, σ SD of the random terms.

Table 4.3 LMM analysis of the FP_{n-1} effects on VG saccade latency.

Dataset	*Model*	*Fixed terms*	$\beta \pm$ SE	*95% CI*	*p value*	*Random terms σ*	
						subject	*resid*
U_{short}	FP_{n-1}.rs1	Intercept	213.04 ± 14.55	184.56, 241.54	$< 2.22 \times 10^{-16}$	33.10	52.31
		FP_{n-1}	0.01 ± 0.01	-0.01, 0.02	0.541		
U_{long}	FP_{n-1}.rs1	Intercept	205.81 ± 20.65	165.36, 246.25	$< 2.22 \times 10^{-16}$	34.39	52.41
		FP_{n-1}	0.01 ± 0.01	-0.01, 0.03	0.176		

CI confidence interval, resid residual, σ SD of the random terms.

Table 4.4 LMM analysis of the sequence effects on VG saccade latency.

Dataset	*Model*	*Fixed terms*	$\beta \pm$ SE	*95% CI*	*p value*	*Random terms σ*	
						subject	*resid*
seq	seq.rs1	Intercept	220.86 ± 5.29	210.37, 231.33	$< 2.22 \times 10^{-16}$	33.45	52.07
		seq	-0.03 ± 0.01	-0.04, -0.02	7.01×10^{-7}		
seq	seq.rs1	Intercept	232.56 ± 5.44	221.76, 243.33	$< 2.22 \times 10^{-16}$	34.50	52.32
		seq	-0.02 ± 0.01	-0.03, -0.01	8.41×10^{-4}		

CI confidence interval, resid residual, σ SD of the random terms.

Equivalence tests were used to check whether the effect size obtained for the non-significant analyses was small enough to be called negligible [198]. Equivalence tests related to the magnitude of difference between the SD of the latency in the B_{short} and B_{long} conditions (t[41] = 5.33, p = 1.93 $\times$ 10^{-6}) as well as U_{short} and U_{long} conditions were significant (t[41] = 3.25, p = 0.001; see Fig. 4.1A). Therefore, the null equivalence hypothesis could be rejected, and the effect size for both analyses was negligible. Finally, the equivalence test of the influence of the FP_{n-1} duration on saccadic latency was significant for the short anchor (p < 2.22 $\times$ 10^{-16}, 98%CI = [0.01, 0.02]), but the test for the long anchor was not conclusive (p = 0.145, 98%CI = [0.01, 0.03]; see Fig. 4.1B). Therefore, the null equivalence hypothesis was rejected, and the negligible character of the effect size was accepted only for the U_{short}.

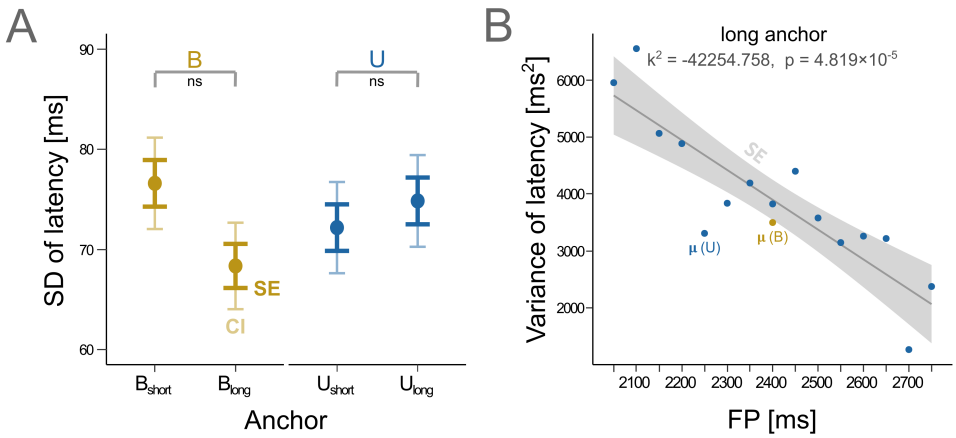

Fig. 4.3 Variance of the visually guided saccade latency in Experiment 4. **(A)** Analysis of the variability of saccadic latencies. SD of saccade latency in different experimental conditions (*dots*), with its SE and 95%CI (*whiskers*). *Horizontal grey lines* indicate paired analysis between conditions (ns - not significant). **(B)** Variance of saccadic latencies plotted against different FP durations. Each *dot* shows the value for the corresponding bin of the U distributions. The *solid line* shows a linear regression with the SE (*grey ribbon*). The yellow dot indicates the average variance around the anchor durations.

Table 4.5 LM and slope analysis for VG saccade latency. The data set was averaged between subjects and distinct FP_n durations.

Dataset	*Formula*	$\beta \pm$ SE	*95% CI*	*p value*	R^2
U_{short}	latency $\sim FP_n$	-0.05 $\pm$ 0.01	-0.07, -0.03	3.01×10^{-5}	0.73
	latency $\sim HR_{rec}$	0.32 $\pm$ 0.07	0.16, 0.48	0.001	0.59
	σ^2(latency) $\sim k^2 * {FP_n}^2 + c$	-18704.92 $\pm$ 7683.92	-35305.02, -2104.83	0.030	0.26
	σ(latency) $\sim HR_{clas}$	-23.32 $\pm$ 3.83	-31.75, -14.89	7.88×10^{-5}	0.75
U_{short}	latency $\sim FP_n$	-0.02 $\pm$ 0.01	-0.04, -0.01	0.001	0.54
	latency $\sim HR_{rec}$	0.16 $\pm$ 0.03	0.09, 0.23	4.77×10^{-4}	0.66
	σ^2(latency) $\sim k^2 * {FP_n}^2 + c$	-42253.76 $\pm$ 7100.72	-57593.93, -26913.58	4.82×10^{-5}	0.71
	σ(latency) $\sim HR_{clas}$	-22.63 $\pm$ 5.60	-34.96, -10.29	0.002	0.56

adj. adjusted, c time-independent source of response variance, k Weber's fraction, σ^2 variance.

4.3.3 A representation of duration in the CNV

The impact of increasing anchor timing on the CNV will be compared for the uncertain conditions: U_{short} and U_{long}. Figure 4.4A shows the results of the cluster-based permutation test ('CBPT') within the 0 - 1250 ms analysis interval. A lower CNV amplitude was detected for the U_{short} compared to the U_{long} condition in cluster (p_{mass} = 0.001; 992 - 1250 ms). Grand average waveforms for U_{short} and U_{long} anchors are plotted in Fig. 4.4B for this cluster. A late CNV was localised on fronto-central, central, and centro-parietal electrodes. Data for all cluster electrodes was then averaged on a subject-by-subject basis. Due to the non-normal distribution of CNV amplitude (Shapiro-Wilk test, p = 0.004), a Kruskal-Wallis Rank Sum Test (KW) was performed to evaluate the difference between the U_{short} and U_{long} CNV amplitudes. The amplitude of the CNV was lower for the U_{short} anchor (*mean* $\pm$ *SD*, -1.52 $\pm$ 0.95 μV) compared to the U_{long} (-0.68 $\pm$ 0.90 μV; $\chi^2(1) = 15.42$, p = 8.60×10^{-5}).

4.3.4 Temporal variability only affects anticipatory saccades

Figure 4.5A describes the latency distribution of early saccades for the short and long anchors, separately. Mixture model analysis indicated that the *mix.2* model assuming the bimodal distribution of early saccades was best fitted to the data of the short anchor (*mix.2* LL = -6481.97 ; *mix.3* LL = -6457.91; *mix.4* LL = -6443.89; *mix.5* LL = -6447.12) and the long anchor blocks (*mix.2* LL = -6668.22; *mix.3* LL = -6611.26; *mix.4* LL = -6603.01; *mix.5* LL = -6575.71). The latency threshold used to separate early saccades into two modes was established at the crossing point between the two Gaussian components, separately for each anchor: 1100 ms for the short and 1650 ms for the long anchor (see Fig. 4.5A). Based on those thresholds 956 saccades were assigned to 1^{st} mode and 2579 saccades were assigned to 2^{nd} mode. Visual inspection of the distribution plots and the mean of 2^{nd} mixture component indicated that 2^{nd} mode was shifted towards the predicted arrival of the 'go' signal with the increasing anchor duration. This is similar to the characteristics of 2^{nd}

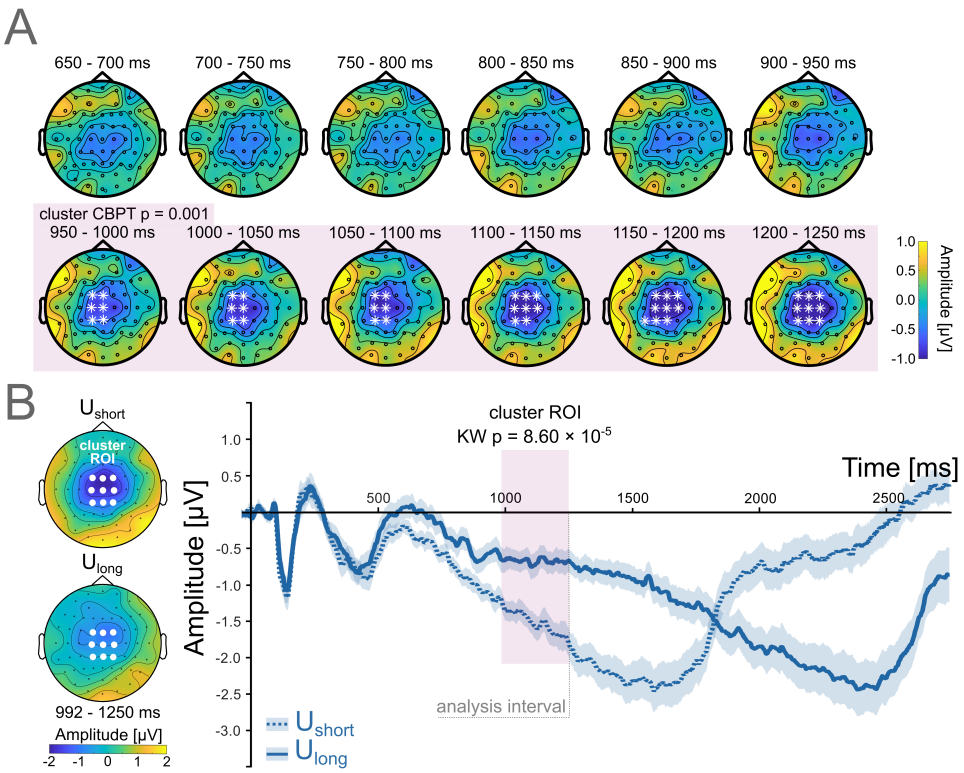

Fig. 4.4 CNV amplitude for U_{short} and U_{long} anchors. (A) Topographic plots in 50 ms time intervals showing the voltage difference between the U_{short} and U_{long} anchors during FP. CBPT indicated a significant negative cluster (992 - 1250 ms, *topo-plots highlighted in pink*) with lower amplitude for the U_{short} anchor than the U_{long} anchor. The channels consecutively recruited into the cluster are marked by *white stars*. *Numerical values* above the topo-plots represent the displayed time window in milliseconds. **(B)** Grand average waveforms represent an activity of the *cluster ROI* created from the 'FCz', 'FC1', 'FC2', 'Cz', 'C1', 'C2', 'CPz', 'CP1', and 'CP2' electrodes averaged for all subjects in U_{short} (*dotted lines*) and U_{long} anchors (*solid lines*). *Ribbons* represent the corresponding 95% SEs. Time 'zero' on the X-axis indicates the offset of the WS. The *vertical dotted line* shows the cutoff point for the analysis interval. The *pink area* represents a window of significant difference between the U_{short} and U_{long} CNV amplitudes detected by CBPT (*cluster*). Scalp topographies represent the brain activity for the U_{short} and U_{long} anchors in the established window of significance. *White dots* indicate the localisation of the cluster grand average electrodes.

mode saccades in different FP durations in Experiment 2. Furthermore, visual assessment of the standard deviation of 2^{nd} mixture component in both anchors indicates that the variability of the anticipatory saccades increased with FP duration. The LMM of the trial-by-trial latencies confirmed the shift of 2^{nd} mode mean with anchor duration (F[1, 2573.17] = 8020.23, p < 2.22 $\times$ 10^{-16}). The LM results indicated that elongating anchor duration significantly increased the standard deviation of 2^{nd} mode saccade latency (F[2, 73] = 17.33, p = 8.51 $\times$ 10^{-5}). However, there was no difference in the SD of 2^{nd} mode saccade latency between the B and U distributions, neither in the short (p = 0.054), nor in the long anchor duration (p = 0.257).

Figure 4.5B illustrates the distribution of early saccades for both levels of temporal uncertainty and both anchors. In order to quantitatively compare the number of 1^{st} and 2^{nd} mode responses for different levels of temporal uncertainty, a GLMM was performed, for each anchor duration, separately. Temporal uncertainty did not influence the number of 1^{st} mode saccades in the short (p = 0.527) or in the long anchor (p = 0.071).

However, temporal uncertainty affected the number of 2^{nd} mode responses in the short anchor (χ^2[1] = 12.64, p = 3.78 $\times$ 10^{-4}) and in the long anchor (χ^2[1] = 6.82, p = 0.009). In the short anchor the occurrence of 2^{nd} mode saccades was less likely in B condition compared to the U condition ($IRR \pm SE$, 0.8 $\pm$ 0.05). In the long anchor 2^{nd} mode saccades were less likely in B condition compared to the U condition (0.9 $\pm$ 0.05).

4.3.5 Correlation between oculomotor responses and CNV amplitude

Given that the CNV is a preparatory signal that occurs before expected events, we tested the hypothesis that it could also partly encode some characteristics of the upcoming motor response. The influence of the CNV amplitude within the time window indicated by the CBPT on the latency of visually guided saccades amplitude was analysed on the trial-by-trial level. The LMM model also included the anchor duration (U_{short} or U_{long}) as a covariate. A main effect of anchor duration (model *full.rs1*, p = 0.003) and amplitude (p = 4.06 $\times$

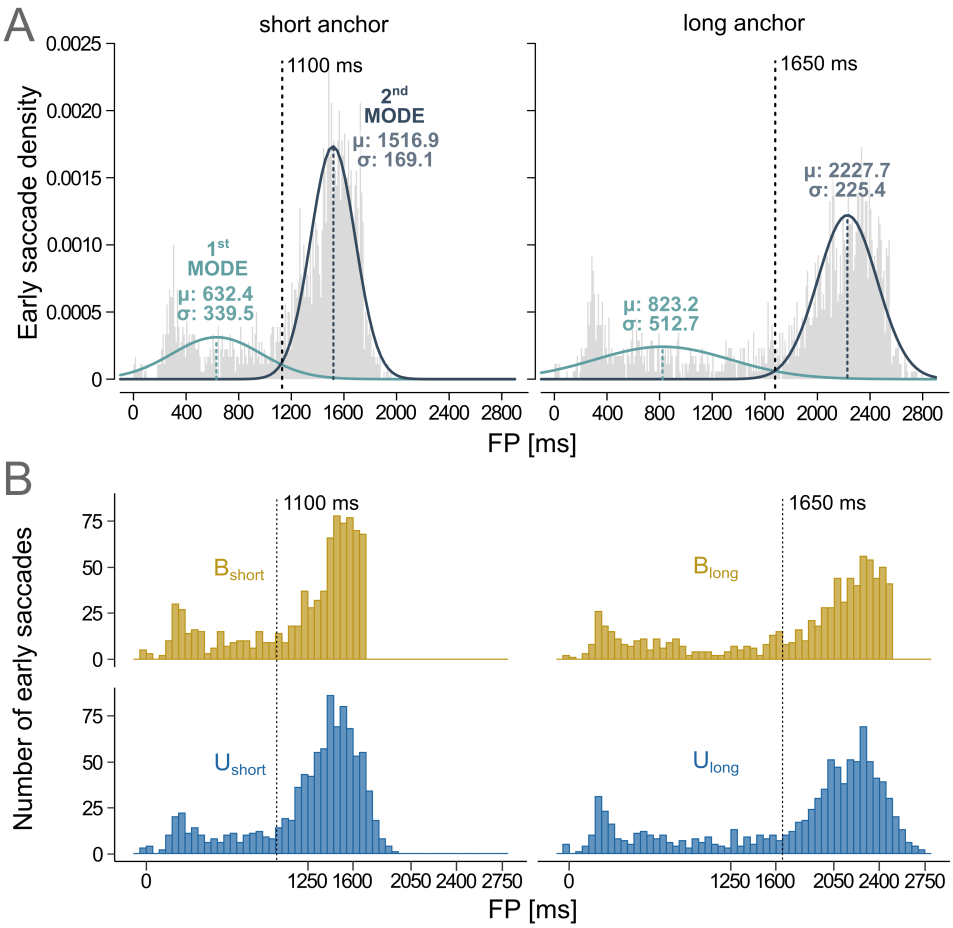

Fig. 4.5 Latency of early saccades in Experiment 4. (A) Latency distribution of early saccades (*grey bars*) and mixture models (*coloured density plots*) added for each TU. Time 'zero' on the X-axis indicates the onset of the FP. A bimodal distribution best describes the data. The *black dashed lines* show the transition between modes and the threshold value for saccade classification, different for each anchor. Labels describe mean (μ, *coloured dashed lines*) and standard deviation (σ) of each mode. **(B)** Latency distributions of early saccades for different distributions and anchors tested.

10-5; see Tab. S4.4 for details) was found. The amplitude of the CNV in the indicated time window increased together with the latency of visually guided saccades. Furthermore, an interaction between the CNV amplitude and the

anchor duration was detected (model *full.rs1*, p = 0.009). The increase of the saccadic latency with the CNV amplitude was detected only for the U_{short} condition ($\beta \pm SE$, 1.34 $\pm$ 0.28, p = 2.57 $\times$ 10^{-6}), while there was no such relationship detected for the long anchor duration (p = 0.278).

The same analysis was repeated to test the influence of the CNV amplitude within the time window indicated by the CBPT on the pupil size from the same time window analysed on the trial-by-trial level. Only a small main effect amplitude (model *amp.rs1*, p = 0.033; see Tab. S4.5 for details) was found and consequently a small increase of the pupil size with the CNV amplitude was detected ($\beta \pm SE$, 0.007 $\pm$ 0.003).

4.4 Discussion

The aim of the present study was to investigate the temporal blurring, HR, and fMTP hypotheses in the oculomotor domain. Subjects were first tested in a baseline condition 'B' with a delay between the warning ('WS') and the 'go' signals that were kept constant, 1600 ms (short anchor) or 2400 ms (long anchor). One hundred B trials with one of these two anchor durations (B_{short} or B_{long}) were first collected. Subsequently, the stimulus-bound temporal uncertainty was increased, and 100 trials of the 'U' distribution were presented (the same anchor duration as in B but σ = 120 ms; see Fig. 4.1 for details). After collecting data using B and U distributions and the first anchor duration, the whole process was repeated with the second anchor duration. The dependent variable analysed in this chapter was saccadic latency.

First, no scalar increase in the variance of latencies between the short (B_{short}) and long (B_{long}) anchor durations (Fig. 4.3A) was observed. This suggests that scalar expectancy was not observed in the present results. Second, a comparison of the U distributions revealed that the slope of the saccadic latency/FP relationship was shallower for long anchors (U_{long}) than for short ones (U_{short}; see Fig. 4.2A; see Tab. 4.1 and Tab. 4.5 for details). These results suggest a reduced sensitivity to the time around the long anchor du-

ration. Third, no latency minimum around the anchor values was observed (see Fig. 4.2A). This result suggests that latency was not directly dependent on the probability of the FP. Fourth, saccadic latencies did not covariate with the duration of the FP in the range of 1500 to 1750 ms in the U_{short} condition and in the range of 2100 to 2550 ms in the U_{long} condition (see Fig. 4.2A). Subjectively, FP durations in the above-mentioned indifference ranges could have been interpreted as equivalent to the two anchor durations. The indifference range was larger for long durations, again suggesting an impact of subjective uncertainty but not as predicted by the temporal blurring or the PDF hypothesis. Therefore, scalar expectancy was not observed when comparing anchor conditions, neither in the B nor U conditions. Within U distributions, the variability of latencies decreased with increasing FP durations (see Tab. 4.5). The gradual decrease of the variability of movement latency could be modelled using the classic HR function (see Tab. 4.5). The HR could therefore have a double impact: reducing movement latency and increasing precision.

Previous research suggested that scalar property would be present only in explicit timing tasks when temporal information is overtly used [270, 83]. However, Piras and Coull [293] suggested that scalar variability was indeed observed in a temporal expectancy task in humans. How could the volatility of scalar expectancy be explained? The oculomotor variant of scalar expectancy was initially proposed by Janssen and Shadlen [173] in the Rhesus monkey, where intensive animal training and reward expectation could have led to the emergence of an explicit representation of elapsed time during the FP, like in prospective timing. Moreover, the type of tested motor response could also play a major role. Indeed, to our knowledge, most human timing studies required a manual response (typically a button press) after a visual or auditory 'go' signal was presented [293, 143, 142, 366, 384, 356] (but for the critical review, see [145]). This could have induced another sensorimotor mapping with explicit attention devoted to producing an accurate manual response and, therefore, scalar expectancy. Previous research has already suggested that saccadic latency could not obey scalar expectancy in the same

way that the reaction time, which is related to manual response [9, 280]. A systematic comparison between the manual and oculomotor responses over the same range of durations and for the same probability distributions remains to be done.

It could also be suggested that the scalar expectancy was not observed in the present study because the temporal preparation itself was reduced. However, a robust reduction in movement latency with increasing FP duration was shown under uncertain conditions. Figure 4.6 shows a schematic comparison of the predictions issued from current hypotheses about temporal preparation (dashed lines) and the experimental results presented here (blue continuous lines and yellow dots). If the PDF hypothesis were true, then the latency-FP relationship should be U-shaped with a minimum around the mean where the 'go' signal timing was the most frequent [143, 142]. This was not observed (see Fig. 4.6A).

If temporal preparation was based on an estimation of the objective (HR_{clas}) or subjective (HR_{subj}) hazard rate (see Fig. 4.6B), then shorter latencies should be observed for long FP durations where these functions reached a maximum. This prediction was confirmed within U distributions. However, the HR_{subj} hypothesis also implies that the variance of latencies should increase with elapsed time. This was not observed here. Together, the best fit of the model to the average latency data was the reciprocal HR (HR_{rec}).

In the current study, two memory-related effects were tested. On the one hand, the memory effect of the previously experienced FP duration (FP_{n-1}) on saccade latency was not observed. This contradicts studies that demonstrated a strong influence of trial history on the saccade latency during trial 'n', even if the total number of trials was rather small (100 - 200 trials) [9, 101, 166]. Authors suggest that the memory of previous FPs could play a role only if the total number of possible 'go' signal timings is small. On the other hand, a sequence effect was found here, as suggested by the fMTP model [384, 318]. Nonetheless, temporal blurring, which was also hypothesised in the fMTP model, was not observed in the current study. In conclusion, the hazard rate

hypothesis explains the empirical data better than other approaches mentioned above. The HR_{rec} function could be used to model the influence of temporal preparation on average latency, whereas the HR_{clas} function could model the reduction of movement variability with elapsed time. These results suggest that temporal blurring does not necessarily occur in the oculomotor domain and that the timing context used in the task, implicit or explicit, could play a major role in the way the brain builds temporal expectation.

Regarding the EEG recordings, we found that, during the foreperiod, the CNV over fronto-central, central, and centro-parietal electrodes had a significantly more negative amplitude during short than long U trials (U_{short} versus U_{long} anchor; see Fig. 4.4B). In agreement with this finding, previous studies showed that the duration between the warning and 'go' stimuli could modulate ramping CNV activity in explicit [265] and implicit timing tasks [295, 111, 178, 34]. Duma and colleagues [111] presented subjects with three blocked conditions in a manual response task: short-biased, long-biased, and uniform. Comparing global temporal predictions for generally shorter and longer trials, they found a more negative CNV for short blocks. Therefore, the CNV could illustrate the optimisation of neuronal excitability during the signal anticipation process. That is, the level of excitability could change with the proximity of the 'go' signal, reflecting the level of motor or perceptual readiness. According to this view, more negative amplitudes would represent a stronger disinhibition of the source regions that build the CNV signal [189]. When the arrival of the 'go' signal was expected sooner in short blocks of trials, the ramping CNV activity would adapt to reach a predetermined excitation threshold faster. This could indicate a higher motor preparation and/or increased readiness to process sensory information when the event is imminent [248, 192]. This was confirmed by the correlation between the CNV amplitude and the latency of VG saccades.

The distribution of early saccades during the FP was bimodal in both anchor durations. As expected, the latency of 2^{nd} mode saccades increased with the elongation of the FP (see Fig. 4.5A). Furthermore, the standard devia-

tion of 2^{nd} mixture component increased with increasing anchor duration. This could further indicate that anticipatory saccades comply with the scalar property of variance that assumes higher variability of latencies in longer foreperiods.

The effect of temporal uncertainty on the number of 1^{st} mode saccades was not observed in Experiment 4. On the other hand, the anticipatory responses were affected by the temporal variability of the 'go' signal onset time in both anchor durations. Most saccades were detected for the uncertain temporal condition, which may indicate that the variable onset time of the 'go' signal renders the planning of the temporally precise saccade difficult.

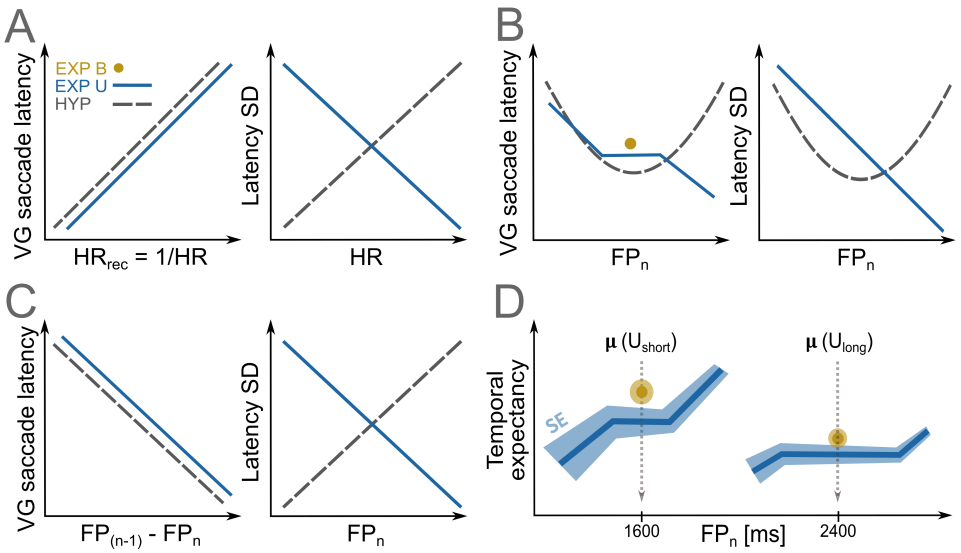

Fig. 4.6 Comparison of dominant hypotheses of temporal preparation and current empirical results. Predictions of temporal preparation models (*grey dotted curves*) versus empirical data (*blue lines* for the uncertainty U condition and *yellow dots* for the baseline B condition) for average latency (*left panels*) and SD (*right panels*). **(A)** *Left panel*: saccadic latency increased as a function of the reciprocal HR (HR_{rec}). *Right panel*: the SD of saccadic latency decreased with increasing FP duration, in contradiction with the temporal blurring hypothesis based on the HR. **(B)** *Left panel*: saccadic latency decreased with the duration of the FP in contradiction with the PDF predictions. Indeed, where the PDF is maximum, the movement latency should be minimal and the 'go' signal timings that are infrequently experienced on the sides of the PDF should evoke longer latencies (inverted U-shape). *Right panel*: probabilistic 'blurring' hypothesis. Movement timing variability should follow an inverted U-shaped distribution. **(C)** *Left panel*: as predicted by the fMTP model, a shorter duration of the FP during trial 'n-1' than during the current trial 'n' is associated with a relatively shorter movement latency. *Right panel*: the fMTP model assumes temporal blurring of the inner representation of FP duration and an increasing saccadic SD for longer FP durations. This is functionally equivalent to the one assumed by the HR hypothesis and was not observed here. **(D)** Hypothetical build-up of temporal expectancy of the 'go' signal for short and long anchor durations.

5

Chapter 5

5.1 Summary of the project

In Chapter 1, we have shown how a simple task like making a good cup of coffee can be disentangled into a series of difficult cognitive and motor decisions. Among these decisions, judgments about time proved to be of great importance. Temporal predictions can be based on explicit or implicit knowledge, previous experience, and the current state of the environment. In order to make optimal decisions, humans must integrate visual and cognitive processing, decision-making and motor control. However, in everyday life, the decision to start a movement could be hazed by temporal uncertainty about the incoming event. How our brain collects, processes, and uses information about temporal uncertainty is a subject of intense research. Chapters 2, 3, and 4 described four experiments of the current project. Experiments were carried out to supplement existing temporal uncertainty research in the oculomotor domain (see Fig. 1.3 in *Overview of the project* subsection).

Before introducing temporal uncertainty, the characteristics of oculomotor responses were tested under different spatial uncertainty conditions. In Experiment 1, a simple foreperiod task was used, where the warning and 'go' signals were separated by a delay period (foreperiod or 'FP'). The task was to make a visually guided saccade towards the 'go' signal as fast as possible after the signal appeared at one of four possible locations. Although the foreperiod's duration was constant throughout the trials, spatial uncertainty about the location of the 'go' signal varied. An explicit cue indicating possi-

ble 'go' signal locations was presented to subjects before the foreperiod. The experiment was a continuation of the work of Hsu et al. [166], aiming to characterise the basic principles of eye movements under spatial uncertainty in the absence of temporal variability. In the next experiments, temporal uncertainty was introduced in various forms. First, temporal uncertainty could be explicitly cued to subjects [9, 82]. In Experiment 3, three different distributions of delay durations were cued. This temporal information was given along with explicit information about the spatial uncertainty of the 'go' signal, similar to the way it was done in Experiment 1. This design allowed us to investigate the coexistence of spatial and temporal uncertainty in different phases of oculomotor preparation. The experiment was performed to contribute to the discussion on possible interactions between spatial and temporal information, which can be found in the recent literature [270, 309].

Secondly, temporal information could emerge implicitly [9, 83]. Therefore, two experiments explored oculomotor responses in a temporally uncertain context where the foreperiod duration was variable between (Experiment 2) and within blocks of trials (Experiment 4).

Crucially, Experiment 4 explored the concept of statistical learning of temporal regularities [75]. It was shown that statistical learning is strongly related to performing a movement [279] and that updating knowledge about the environment's regularities could be rewarding in itself [396]. Several theories aimed to explain the rise of expectation evoked by implicit learning of temporal regularities (for review, see [270]). Some models explain temporal expectation using the hazard rate function ('HR' [155, 368, 173]). HR describes the change in the probability that an event will occur, given that it has not yet occurred [269]. However, HR calculations are complex [214]. Therefore, other models are based on the simpler assumption that the probability density function is used to guide temporal expectation [143, 142, 53]. Furthermore, the HR hypothesis fails to account for the sequential FP effect found in implicit timing tasks [214]. This motivated the creation of new hypotheses incorporating the influence of trial history [377, 318].

Most of the hypotheses mentioned above were built on the results of manual reaction time tasks. However, saccadic eye movements, not limb movements, are usually the first reactions to a stimulus. In most cases, saccades towards the new stimulus precede a hand movement or a re-direction of the person's gait [277, 232]. The fixation period that follows gives the subject crucial information about the new object [398, 347, 211]. This information could later be used to guide future decisions of the oculomotor and motor systems. Oculomotor responses were previously shown to depend on the temporal predictability of an upcoming event. Therefore, they could be regarded as a marker of expectation [94, 355, 81].

Finally, related oculomotor research suggests that the scalar property of variance, widely observed in explicit timing tasks [270, 83], could not be present in implicit tasks [9] (but see [293] for a related discussion). For all the above-mentioned reasons, Experiment 4 was designed to reconsider existing temporal expectation hypotheses in the context of oculomotor responses.

In Chapter 4, the electrophysiological results of Experiment 4 were also presented. Based on previous EEG research on temporal expectation [190, 191, 189, 11, 91], the contingent negative variation ('CNV') is proposed as a candidate neural representation of temporal expectation. The *ramping* CNV activity recorded during the foreperiod could be a reflection of the decision processes modelled by the LATER model [63, 272] or DDM [301, 21, 337].

As presented in Chapter 1, an intersection between brain regions that guide saccadic eye movements and the psycho-sensory pupillary response could exist (the *common drive hypothesis* [321, 388]). The scheme presented in Figure 1.1B and 1.1C suggests that superior colliculus activity could be shared between the saccadic and pupillary neuronal pathways. The superior colliculus transfers information to and from the midbrain and pons [323, 168], which involve crucial structures like the raphe nuclei [68] and the locus coeruleus [147].

It is also worth mentioning that oculomotor-related activity of the superior colliculus is strongly influenced by the supplementary motor area ('SMA'),

supplementary and frontal eye fields, and basal ganglia [183]. TThe localization of these structures overlaps with the area of CNV-related effects presented in Chapter 4. The SMA was previously stipulated as a candidate for the source of the CNV signal [155]. Activation of the SMA and basal ganglia was shown when the representation of the timed interval was internally specified [129]. Therefore, it is plausible to suggest that similar neuronal areas could maintain the saccadic, pupillary, and electrophysiological measurements tested in the current project. Those areas could be all susceptible to changes related to temporal expectation.

5.1.1 Saccadic latency in uncertain environments

Saccadic characteristics are influenced by reward [398]. However, it was also suggested that, for an oculomotor mechanism, reduced visual uncertainty achieved by executing a saccade towards a new target is rewarding in itself [245]. It may be especially true if there is already some amount of spatial or temporal uncertainty in the contextual information about the surroundings, and each target arrival provides the observer with additional information about the structure of this uncertainty [324].

Saccades have previously been shown as susceptible to spatial uncertainty [138, 66]. The first outcome of the current project concerns the latency of VG saccades. Regardless of whether the design of the experiment assumed only spatial uncertainty (Experiment 1), spatial uncertainty with implicit temporal variability (Experiment 2), or spatial uncertainty with explicit temporal variability (Experiment 3), the latency of VG saccades always increased with spatial uncertainty (see the 'LATENCY' label for Experiments 1, 2 and 3 in Fig. 5.1). In other words, the introduction of a temporal source of variability did not affect the strong susceptibility of VG saccades to spatial uncertainty. Saccadic latency consequently increased as the number of possible locations of the future 'go' signal increased. The results indicated that the latency of visually guided saccades in Experiment 1 obeyed Hick's law [158]. This finding breached recent suggestions that Hick's law does not

apply to the oculomotor domain [194]. In this project, saccadic latency was susceptible to the information gain related to each spatial uncertainty condition. Knowing the exact location of the 'go' signal shortened the latency of VG saccades. This improvement in saccadic performance could be related to attention allocation strategies. If only one possible location of the future target is expected, attention could be undividedly shifted to the anticipated location even before the 'go' signal appears [22, 290]. However, the latency results of Experiment 2 did not obey HL (se Fig. 2.6A for details). This could indicate that temporal variability introduced into the task could disrupt this competition for attention. This result was unexpected and novel, and illustrates a strong interaction between temporal and spatial uncertainty.

A visual discrimination task designed by Rohenkohl et al. [309] indicated that, in the presence of two sources of uncertainty, predicting the timing of the stimulus is worth the effort only when its location is known. On the other hand, Tal-Perry et al. [356] suggested that implicitly built temporal expectations are independent of spatial attention. However, both research groups used different types of tasks. It was recently suggested that the codependence between spatial and temporal information could be highly dependent on the exact type of task at hand [282, 356]. Both experiments were also testing only manual responses. That is why it is valuable to revisit the relationship between spatial and temporal information in the oculomotor domain, especially since it was suggested that some beneficial link between spatial and temporal processing could occur for the oculomotor response [270]. However, the results of Experiment 3 have argued against the benefit hypothesis. Although both explicit temporal and spatial uncertainty increased the latency of oculomotor responses, no interaction between both types of information was detected. Therefore, no *canonical uncertainty* or *summary statistics* were used by the oculomotor domain [16]. More research is needed to establish whether the lack of spatio-temporal interdependence is an effect of separate attentional mechanisms operating for each type of uncertainty [82, 230, 126, 393, 66] or the task used in this specific experiment [282, 356].

The work of Ameqrane et al. [9] suggested that, in the absence of spatial

uncertainty, saccadic latency depends on the length of the blocked FP duration (so-called *fixed foreperiod effect*). Current results of Experiment 2 showed that the introduction of spatial uncertainty did not alter the effect (see the 'LATENCY' label for Experiment 2 in Fig. 5.1). The latency of saccades still increased with the duration of the FP, suggesting that prompt reaction of the eye is more difficult to achieve when motor preparation must be sustained for longer. However, similarly to Experiment 3, no interaction was found between spatial uncertainty and FP duration, which could suggest that the duration of oculomotor anticipation does not influence the eye's strategy to process spatial uncertainty.

Cueing the exact duration of the upcoming foreperiod is a straightforward task, usually implemented by controlling the display of a visual object (e.g., a disk [9]) that lasts the same amount of time as the upcoming FP. However, cueing the temporal variability of the incoming 'go' signal is more difficult. It assumes that subjects must create an indirect mapping between the cue symbol and the distribution of the possible FP durations. In Experiment 3, such mapping between the visual cue (star symbol with different numbers of arms) and the kurtosis of FP distribution (see Fig. 3.1) was first established during the training phase. Subjects were informed that different star shaped symbols were associated with different ranges of possible FP durations used in the trial. The number of arms in the star increased with the kurtosis of FP distribution. The results indicated that saccadic latency increased with cued FP variability, suggesting that the correct association emerged (see the 'LATENCY' label for Experiments 3 in Fig. 5.1). Latency results followed the ones observed for spatial uncertainty - the more uncertain the aspect of the future 'go' signal, the longer the latency of a saccade.

Saccadic latency observed in Experiments 1, 2, and 3 could be explained by means of evidence accumulation in models such as LATER [63, 272] or DDM [301]. The arrival of the warning signal started the evidence accumulation phase, during which the rate of accumulation indicated the amount of information about the incoming signal or the difficulty of making the decision [258]. Top-down processes, like the history of previous saccades, could

also modify this rate. The results from Experiment 1 indicated that spatial uncertainty modulated the rate of evidence accumulation in DDM ('R_V/T_C' model; see Fig. 2.4D) and confirmed that saccadic latencies could be explained by the opponent Poisson model [21, 337]. Therefore, it could be suggested that information about spatial uncertainty of the incoming 'go' signal is represented by the sum of excitatory and inhibitory neuronal spikes that build the drift rate [21, 337]. Indeed, it was previously demonstrated that the activity of saccade-related neurons in the SC can be altered by the uncertainty of the 'go' signal [29, 260]. However, the lack of the interaction effect in Experiment 3 indicated that information about spatial and temporal uncertainty of a 'go' signal is not accumulated by the same collection of neurons. Spatial and temporal information could have a separate impact on the drift to a decision threshold assumed by DDM. The results suggest that different types of uncertainty could be encoded by different neuronal groups and utilised at different stages of the saccade preparation and execution.

To summarise, in the context of spatial uncertainty, saccadic latency obeyed HL only in the absence of temporal uncertainty. At the same time, shorter saccadic latencies were observed in the absence of spatial uncertainty regardless of the type of temporal uncertainty used in the given task. The results of Experiment 2 confirmed the fixed foreperiod effect on saccadic latency. However, previously suggested interaction of spatial and temporal information, observed on the manual response latency, was not observed for saccades. However, plotting the latency-FP effect for all FP durations in a temporally uncertain context yielded interesting conclusions. Those will be discussed in the next subsection.

5.1.2 Saccades differ from manual responses

Important differences come to light when comparing models of temporal expectation built on manual reaction time data or saccadic latencies. First, results of Experiment 4 demonstrated that the latency-FP function was not U-shaped (see Fig. 4.2A). Therefore, the obtained results do not support the

hypothesis that temporal expectation takes the form of the reciprocal of the Gaussian distribution [143]; [142]. Secondly, the history of previously experienced FP durations played little role in the formation of the saccadic movement in the current trial. Therefore, the formalised Multiple Trace Theory of Temporal Preparation [318] was not suited to explain the saccadic latency data. Instead, a reciprocal of the hazard function calculated from Gaussian distributions best explained obtained results. However, it must be noted that even the HR did not capture all features of the latency-FP function observed in Experiment 4. This suggests that how the oculomotor system uses temporal expectation to form a saccadic response differs from motor systems managing manual reactions.

Finally, following observations from related research [9, 280], no scalar property of timing was found in the saccadic latency results of Experiment 4. This was shown by the slope analysis (see Fig. 4.3B) and by comparing the SD of the latency between short and long anchor durations (see Fig. 4.3A). This further demonstrates the difference between the oculomotor and manual reactions.

5.1.3 Do not bet on the unknown when planning a saccade

Saccadic maximum velocity was previously shown to be influenced by arousal. Alleviated arousal levels could result from high reward possibility [327], level of individual motivation [257], or task difficulty [104]. In turn, arousal changes could be responsible for modulating maximal firing rates of burst neurons during the saccadic movement, causing high V_{max} [104, 259]. In this project, we demonstrated that manipulating the level of spatial uncertainty also changed the V_{max} of visually guided saccades. Eye velocity was higher when no spatial uncertainty was present in the given trial (SU_1 condition; see the 'V_{MAX}' label for Experiments 1 in Fig. 5.1). The certainty about the future location of the 'go' signal could indeed increase arousal levels. In contrast, when the exact location of the 'go' signal was ambiguous (SU_2, SU_3, SU_4 conditions), oculomotor inhibition could be applied to optimise motor preparation

in an uncertain environment [14]. The absence of an external reward (arbitral points, monetary incentive, or positive feedback collected for fast responses) could make the effort that is put in the uncertain condition disproportionate to the benefits [47]. Cautious allocation of the oculomotor resources could encourage the "do not bet on the unknown" strategy [287]. In the work of Payzan-LeNestour and Bossaerts [287], two different strategies were proposed to explain behaviour in uncertain environments. On the one hand, *curiosity* motive could play a role when the exploration approach has the potential to broaden the reward opportunity. On the other hand, a *cautiousness* motive or "do not bet on the unknown" strategy could be used when a potential mistake is rather unprofitable. If nothing additional is achieved by executing a fast response in ambiguous conditions, cautious optimisation of resources could be the optimal choice.

The oculomotor system could 'choose' the "do not bet on the unknown" strategy also when an explicit form of temporal uncertainty was introduced. In Experiment 3, the V_{max} of visually guided saccades was strongly decreased in spatially uncertain conditions (SU_2 and SU_3; see the 'V_{MAX}' label for Experiment 3 in Fig. 5.1), regardless of the amount of temporal uncertainty introduced in the given trial. Interestingly, however, the implicit form of temporal uncertainty used in Experiment 2 suppressed the effect of spatial uncertainty (see the 'V_{MAX}' label for Experiment 2 in Fig. 5.1). It seems that introducing variable FP durations in a blocked design FP was enough to remove the arousing aspect of knowing exactly the location of the future 'go' signal. It could be hypothesized that when the duration of the anticipated target delay was vague, and its variability not cued, then certain spatial information is no longer associated with increased arousal. At the same time, results of Experiment 3 suggest that when two sources of uncertainty were introduced, spatial uncertainty could be prioritised by mechanisms maintaining saccadic velocity. Further, temporal uncertainty affected V_{max} only when spatial uncertainty of the 'go' signal was absent.

To sum up, the maximal velocity of the eye does not fully reflect the effect of complex spatio-temporal uncertainty on oculomotor anticipation. Al-

though the "do not bet on the unknown" strategy could be applied in spatially uncertain contexts even in the presence of explicit temporal uncertainty, implicit temporal variability cancels the arousing effect of certain spatial information.

5.1.4 Early saccades to probe oculomotor readiness

Oculomotor inhibition plays a permissive role, allowing saccades to occur at the right time after the appearance of the 'go' signal. However, a lack of inhibition could manifest itself through the occurrence of uninstructed saccades during the delay period [281]. If an uninstructed saccade occurs, the movement blurs vision and delays the gathering of meaningful information. The occurrence of an uninstructed saccade is therefore usually regarded as an 'error'. However, uninstructed saccades could provide valuable information about the state of inhibitory oculomotor control and probe impulsivity [166, 105, 112, 204, 58]. Attempts to use early saccades as markers of impulsivity have already been made in health and disease [166, 102, 9], suggesting the existence of a bimodal pattern of saccades during the FP. 1^{st} mode of the distribution was observed just after the extinction of the warning signal and could represent *impulsive* saccades. 2^{nd} mode, rising later during the foreperiod, could illustrate truly *anticipatory* saccades.

In this project, all four experiments confirmed the occurrence of early saccades, supporting findings from previous works. The results of the mixture models analysis repeatedly demonstrated that the bimodal distribution was best fitted to the distribution of early saccades during the foreperiod. This bimodal distribution was observed in the fixed (see Fig. 2.3A) and variable foreperiod tasks, with implicit temporal uncertainty (see Fig. 2.8A and Fig. 4.5A) and with explicit temporal uncertainty (see Fig. 3.4A). However, the percentage of early saccades in all experiments varied: 5.5%, 10%, 15%, and 22% in Experiments 1, 2, 3, and 4, respectively. Due to the small and varied number of early saccades between subjects and tasks, the conclusions drawn from the analysis of early saccades must be taken with caution.

In all experiments, 1^{st} mixture component was fitted close to the beginning of the foreperiod, just after the onset and extinction of the warning signal. This could indicate that 1^{st} mode saccades were indeed evoked by the arrival of the WS. The function of the WS was to mark the beginning of the foreperiod and initialise the build-up of oculomotor readiness. This increased readiness could mean a reduced oculomotor inhibition and result in premature, *'impulsive'* saccades. 1^{st} mode impulsive saccades were also susceptible to changes in spatial uncertainty.

Furthermore, in Experiment 1 and Experiment 2, the highest number of 1^{st} mode saccades were observed for the 'no spatial uncertainty' condition (SU_1; see the corresponding '$EARLY_{1st}$' label in Fig. 5.1). This result could be a byproduct of the "do not bet on the unknown" strategy that promotes the engagement of oculomotor resources in stable environments. When the future location of the 'go' signal is predictable, the probability of executing a fast and correct saccade is high and facilitates oculomotor engagement. In the absence of negative feedback, impulsive saccades could be a small price to pay for the execution of fast responses to the 'go' signal. Interestingly, the effect of spatial uncertainty on 1^{st} mode saccades was cancelled in Experiment 3, when the distribution of FP duration was manipulated explicitly, and in Experiment 4, when the FP distribution was manipulated implicitly (see the corresponding '$EARLY_{1st}$' labels in Fig. 5.1). Therefore, it could be hypothesized that the anticipated FP variability could also engage a "do not bet on the unknown" strategy, globally increasing oculomotor inhibition, even when the location of the future 'go' signal is known.

Interestingly, a separate effect of FP duration on 1^{st} mode saccades was shown in Experiment 2. Impulsive saccades were most frequently observed for the shorter FP (400 ms; see the '$EARLY_{1st}$' label in Fig. 5.1). It is possible that a shorter foreperiod duration could have increased the propensity to respond quickly compared to longer FP durations (900 ms, 1400 ms, 1900 ms). Alternatively, the temporal proximity of the 'go' signal could have induced a relatively early release of inhibition. For short FPs, the correct visually guided saccade must be executed almost immediately after the warning signal ex-

tinction. The deployment of a fast and correct visually guided saccade could be therefore made at the cost of the increased amount of impulsive responses, especially in the absence of negative reinforcement or feedback.

In Experiment 1, the mean of 2^{nd} mixture component approached the duration of the FP. In Experiment 2, the mixture analysis was conducted separately for each FP duration and the latency and standard deviation of 2^{nd} mode saccades increased with the duration of the FP (see Fig. 2.8A). Further, in Experiment 4, when the anchor FP distribution could be either 1600 ms or 2400 ms, the mean of 2^{nd} mode saccades followed the anchor duration and the standard deviation of 2^{nd} mode increased for longer foreperiods. The increasing slope of the latency distribution of 2^{nd} mode saccades approaching the mean duration of the FP in a given condition strongly suggests that the occurrence of anticipatory saccades is dependent on temporal expectation. Changes in the standard deviation of 2^{nd} mixture component also suggest that anticipatory saccades could obey the *scalar property of variance*. This is interesting, especially as the results of Experiment 4 indicated that the variance of visually guided saccades did not conform to the scalar property (see Fig. 4.3). This further highlights the differences between saccades evoked as a reaction to the 'go' signal and the responses driven by intentional temporal anticipation.

Further, in Experiment 3 when temporal uncertainty was introduced by manipulating the kurtosis of the FP distribution with the mean of this distribution constant, parameters of 2^{nd} mixture component were changed accordingly. The mean of 2^{nd} mixture component remained constant across TU conditions but the standard deviation increased together with temporal uncertainty (see Fig. 3.1B). Surprisingly, this relationship between the variance of anticipatory saccades and the kurtosis of the FP distribution was not confirmed in Experiment 4, as there was no difference in the SD of 2^{nd} mode saccade latency between the B and U distributions, regardless of the anchor duration tested. Future experiments are needed to establish if this could be a result of the implicit character of the FP distributions in Experiment 4.

All three experiments manipulating spatial uncertainty indicated the highest number of early saccades (both modes included) for the 'no spatial uncertainty' condition (SU_1; see the '$EARLY_{2nd}$' label in Fig. 5.1). According to the 'do not bet on the unknown' strategy, knowing exactly where to direct a visually guided saccade could increase subjects' engagement in executing it as fast as possible. This, in turn, could increase the number of anticipatory saccades that are a reflection of the anticipation of the timing of the 'go' signal [9]. Consequently, a decrease in the number of early saccades in spatially uncertain conditions (SU_2, SU_3, SU_4 conditions) could be a reflection of strengthened oculomotor inhibition put to work when the environment provides ambiguous information about future events.

Further, 2^{nd} mode saccades occurred *more* often in conditions with higher explicit (Experiment 3) or implicit temporal uncertainty (Experiment 4, see the '$EARLY_{2nd}$' label in Fig. 5.1). This could be explained by the anticipatory character of 2^{nd} mode saccades. In both experiments, high temporal uncertainty was created by increasing kurtosis of the FP distribution which decreased the frequency of anchor FP duration. If subjects attempted to anticipate the 'go' signal at the anchor of the FP distribution, increasing kurtosis meant that more of those attempts were ill-timed. It is noteworthy, that 1^{st} mode, impulsive responses were never affected by temporal uncertainty of the FP (see the '$EARLY_{1st}$' label in Fig. 5.1).

It is also worth noting that manipulating the duration of the FP in Experiment 2 further highlighted the distinction between 1^{st} and 2^{nd} mode saccadic responses. Anticipatory saccades were shown to have generally a larger amplitude and higher V_{max} compared to 1^{st} mode saccades. In contrast with 1^{st} mode saccades, the V_{max} and latency parameters of 2^{nd} mode responses changed with FP duration.

In summary, all experiments confirmed the bimodal pattern of saccades during the FP. *Impulsive*, 1^{st} mode saccades, probably driven by lowered oculomotor inhibition and a speed imperative, could be evoked by the extinction of the WS. Impulsive saccades were especially numerous in conditions of 'no

spatial uncertainty' and short foreperiods when the inhibition is levelled by the certainty of the response direction or the need for a fast oculomotor reaction. 2^{nd} mode, *anticipatory* saccades were modulated not only by the extent of spatial uncertainty but also by the length of the foreperiod. The mean latency of 2^{nd} mode moved together with the expected arrival of the 'go' signal. Furthermore, the SD of 2^{nd} mode increasing with FP duration indicated that the anticipatory saccades could obey the scalar property of variance like in explicit timing tasks.

Both types of saccades could operate under the 'do not bet on the unknown' strategy. High spatial predictability of the incoming 'go' signal could alleviate arousal and promote oculomotor disinhibition. Furthermore, the gradual increase in the number of anticipatory saccades towards the expected arrival of the 'go' signal (the slope of 2^{nd} mode) seems to reflect the ramping decision-making activity observed in time neurons and proposed by the DDM [301] and LATER models [63, 272]. Anticipatory saccades could directly illustrate how the brain represents the temporal expectation of the event [64, 280] and advances the oculomotor preparation according to that representation [84].

5.1.5 Pupillary responses reflect two distinct decision making strategies

First and foremost, alterations of pupil size maintain a high quality of vision by changing the amount of light that enters the eye. However, the psychosensory pupil response, or 'PPR' is hypothesised to also reflect the prediction process related to changes in the environment [264, 98]. A larger pupil dilation could be the result of increased arousal evoked by a novel surprising event. Consequently, the arrival of a non-surprising event that already fits existing internal expectations about the environment would make the pupil comparably less dilated [278, 403, 187, 202, 296, 4].

However, it has been reported that there could be a negative correlation between the latency of a saccade evoked by an event and the preceding pupillary response [388, 172, 389, 165]. Jainta et al. [172] showed that pupil size

preceding a visually guided saccade could be negatively correlated with its latency. Indeed, in Experiment 1 of the present thesis, trials without spatial uncertainty (SU_1 condition) evoked shorter VG saccade latencies and stronger pupillary dilation (see the 'PUPIL' label in Fig. 5.1). This experimental condition was also related to the highest V_{max} and numerous early saccades. A positive relationship between pre-saccadic pupil size, saccadic maximum velocity and the number of early saccades was also shown by Wang et al. [389]. This connection between the pupillary response and saccade characteristics could exist due to the coordination of these behaviors by the superior colliculus which is a part of the neuronal pathways of both of those mechanisms (the *common drive hypothesis* [321, 388]).

The results of Experiment 1 suggested that, as for the V_{max} of visually guided saccades or the number of early saccadic responses, the pupillary response could conform to an implicit "do not bet on the unknown" strategy [287]. When uncertainty is expected (SU_2, SU_3, SU_4 conditions) and no additional reward is granted for risking a fast response, then the oculomotor system (including pupil size control) could lean towards a cautious response strategy and increase oculomotor inhibition. Therefore, pupil dilation, saccadic V_{max}, and impulsive responses could be diminished.

However, Experiments 2 and 3 indicated that this effect of spatial uncertainty on the pupillary response was reduced by temporal variability between blocks of trials (blocked variable foreperiod in Experiment 2 and cued temporal uncertainty in Experiment 3; see the 'PUPIL' label in Fig. 5.1). It could be suggested that in these two experiments, the pupillary response was dominated by temporal uncertainty between blocks. This observation suggests an independence of the impact of the two sources of uncertainty on pupil size.

When it comes to time-related effects on the pupillary response, previous studies indicate that pupil size could reflect decision-making under changing temporal expectations [203, 296, 261, 395, 46]. Crucially, in variable foreperiod tasks, pupil dilation could occur earlier for temporally imminent stimuli [2].

In the current project, similar effects were observed for Experiments 2 and 3. In Experiment 2, a stronger dilation was observed in blocks with shorter FP durations. In Experiment 3, the pupil was more dilated if the shorter FP duration could occur in a given trial as indicated by the temporal cue. Observed pupil dilation, increasing more if the movement or decision were imminent, reinforces the proposed association between pupil size changes and ramping decision-making activity in DDM models [21]. The behaviour of the pupil also resembles the slope of 2^{nd} mode, anticipatory saccades, rising as the expected arrival time of the 'go' signal approaches. At the same time, Akdoğan et al. [2] did not find any trial-to-trial correlation between pupil dilation and response latency. In this project, the correlation between the occurrence of anticipatory saccades and pupillary response during the FP cannot be carried out. Early saccades are a source of noise in the pupil traces and were removed from the analysis. Future research could answer the question of whether anticipatory saccades and pupillary response could be commonly driven by the same mechanisms during the FP [388, 321].

To sum up, it could be suggested that, as observed for the saccadic V_{max}, the occurrence of the 'do not bet on the unknown' strategy in the pupillary response is not dependent on the type of uncertainty (spatial or temporal) but on the number of different sources of uncertainty presented in a given task.

5.1.6 Neuronal excitability increases for imminent decisions

The contingent negative variation ('CNV') has been proposed to reflect cognitive and/or motor preparation processes that precede the arrival of the 'go' signal. The CNV is often recorded from fronto-central scalp areas. Its source could be located in the SMA and/or the pre-SMA [83, 192]. Crucially, those structures neighbour other brain areas involved in oculomotor control [24].

Previous studies indicated that the amplitude of the CNV recorded during stimulus anticipation could be more negative when some aspects of the incoming stimulus are uncertain [124, 195]. Those results were interpreted in terms of attention allocation. Unpredictable stimuli could require more

attentional resources invested into their anticipation and processing. The extent of this attention allocation could be represented by a lower amplitude of the CNV (for review, see [248, 192]). At the same time, research on temporal processing indicated that more negative CNV could be evoked by durations repeatedly presented during the task [394, 34]. Furthermore, studies showed that the CNV signal was more negative for trials in which the foreperiod was generally shorter [209, 91, 34]. This could indicate that the CNV signal represents a form of cognitive or motor *readiness* to process an incoming stimulus [136, 84]. Consequently, the CNV signal could illustrate the optimisation of neuronal excitability that changes as FP elapses. According to this view, more negative CNV amplitudes would represent a stronger disinhibition of its source regions and therefore heightened excitability that facilitates the execution of movement [189].

The results obtained in Chapter 4 further support the above-mentioned hypothesis. During the foreperiod, the CNV over fronto-central, central, and centro-parietal electrodes presented a significantly more negative amplitude during U_{short} than U_{long} trials (see Fig. 4.4B). This indicates an increased neuronal excitability for short FPs, evoked by the anticipation of an imminent 'go' signal. Fast-approaching 'go' signal could 'push' the ramping CNV activity to reach a predetermined excitation threshold faster compared to trials with long FPs. This suggests that levels of neuronal excitability required to achieve optimal motor or perceptual readiness depend on FP duration.

The CNV activity in Experiment 4 resembled not only the assumptions of the ramping decision-making models but also the pupil-related observations of Akdoğan et al. [2]. CNV and pupillary signals appear to develop under the common rule: favouring the imminent 'go' signals, perhaps illustrating some aspects of temporal expectation. However, it must be stressed that in this project, the positive, trial-by-trial correlation between pupil size and the CNV in Experiment 4 was small ($p = 0.033$) and therefore requires stronger empirical evidence. Similarly to the pupillary traces, the CNV signal can also be artifacted by the occurrence of the early saccades during the foreperiod. For that reason, a direct correlation between the slope of the CNV and the rise

of the number of anticipatory saccades during the FP could not be conducted.

In a foreperiod task with [215] and without temporal cue [390], as well as in a random-dot motion task [42], the latency of response to a 'go' signal was correlated with the amplitude of the CNV. In both cases, a more negative amplitude of the slow component predicted shorter latencies. In contrast, Kóbor et al. [195] reported no significant correlations between key-press latency and CNV amplitude in a four-choice reaction time task. In his study, subjects were presented with predictable and unpredictable streams of targets. The results showed that the level of target predictability modulated CNV amplitude. Similarly, a detailed regression analysis was executed on the foreperiod go-no-go task [368]. Dissecting the sources of the latency variability in the task indicated that only a small part of the latency effects depended on the amplitude of the CNV.

Previous research suggests that the CNV signal illustrates the optimisation of neuronal excitability during anticipation. In Chapter 4, a trial-by-trial relationship between the CNV signal and the latency of VG saccades was found. The amplitude of the CNV increased together with the latency of visually guided saccades, but only for the U_{short} condition. This indicates that changes in neuronal excitability illustrated by the CNV are linked to the latency of visually guided saccades. However, this relationship could be observed only when the expected arrival time of the 'go' signal is imminent (U_{short} condition). When the overall duration of the FP was longer, this link could be delayed in time or not required at all. This result provides further evidence to existing suggestions that the relationship between the CNV and behavioural performance is not linear but reflects complex resource optimisation processes [57] (for review, see [189]). The absence of scientific consensus on the possible relationship between the CNV signal and behavioural responses highlights the need for more studies.

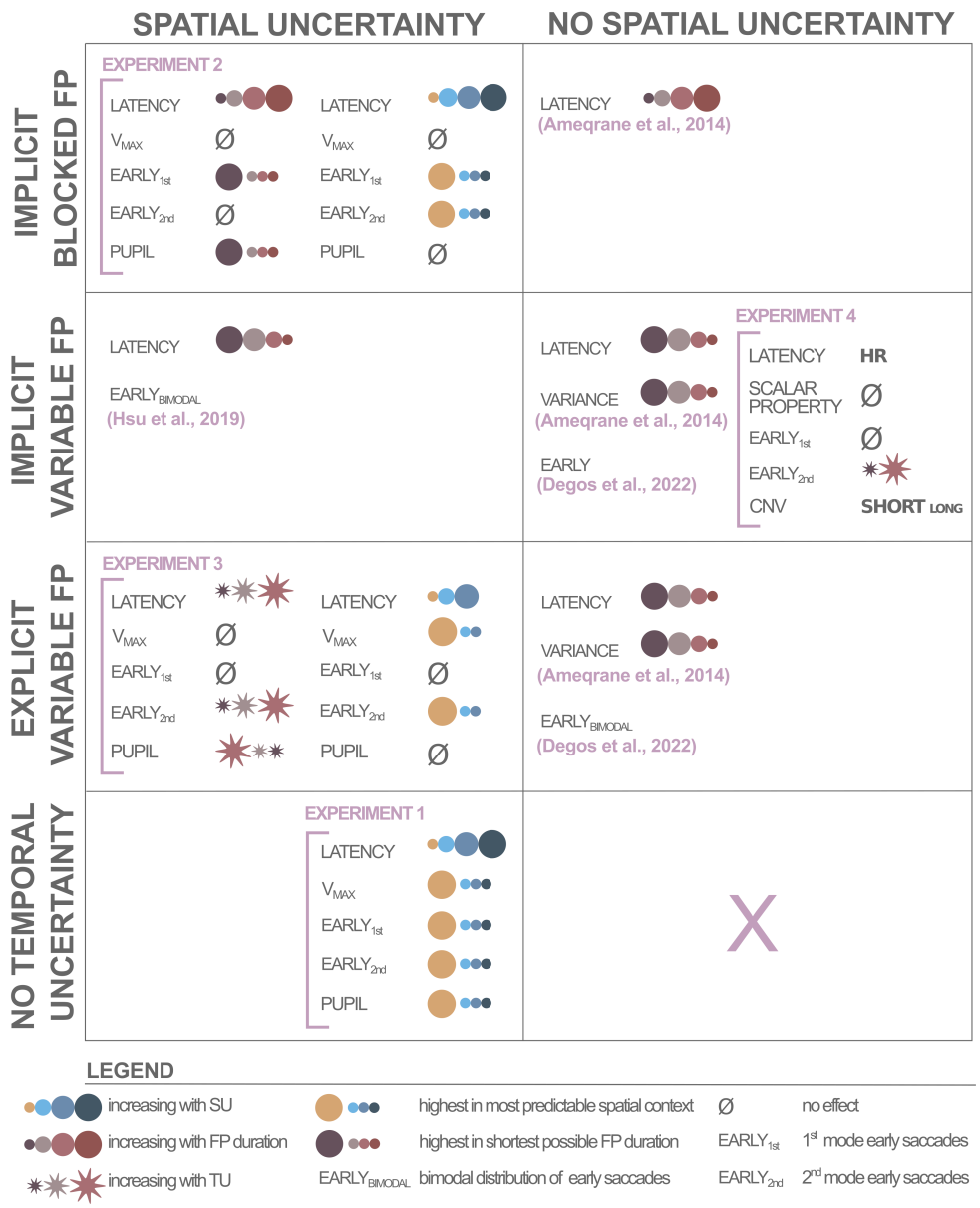

Fig. 5.1 Summary of current findings. In addition to previously published results [9, 166, 102], the table includes a summary of current findings. Results of each experiment are presented in a *column* based on the role of spatial uncertainty in the experimental design. *Rows* indicate the type of FP task used. *Coloured pictograms* are described in the legend. The summary includes effects related to the parameters of the VG saccades (latency, variance, V_{max}), the distribution of early saccades and the pupillary response.

5.1.7 Future directions - Impulsivity testing in health and disease

Differences between impulsive and anticipatory saccades could help to improve the diagnosis of impulsivity-related behaviours. Impulse control disorders ('ICD' [322]) can co-occur with diseases such as Parkinson's disease ('PD' [393, 119, 386, 271]), Major Depressive Disorder ('MDD' [166, 118, 77]), or dementia [316]. Those conditions are characterised by a non-definite list of behaviours resulting from impairments of cognitive inhibition: compulsive gambling, shopping, hypersexuality, and binge eating [118, 369]. Furthermore, purely motor signs of increased inhibition can be observed, e.g., akinesia, bradykinesia, tremor, and rigidity [256, 228].

However, PD can also be characterised by the occurrence of involuntary movements [333] and impaired decision-making was also demonstrated for those patients [288, 402]. At its core, PD of idiopathic ('iPD') or genetic origin [130, 7] is manifested by degeneration of midbrain dopaminergic cells [288]. However, the functional explanation of symptoms is complex. Results suggest that some motor problems related to the progress of PD could not be due to impairments in the execution of the movement but rather could be a result of altered motivation and motor inhibition [101, 180, 243]. Oculomotor responses (for the description of saccadic intrusions related to neurodegenerative diseases, see [281]) could serve as a valuable tool to uncover the impulsivity-related characteristics of the disease. Degos et al. [102] showed that in iPD patients, temporal uncertainty caused an increase in the probability of occurrence of impulsive saccade sequences, trial after trial. Furthermore, after introducing dopamine agonists, the number of impulsive saccades was decreased for the benefit of anticipatory ones. The authors suggest that the increased trial-by-trial probability of executing an impulsive saccade could be an oculomotor sign of impulsivity [102].

In the work of Hsu et al. [166], MDD patients executed twice the number of early saccades ($\sim$ 31%) compared to a healthy control group ($\sim$ 14%, [166]). Early saccades recorded from MDD patients had also shorter latencies. Those results further indicate that impairments of inhibitory control related

to diseases such as MDD can be detected by probing oculomotor behaviour. Future investigation of oculomotor response patterns could improve our understanding of the underlying mechanism of ICDs and their environmental triggers. Finally, further research could provide information about future behavioural therapies of ICDs.

At the same time, individuals can present non-dysfunctional manifestations of impulsivity related to personality. One can be described as impulsive if one tends to act without precaution or foresight, even without the ICD diagnosis [118, 89, 24]. The results presented in this project indicate that patterns of impulsive and anticipatory saccades can also be observed among healthy control groups. Therefore, the results of the current project not only provide a comparison for future research on ICD populations but can also inform the research on personality types.

Importantly, in this project, no correlation was found between the characteristics of oculomotor behaviour and the results of subjective impulsivity questionnaires (*Intolerance of Uncertainty* [62, 123]; *Barratt Impulsivity* [27, 286]; *Generalised Anxiety Disorder* [342]). Future research is necessary to determine whether behavioural testing could actually be better than questionnaires.

5.1.8 Conclusions

The current project illustrates several important characteristics of the oculomotor system under varying levels of spatial and temporal uncertainty. Firstly, the latency of visually guided saccades repeatedly increases with spatial uncertainty. The logarithmic relationship between saccade latency and spatial surprise illustrated by Hick's law is suppressed by introducing some form of implicit temporal uncertainty. However, no evidence was shown for an interaction effect of explicitly cued spatial and temporal uncertainties on oculomotor responses. Secondly, the oculomotor system likely represents the implicit trial-by-trial foreperiod variability as a hazard rate. However, unlike for manual response tasks, no scalar expectancy is presented for the visually guided saccadic movement. Next, saccadic velocity and pupil dilation in-

dicate that, under spatially uncertain conditions and without an additional reward, the system likely chooses an implicit "do not bet on the unknown" strategy of resource allocation. Crucially, this strategy is suppressed by introducing some form of temporal uncertainty in the task. While saccadic velocity does not directly reflect changes in foreperiod duration, the pupillary response selectively illustrates temporal expectation.

Early saccades observed before the 'go' signal had a bimodal distribution and contrasting characteristics. 1^{st} mode, occurring early into the FP, illustrated impulsive responses, sensitive to the fast-approaching arrival time of the 'go' signal. 2^{nd} mode, with a latency adjusted to temporal expectation, described cognitively driven, anticipatory saccades. Both modes were also influenced by the top-down inhibitory process deployed in spatially uncertain conditions.

Finally, the CNV observed over fronto-central, central and centro-parietal brain regions showed more negative amplitudes for fast-approaching 'go' signals. Those negative amplitudes, representing a strong disinhibition of the source regions, could illustrate a state of increased motor or perceptual readiness, higher for shorter foreperiods. This hypothesis was strengthened by the observed positive correlation between CNV amplitude and the latency of visually guided saccades.

The current doctoral project demonstrated that human oculomotor responses are sensitive to spatial and temporal uncertainty. The lack of an additional reward for fast responses made the behavioural tasks presented in this project similar to everyday situations. Performing a saccadic movement in everyday life is almost never promoted with a reward other than reduced visual uncertainty. In order to produce optimal and stable oculomotor performance, such as fast and precise saccadic responses, the available resources must be strategically allocated. Here, we demonstrated that the cautious strategy used by the oculomotor systems favours increased resource allocation only in predictable environments. On the other hand, spatially or temporally uncertain contexts could cause increased oculomotor inhibition.

6

Supplementary Materials

6.1 Chapter 2

Table S2.1 Model selection for statistical analyses in Experiment 1. BIC values derived from REML models.

Outcome	*Model*	*Formula*	BIC_{REML}
VG saccade latency	full.rs1	latency ~ SU + (1 | subject)	48787.51
	full.rs2	latency ~ SU + (1 + SU | subject)	DNC
VG saccade V_{max}	full.rs1	V_{max} ~ SU + (1 | subject)	50897.24
	full.rs2	V_{max} ~ SU + (1 + SU | subject)	DNC
pupil size	full.rs1	pupil size ~ SU + (1 | subject)	18841.85
	full.rs2	pupil size ~ SU + (1 + SU | subject)	DNC
1^{st} mode saccade count	full.rs1	count ~ SU + (1 | subject)	271.67
	full.rs2	count ~ SU + (1 + SU | subject)	305.94
2^{nd} mode saccade count	full.rs1	count ~ SU + (1 | subject)	354.90
	full.rs2	count ~ SU + (1 + SU | subject)	DNC

DNC model did not converge.

Table S2.2 Model selection for statistical analyses in Experiment 2. BIC values derived from REML models.

Outcome	*Model*	*Formula*	BIC_{REML}
VG saccade latency	full.rs1	latency ~ SU * FP + (1 | subject)	78333.95
	full.rs2	latency ~ SU * FP + (1 + SU | subject)	DNC
	full.rs3	latency ~ SU * FP + (1 + FP | subject)	77864.13
	full.rs4	latency ~ SU * FP + (1 + SU * FP | subject)	DNC
VG saccade V_{max}	full.rs1	V_{max} ~ SU * FP + (1 | subject)	86012.16
	full.rs2	V_{max} ~ SU * FP + (1 + SU | subject)	DNC
	full.rs3	V_{max} ~ SU * FP + (1 + FP | subject)	85891.74
	full.rs4	V_{max} ~ SU * FP + (1 + FP | subject)	DNC
pupil size	full.rs1	pupil size ~ FP + (1 | subject)	5367.88
	full.rs2	pupil size ~ FP + (1 + FP | subject)	DNC

DNC model did not converge.

Table S2.3 The influence of spatial uncertainty and FP duration on the latency of VG saccades. REML-calculated LMM model statistics calculated using Type III ANOVA. BIC values derived from ML models.

Model	BIC_{ML}	*Fixed terms*	df	*F value*	*p value*	*Random terms σ*	
						subject	*resid*
full.rs3	78231.44	SU	3, 7495.04	40.94	$< 2.22 \times 10^{-16}$	27.26	42.28
		FP	1, 23.56	24.85	4.54×10^{-5}		
		SU * FP	3, 7501.65	0.72	0.540		
SU.rs3	78215.52	SU	3, 7497.43	40.95	$< 2.22 \times 10^{-16}$	27.47	42.28
FP.rs3	78301.86	FP	1, 23.52	24.88	4.51×10^{-5}	26.97	42.62

df degrees of freedom, *resid* residual, σ SD of the random terms.

Table S2.4 The influence of spatial uncertainty and FP duration on the V_{max} of VG saccades. REML-calculated LMM model statistics calculated using Type III ANOVA. BIC values derived from ML models.

Model	BIC_{ML}	*Fixed terms*	df	*F value*	*p value*	*Random terms σ*	
						subject	*resid*
full.rs3	86003.55	SU	3, 7671.92	3.19	0.025	84.22	62.30
		FP	1, 24.07	5.70	0.023		
		SU * FP	3, 7660.74	0.21	0.890		
SU.rs3	85973.78	SU	3, 7673.47	3.16	0.024	84.19	62.29
FP.rs3	85960.02	FP	1, 23.94	5.60	0.026	84.05	62.31

df degrees of freedom, *resid* residual, σ SD of the random terms.

Table S2.5 The log-likelihood of the mixture models fitted to the distribution of early saccades in Experiment 2.

FP duration	*Log-Likelihood*			
	mix.2	mix.3	mix.4	mix.5
400 ms	-1020.63	-1011.12	-1009.66	-1008.95
900 ms	-938.54	-926.68	-927.72	-923.98
1400 ms	-786.50	-775.42	-776.85	-782.52
1900 ms	-794.67	-785.71	-784.53	-776.54

Table S2.6 Model selection for statistical analyses in Experiment 2. BIC values derived from REML models.

Outcome	*Model*	*Formula*	BIC_{REML}
early saccade latency	full.rs1	latency ~ mode * FP + (1 | subject)	14203.47
	full.rs2	latency ~ mode * FP + (1 + mode | subject)	DNC
	full.rs3	latency ~ mode * FP + (1 + FP | subject)	DNC
	full.rs4	latency ~ mode * FP + (1 + mode * FP | subject)	DNC
early saccade count	full.rs1	count ~ mode * FP + (1 | subject)	1001.016
	full.rs2	count ~ mode * FP + (1 + mode | subject)	977.50
	full.rs3	count ~ mode * FP + (1 + FP | subject)	980.48
	full.rs4	count ~ mode * FP + (1 + mode * FP | subject)	959.95
early saccade V_{max}	full.rs1	V_{max} ~ mode * FP + (1 | subject)	12708.44
	full.rs2	V_{max} ~ mode * FP + (1 + mode | subject)	DNC
	full.rs3	V_{max} ~ mode * FP + (1 + FP | subject)	DNC
	full.rs4	V_{max} ~ mode * FP + (1 + mode * FP | subject)	DNC
early saccade amplitude	full.rs1	amp ~ mode * FP + (1 | subject)	5088.86
	full.rs2	amp ~ mode * FP + (1 + mode | subject)	DNC
	full.rs3	amp ~ mode * FP + (1 + FP | subject)	5101.63
	full.rs4	amp ~ mode * FP + (1 + mode * FP | subject)	DNC
early saccade count	full.rs1	count ~ mode * SU + (1 | subject)	940.13
	full.rs2	count ~ mode * SU + (1 + mode | subject)	909.53
	full.rs3	count ~ mode * SU + (1 + SU | subject)	DNC
	full.rs4	count ~ mode * SU + (1 + mode * SU | subject)	DNC
early saccade V_{max}	full.rs1	V_{max} ~ mode * SU + (1 | subject)	12671.65
	full.rs2	V_{max} ~ mode * SU + (1 + mode | subject)	DNC
	full.rs3	V_{max} ~ mode * SU + (1 + SU | subject)	DNC
	full.rs4	V_{max} ~ mode * SU + (1 + mode * SU | subject)	DNC
early saccade amplitude	full.rs1	amp ~ mode * SU + (1 | subject)	5005.44
	full.rs2	amp ~ mode * SU + (1 + mode | subject)	5012.19
	full.rs3	amp ~ mode * SU + (1 + SU | subject)	5050.36
	full.rs4	amp ~ mode * SU + (1 + mode * SU | subject)	DNC

DNC model did not converge.

Table S2.7 The influence of FP duration and mode on the latency of early saccades in Experiment 2. REML-calculated LMM model statistics calculated using Type III ANOVA. BIC values derived from ML models.

Model	BIC_{ML}	*Fixed terms*	df	*F value*	*p value*	*Random terms σ*	
						subject	*resid*
full.rs1	14203.47	mode	1, 1031.33	0.02	0.009	70.77	227.43
		FP	1, 1032.00	424.41	$< 2.22 \times 10^{-16}$		
		mode * FP	1, 1031.98	366.27	$< 2.22 \times 10^{-16}$		
mode.rs1	15027.27	mode	1, 1031.70	913.06	$< 2.22 \times 10^{-16}$	93.23	341.94
FP.rs1	15018.98	FP	1, 1028.09	926.99	$< 2.22 \times 10^{-16}$	136.97	338.44

df degrees of freedom, *resid* residual, σ SD of the random terms.

Table S2.8 The influence of FP duration and mode on the latency of early saccades in Experiment 2. REML-calculated LMM model statistics calculated using Type III ANOVA. BIC values derived from ML models.

Fixed terms	*df*	*F value*	*p value*
mode	1	24.41	2.99×10^{-6}
FP	1	57.47	1.50×10^{-11}
mode * FP	1	34.68	4.82×10^{-8}

df degrees of freedom.

Table S2.9 The influence of FP duration and mode on the number of early saccades in Experiment 2. ML-calculated GLMM model statistics calculated using the Type III Wald χ^2 test.

Model	BIC_{ML}	*Fixed terms*	df	χ^2	*p value*	*Random terms σ*
						subject
full.rs4	959.95	mode	1	1.19	0.276	0.57
		FP	1	1.15	0.284	
		mode * FP	1	11.67	6.34×10^{-4}	
mode.rs4	959.39	mode	1	0.47	0.493	0.52
FP.rs4	959.47	FP	1	0.39	0.535	0.51

df degrees of freedom, σ SD of the random terms.

Table S2.10 The influence of FP duration and mode on the V_{max} of early saccades in Experiment 2. REML-calculated LMM model statistics calculated using Type III ANOVA. BIC values derived from ML models.

Model	BIC_{ML}	*Fixed terms*	df	*F value*	*p value*	*Random terms σ*	
						subject	*resid*
full.rs1	12707.33	mode	1, 1013.80	14.56	1.44×10^{-4}	94.63	108.23
		FP	1, 1014.83	0.04	0.850		
		mode * FP	1, 1015.91	6.94	0.009		
mode.rs1	12701.23	mode	1, 1015.27	8.04	0.005	95.05	108.53
FP.rs1	12709.20	FP	1, 1015.58	0.06	0.811	95.98	108.93

df degrees of freedom, *resid* residual, σ SD of the random terms.

Table S2.11 The influence of FP duration and mode on the amplitude of early saccades in Experiment 2. REML-calculated LMM model statistics calculated using Type III ANOVA. BIC values derived from ML models.

Model	BIC_{ML}	*Fixed terms*	df	*F value*	*p value*	*Random terms σ*	
						subject	*resid*
full.rs1	5088.86	mode	1, 1012.85	16.79	0.038	2.13	2.71
		FP	1, 1014.36	4.33	4.51×10^{-5}		
		mode * FP	1, 1015.64	2.54	0.112		
mode.rs1	5086.17	mode	1, 1013.92	18.94	1.48×10^{-5}	2.20	2.72
FP.rs1	5103.88	FP	1, 1014.67	1.06	0.303	2.18	2.74

df degrees of freedom, *resid* residual, σ SD of the random terms.

Table S2.12 The influence of spatial uncertainty and mode on the number of early saccades in Experiment 2. ML-calculated GLMM model statistics calculated using the Type III Wald χ^2 test.

Model	BIC_{ML}	*Fixed terms*	df	χ^2	*p value*	*Random terms σ*
						subject
full.rs2	909.53	mode	1	5.14	0.023	0.82
		SU	3	434.22	$< 2.22 \times 10^{-16}$	
		mode * SU	3	2.47	0.480	
mode.rs2	1318.63	mode	1	3.96	0.047	0.69
SU.rs2	896.32	SU	3	435.44	$< 2.22 \times 10^{-16}$	0.77

df degrees of freedom, σ SD of the random terms.

Table S2.13 The influence of spatial uncertainty and mode on the V_{max} of early saccades in Experiment 2. REML-calculated LMM model statistics calculated using Type III ANOVA. BIC values derived from ML models.

Model	BIC_{ML}	*Fixed terms*	df	*F value*	*p value*	*Random terms σ*	
						subject	*resid*
full.rs1	12726.09	mode	1, 1010.95	10.86	0.001	93.07	108.00
		SU	3, 1010.17	3.33	0.019		
		mode * SU	3, 1006.85	1.78	0.150		
mode.rs1	12701.23	mode	1, 1015.27	8.04	0.005	95.05	108.53
SU.rs1	12712.86	SU	3, 1014.36	3.42	0.017	93.89	108.55

df degrees of freedom, *resid* residual, σ SD of the random terms.

Table S2.14 The influence of spatial uncertainty and mode on the amplitude of early saccades in Experiment 2. REML-calculated LMM model statistics calculated using Type III ANOVA. BIC values derived from ML models.

Model	BIC_{ML}	*Fixed terms*	df	*F value*	*p value*	*Random terms σ*	
						subject	*resid*
full.rs1	5005.44	mode	1, 1011.79	31.45	2.64×10^{-8}	1.87	2.57
		SU	3, 1010.35	40.65	$< 2.22 \times 10^{-16}$		
		mode * SU	3, 1005.59	1.80	0.147		
mode.rs1	5086.17	mode	1, 1013.92	18.94	1.48×10^{-5}	2.20	2.72
SU.rs1	5011.11	SU	3, 1015.08	37.81	$< 2.22 \times 10^{-16}$	1.87	2.61

df degrees of freedom, *resid* residual, σ SD of the random terms.

6.2 Chapter 3

Table S3.1 Model selection for statistical analyses in Experiment 3. BIC values derived from REML models.

Outcome	*Model*	*Formula*	BIC_{REML}
VG saccade latency	full.rs1	latency ~ SU * TU + (1 | subject)	-472.28
	full.rs2	latency ~ SU * TU + (1 + SU | subject)	DNC
	full.rs3	latency ~ SU * TU + (1 + TU | subject)	DNC
	full.rs4	latency ~ SU * TU + (1 + SU * TU | subject)	DNC
VG saccade V_{max}	full.rs1	V_{max} ~ SU * TU + (1 | subject)	46567.91
	full.rs2	V_{max} ~ SU * TU + (1 + SU | subject)	DNC
	full.rs3	V_{max} ~ SU * TU + (1 + TU | subject)	DNC
	full.rs4	V_{max} ~ SU * TU + (1 + SU * TU | subject)	DNC
pupil size	full.rs1	pupil size ~ SU + (1 | subject)	10238.40
	full.rs2	pupil size ~ SU + (1 + SU | subject)	DNC
pupil size	full.rs1	pupil size ~ TU + (1 | subject)	10221.74
	full.rs2	pupil size ~ TU + (1 + TU | subject)	10257.33
1^{st} mode saccade count	full.rs1	count ~ SU * TU + (1 | subject)	510.36
	full.rs2	count ~ SU * TU + (1 + SU | subject)	536.93
	full.rs3	count ~ SU * TU + (1 + TU | subject)	531.75
	full.rs4	count ~ SU * TU + (1 + SU * TU | subject)	DNC
2^{nd} mode saccade count	full.rs1	count ~ SU * TU + (1 | subject)	1037.05
	full.rs2	count ~ SU * TU + (1 + SU | subject)	1054.09
	full.rs3	count ~ SU * TU + (1 + TU | subject)	1063.37
	full.rs4	count ~ SU * TU + (1 + SU * TU | subject)	DNC

DNC model did not converge.

Table S3.2 The influence of spatial and temporal uncertainty on the latency of VG saccades in Experiment 3. REML-calculated LMM model statistics calculated using Type III ANOVA. BIC values derived from ML models.

Model	BIC_{ML}	*Fixed terms*	df	*F value*	*p value*	*Random terms σ*	
						subject	*resid*
full.rs1	-541.45	SU	2, 4155.10	89.69	$< 2.2 \times 10^{-16}$	0.09	0.22
		TU	2, 4154.43	74.20	$< 2.2 \times 10^{-16}$		
		SU * TU	4, 4154.10	0.32	0.865		
SU.rs1	-444.01	SU	2, 4161.13	87.26	$< 2.2 \times 10^{-16}$	0.09	0.23
FP.rs1	-414.60	TU	2, 4160.54	71.97	$< 2.2 \times 10^{-16}$	0.09	0.23

df degrees of freedom, *resid* residual, σ SD of the random terms.

Table S3.3 The influence of spatial and temporal uncertainty on the V_{max} of VG saccades in Experiment 3. REML-calculated LMM model statistics calculated using Type III ANOVA. BIC values derived from ML models.

Model	BIC_{ML}	*Fixed terms*	df	*F value*	*p value*	*Random terms σ*	
						subject	*resid*
full.rs1	46602.94	SU	2, 4087.54	15.65	1.70×10^{-7}	55.49	66.92
		TU	2, 4087.37	0.74	0.478		
		SU * TU	4, 4087.26	0.91	0.458		
SU.rs1	46558.18	SU	2, 4093.53	15.72	1.59×10^{-7}	55.46	66.91
FP.rs1	46588.03	TU	2, 4093.38	0.74	0.479	55.37	67.16

df degrees of freedom, *resid* residual, σ SD of the random terms.

Table S3.4 The log-likelihood of the mixture models fitted to the distribution of early saccades in Experiment 3.

Temporal uncertainty	*Log-Likelihood*			
	mix.2	mix.3	mix.4	mix.5
TU_1	-1255.36	-1240.35	-1236.66	-1234.01
TU_2	-1360.69	-1362.36	-1354.88	-1359.19
TU_3	-1511.71	-1477.73	-1474.71	-1474.11

Table S3.5 The influence of spatial and temporal uncertainty on the number of 1^{st} mode saccades in Experiment 3. ML-calculated GLMM model statistics calculated using the Type III Wald χ^2 test.

Model	BIC_{ML}	*Fixed terms*	df	χ^2	*p value*	*Random terms* σ
						subject
full.rs1	510.36	SU	2	1.55	0.460	1.28
		TU	2	4.99	0.083	
		SU * TU	4	1.89	0.756	
SU.rs1	485.03	SU	2	1.45	0.484	1.28
TU.rs1	481.54	TU	2	4.95	0.084	1.28

df degrees of freedom, σ SD of the random terms.

Table S3.6 The influence of spatial and temporal uncertainty on the number of 2^{nd} mode saccades in Experiment 3. ML-calculated GLMM model statistics calculated using the Type III Wald χ^2 test.

Model	BIC_{ML}	*Fixed terms*	df	χ^2	*p value*	*Random terms σ* *subject*
full.rs1	1037.05	SU	2	30.86	1.99×10^{-7}	0.92
		TU	2	9.98	0.007	
		SU * TU	4	0.13	0.998	
SU.rs1	1013.95	SU	2	30.90	1.95×10^{-7}	0.92
TU.rs1	1034.41	TU	2	9.98	0.007	0.92

df degrees of freedom, σ SD of the random terms.

6.3 Chapter 4

Table S4.1 Model selection for statistical analyses in Experiment 4. BIC values derived from REML models.

Variable	*Model*	*Formula*	BIC_{REML}	
			U_{short}	U_{long}
FP_n	full.rs1	latency $\sim FP_n$ + (1 | subject)	29952.28	30989.44
	full.rs2	latency $\sim FP_n$ + (1 + FP_n | subject)	DNC	DNC
HR_{rec}	full.rs1	latency $\sim HR_{rec}$ + (1 | subject)	29952.58	30986.09
	full.rs2	latency $\sim HR_{rec}$ + (1 + HR_{rec} | subject)	29961.90	DNC
FP_{n-1}	full.rs1	latency $\sim FP_{n-1}$ + (1 | subject)	29993.69	30998.53
	full.rs2	latency $\sim FP_{n-1}$ + (1 + FP_{n-1} | subject)	DNC	DNC
seq	full.rs1	latency $\sim$ seq + (1 | subject)	29970.18	30989.88
	full.rs2	latency $\sim$ seq + (1 + seq | subject)	DNC	DNC

DNC model did not converge, *seq* sequence.

Table S4.2 Model selection for statistical analyses of distribution effects on early saccades in Experiment 4. BIC values derived from REML models.

Outcome	*Model*	*Formula*	BIC_{REML}
1^{st} mode saccade count in short anchor	full.rs1	count $\sim$ dist + (1 | subject)	344.03
	full.rs2	count $\sim$ dist + (1 + dist | subject)	DNC
1^{st} mode saccade count in long anchor	full.rs1	count $\sim$ dist + (1 | subject)	373.53
	full.rs2	count $\sim$ dist + (1 + dist | subject)	DNC
2^{nd} mode saccade count in short anchor	full.rs1	count $\sim$ dist + (1 | subject)	562.01
	full.rs2	count $\sim$ dist + (1 + dist | subject)	DNC
2^{nd} mode saccade count in long anchor	full.rs1	count $\sim$ dist + (1 | subject)	484.07
	full.rs2	count $\sim$ dist + (1 + dist | subject)	DNC

dist distribution, *DNC* model did not converge.

Table S4.3 Model selection for statistical analyses of anchor effects on early saccades in Experiment 4. BIC values derived from REML models.

Outcome	*Model*	*Formula*	BIC_{REML}
VG saccade latency	full.rs1	latency ~ amp * anchor + (1 | subject)	52003.10
	full.rs2	latency ~ amp * anchor + (1 + amp | subject)	DNC
	full.rs3	latency ~ amp * anchor + (1 + anchor | subject)	51960.50
	full.rs4	latency ~ amp * anchor + (1 + amp * anchor | subject)	DNC
pupil size	full.rs1	pupil size ~ amp * anchor + (1 | subject)	19413.32
	full.rs2	pupil size ~ amp * anchor + (1 + amp | subject)	19420.90
	full.rs3	pupil size ~ amp * anchor + (1 + anchor | subject)	19428.48
	full.rs4	pupil size ~ amp * anchor + (1 + amp * anchor | subject)	DNC

amp amplitude of the CNV, *dist* distribution, *DNC* model did not converge.

Table S4.4 The influence of CNV amplitude and anchor on the VG saccade latency in Experiment 4. REML-calculated LMM model statistics calculated using Type III ANOVA. BIC values derived from ML models.

Model	BIC_{ML}	*Fixed terms*	df	*F value*	*p value*	*Random terms σ*	
						subject	*resid*
full.rs3	51968.19	amp	1, 4785.90	16.88	4.06×10^{-5}	29.50	51.30
		anchor	1, 38.74	10.44	0.003		
		amp * anchor	1, 4786.09	6.77	0.009		
anchor.rs3	51974.43	anchor	1, 36.43	15.16	4.05×10^{-4}	29.55	51.42
amp.rs3	51969.43	amp	1, 4793.54	17.57	2.82×10^{-5}	29.51	51.34

amp amplitude of the CNV, *df* degrees of freedom, *dist* distribution, *resid* residual, σ SD of the random terms.

Table S4.5 The influence of CNV amplitude and anchor on pupil size in Experiment 4. REML-calculated LMM model statistics calculated using Type III ANOVA. BIC values derived from ML models.

Model	BIC_{ML}	*Fixed terms*	df	*F value*	*p value*	*Random terms σ*	
						subject	*resid*
full.rs1	19385.37	amp	1, 6584.10	5.25	0.022	0.21	1.04
		anchor	1, 6556.10	2.01	0.156		
		amp * anchor	1, 6562.91	0.54	0.461		
anchor.rs1	19373.64	anchor	1, 6554.93	2.11	0.146	0.20	1.04
amp.rs1	19371.22	amp	1, 6583.91	4.53	0.033	0.21	1.04

amp amplitude of the CNV, *df* degrees of freedom, *dist* distribution, *resid* residual, σ SD of the random terms.

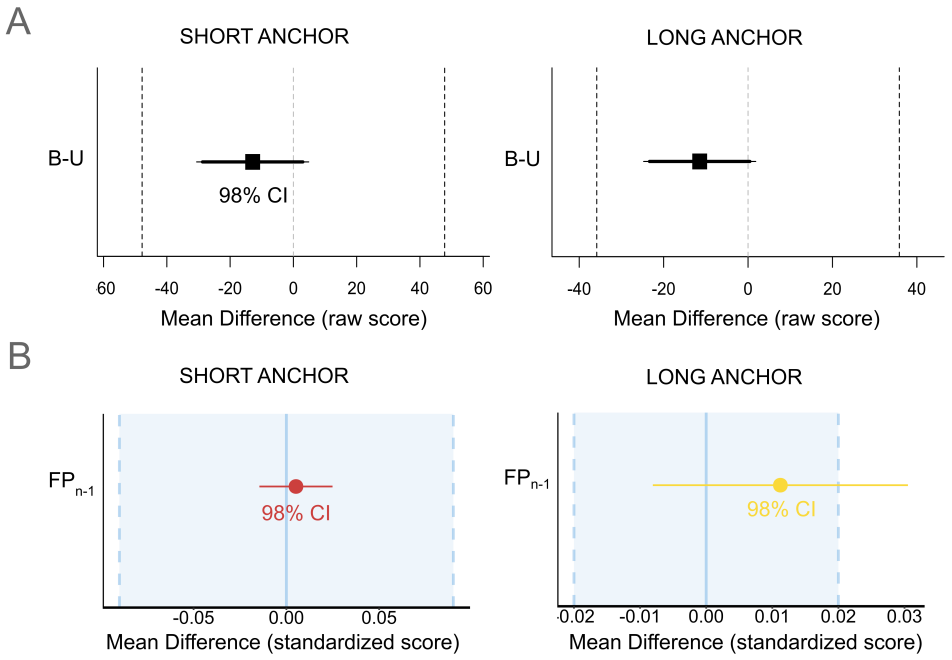

Fig. S4.1 Results of the equivalence test in Experiment 4. (A) Equivalence test results for the SD of VG saccade latency. A *black square* shows mean difference (B - U) in raw scores with 98% CI (*black horizontal line*). **(B)** Equivalence test results for the FP_{n-1} effects on the VG saccade latency. *Coloured dot* shows the mean effect size in standardised scores with 98% CI (*horizontal coloured line*).

Bibliography

[1] Abeles, D., Amit, R., Tal-Perry, N., Carrasco, M., and Yuval-Greenberg, S. (2020). Oculomotor inhibition precedes temporally expected auditory targets. *Nat Commun*, 11(1):3524.

[2] Akdoğan, B., Balcı, F., and Van Rijn, H. (2016). Temporal Expectation Indexed by Pupillary Response. *Timing Time Percept*, 4(4):354–370.

[3] Akkal, D., Escola, L., Bioulac, B., and Burbaud, P. (2004). Time predictability modulates pre-supplementary motor area neuronal activity:. *NeuroReport*, 15(8):1283–1286.

[4] Alamia, A., VanRullen, R., Pasqualotto, E., Mouraux, A., and Zenon, A. (2019). Pupil-Linked Arousal Responds to Unconscious Surprisal. *J. Neurosci.*, 39(27):5369–5376.

[5] Albares, M., Lio, G., Criaud, M., Anton, J., Desmurget, M., and Boulinguez, P. (2014). The dorsal medial frontal cortex mediates automatic motor inhibition in uncertain contexts: Evidence from combined fMRI and EEG studies. *Human Brain Mapping*, 35(11):5517–5531.

[6] Albert, J., López-Martín, S., Hinojosa, J. A., and Carretié, L. (2013). Spatiotemporal characterization of response inhibition. *NeuroImage*, 76:272–281.

[7] Alcalay, R. N., Caccappolo, E., Mejia-Santana, H., Tang, M. X., Rosado, L., Orbe Reilly, M., Ruiz, D., Louis, E. D., Comella, C. L., Nance, M. A., Bressman, S. B., Scott, W. K., Tanner, C. M., Mickel, S. F., Waters, C. H., Fahn, S., Cote, L. J., Frucht, S. J., Ford, B., Rezak, M., Novak, K. E., Friedman, J. H., Pfeiffer, R. F., Marsh, L., Hiner, B., Payami, H., Molho, E., Factor, S. A., Nutt, J. G., Serrano, C., Arroyo, M., Ottman, R., Pauciulo, M. W., Nichols, W. C., Clark, L. N., and Marder, K. S. (2014). Cognitive and Motor Function in Long-Duration *PARKIN* -Associated Parkinson Disease. *JAMA Neurol*, 71(1):62.

[8] Allman, M. J., Teki, S., Griffiths, T. D., and Meck, W. H. (2014). Properties of the Internal Clock: First- and Second-Order Principles of Subjective Time. *Annu. Rev. Psychol.*, 65(1):743–771.

[9] Ameqrane, I., Pouget, P., Wattiez, N., Carpenter, R., and Missal, M. (2014). Implicit and Explicit Timing in Oculomotor Control. *PLoS ONE*, 9(4):e93958.

[10] Ameqrane, I., Wattiez, N., Pouget, P., and Missal, M. (2015). A subanesthetic dose of ketamine in the Rhesus monkey reduces the occurrence of anticipatory saccades. *Psychopharmacology*, 232(19):3563–3572.

[11] Amit, R., Dekel, A., Carrasco, M., and Yuval-Greenberg, S. (2019). Oculomotor inhibition reflects temporal expectations. *NeuroImage*, 184:279–292.

[12] Aron, A. R., Behrens, T. E., Smith, S., Frank, M. J., and Poldrack, R. A. (2007). Triangulating a Cognitive Control Network Using Diffusion-Weighted Magnetic Resonance Imaging (MRI) and Functional MRI. *J. Neurosci.*, 27(14):3743–3752.

[13] Aron, A. R. and Poldrack, R. A. (2006). Cortical and Subcortical Contributions to Stop Signal Response Inhibition: Role of the Subthalamic Nucleus. *J. Neurosci.*, 26(9):2424–2433.

[14] Ashton, M. C. (2013). 5 Biological Bases of Personality. In Ashton, M. C., editor, *Individual Differences and Personality*, pages 101–121. Elsevier.

[15] Aston-Jones, G. and Cohen, J. D. (2005). An integrative theory of locus coeruleus-norepinephrine function: adaptive gain and optimal performance. *Annu. Rev. Neurosci.*, 28(1):403–450.

[16] Bach, D. R. and Dolan, R. J. (2012). Knowing how much you don't know: a neural organization of uncertainty estimates. *Nat Rev Neurosci*, 13:572–586.

[17] Bachurina, V. and Arsalidou, M. (2022). Multiple levels of mental attentional demand modulate peak saccade velocity and blink rate. *Heliyon*, 8(1):e08826.

[18] Badde, S. (2020). Oculomotor freezing reflects tactile temporal expectation and aids tactile perception. *Nature Communications*, 11:3341.

[19] Bahill, A. T., Clark, M. R., and Stark, L. (1975). The main sequence, a tool for studying human eye movements. *Mathematical Biosciences*, 24(3-4):191–204.

[20] Baker, C. I., Olson, C. R., and Behrmann, M. (2004). Role of Attention and Perceptual Grouping in Visual Statistical Learning. *Psychol Sci*, 15(7):460–466.

[21] Balcı, F. and Simen, P. (2016). A decision model of timing. *Current Opinion in Behavioral Sciences*, 8:94–101.

[22] Baldauf, D. and Deubel, H. (2009). Attentional Selection of Multiple Goal Positions Before Rapid Hand Movement Sequences: An Event-related Potential Study. *Journal of Cognitive Neuroscience*, 21(1):18–29.

[23] Barbot, A. and Carrasco, M. (2017). Attention Modifies Spatial Resolution According to Task Demands. *Psychol Sci*, 28(3):285–296.

[24] Bari, A. and Robbins, T. W. (2013). Inhibition and impulsivity: Behavioral and neural basis of response control. *Progress in Neurobiology*, 108:44–79.

[25] Barnes, R. and Jones, M. R. (2000). Expectancy, Attention, and Time. *Cognitive Psychology*, 41(3):254–311.

[26] Barr, D. J., Levy, R., Scheepers, C., and Tily, H. J. (2013). Random effects structure for confirmatory hypothesis testing: Keep it maximal. *Journal of Memory and Language*, 68(3):255–278.

[27] Barratt, E. S. (1965). Factor Analysis of Some Psychometric Measures of Impulsiveness and Anxiety. *Psychol Rep*, 16(2):547–554.

[28] Basso, M. A. and May, P. J. (2017). Circuits for Action and Cognition: A View from the Superior Colliculus. *Annu. Rev. Vis. Sci.*, 3(1):197–226.

[29] Basso, M. A. and Wurtz, R. H. (1997). Modulation of neuronal activity by target uncertainty. *Nature*, 389(6646):66–69.

[30] Bates, D., Mächler, M., Bolker, B., and Walker, S. (2015). Fitting Linear Mixed-Effects Models Using lme4. *J. Stat. Soft.*, 67(1):1–48.

[31] Bates, D. and Maechler, M. and Bolker, B. and Walker, S. (2025). lme4. *[manual]*.

[32] Batterink, L. J., Paller, K. A., and Reber, P. J. (2019). Understanding the Neural Bases of Implicit and Statistical Learning. *Topics in Cognitive Science*, 11(3):482–503.

[33] Bausenhart, K. M., Rolke, B., and Ulrich, R. (2008). Temporal preparation improves temporal resolution: Evidence from constant foreperiods. *Perception & Psychophysics*, 70(8):1504–1514.

[34] Baykan, C., Zhu, X., Zinchenko, A., and Shi, Z. (2024). Blocked versus interleaved: How range contexts modulate time perception and its EEG signatures. *Psychophysiology*, 61(8):e14585.

[35] Becker, J., Viertler, M., Korn, C. W., and Blank, H. (2024). The pupil dilation response as an indicator of visual cue uncertainty and auditory outcome surprise. *Eur J of Neuroscience*, 59(10):2686–2701.

[36] Beierholm, U., Guitart-Masip, M., Economides, M., Chowdhury, R., Düzel, E., Dolan, R., and Dayan, P. (2013). Dopamine Modulates Reward-Related Vigor. *Neuropsychopharmacol*, 38(8):1495–1503.

[37] Benaglia, T., Chauveau, D., Hunter, D., and Young, D. (2009). mixtools: An r package for analyzing finite mixture models. *Journal of Statistical Software*, 32(6):1–29.

[38] Benaglia, T. and Chauveau, D. and Hunter, D.R. and Young, D. (2022). mixtools: An r package for analyzing finite mixture models. *[manual]*.

[39] Bisley, J. W. and Goldberg, M. E. (2010). Attention, Intention, and Priority in the Parietal Lobe. *Annu. Rev. Neurosci.*, 33(1):1–21.

[40] Bizo, L. A., Chu, J. Y. M., Sanabria, F., and Killeen, P. R. (2006). The failure of Weber's law in time perception and production. *Behavioural Processes*, 71(2-3):201–210.

[41] Bode, S., Bennett, D., Sewell, D. K., Paton, B., Egan, G. F., Smith, P. L., and Murawski, C. (2018). Dissociating neural variability related to stimulus quality and response times in perceptual decision-making. *Neuropsychologia*, 111:190–200.

[42] Boehm, U., van Maanen, L., Forstmann, B., and van Rijn, H. (2014). Trial-by-trial fluctuations in CNV amplitude reflect anticipatory adjustment of response caution. *NeuroImage*, 96:95–105.

[43] Bolker, B. M., Brooks, M. E., Clark, C. J., Geange, S. W., Poulsen, J. R., Stevens, M. H. H., and White, J.-S. S. (2009). Generalized linear mixed models: a practical guide for ecology and evolution. *Trends in Ecology & Evolution*, 24(3):127–135.

[44] Bostan, A. C. and Strick, P. L. (2018). The basal ganglia and the cerebellum: nodes in an integrated network. *Nat Rev Neurosci*, 19(6):338–350.

[45] Boutachkourt, A., Drążyk, D., and Missal, M. (2024). Gazing into spatiotemporal 'known unknowns': the influence of uncertainty on pupil size and saccadic eye movements. *Sci Rep*, 14(1):17509.

[46] Bradshaw, J. (1968). Pupillary changes and reaction time with varied stimulus uncertainty. *Psychonomic Science*, 13(2):69–17.

[47] Braver, T. S. (2012). The variable nature of cognitive control: a dual mechanisms framework. *Trends in Cognitive Sciences*, 16(2):106–113.

[48] Brenner, J. M., Beltramo, R., Gerfen, C. R., Ruediger, S., and Scanziani, M. (2023). A genetically defined tecto-thalamic pathway drives a system of superior-colliculus-dependent visual cortices. *Neuron*, 111(14):2247–2257.e7.

[49] Breton-Provencher, V., Drummond, G. T., Feng, J., Li, Y., and Sur, M. (2022). Spatiotemporal dynamics of noradrenaline during learned behaviour. *Nature*, 606(7915):732–738.

[50] Brooks, M. E., Kristensen, K., van Benthem, K., Magnusson, A., Berg, C., Nielsen, A., Skaug, H., Maechler, M., and Bolker, B. (2017). glmmtmb balances speed and flexibility among packages for zero-inflated generalized linear mixed modeling. *The R Journal*, 9(2):378–400.

[51] Brooks, M. E. and Kristensen, K. and van Benthem, K.J. and Magnusson, A. and Berg, C.W. and Nielsen, A. and Skaug, H.J. and Maechler, M. and Bolker, B.M. (2024). glmmtmb balances speed and flexibility among packages for zero-inflated generalized linear mixed modeling. *[manual]*.

[52] Brunyé, T. T. and Gardony, A. L. (2017). Eye tracking measures of uncertainty during perceptual decision making. *International Journal of Psychophysiology*, 120:60–68.

[53] Bueti, D., Bahrami, B., Walsh, V., and Rees, G. (2010). Encoding of Temporal Probabilities in the Human Brain. *Journal of Neuroscience*, 30(12):4343–4352.

[54] Buhusi, C. V. and Meck, W. H. (2005). What makes us tick? Functional and neural mechanisms of interval timing. *Nat Rev Neurosci*, 6(10):755–765.

[55] Buhusi, C. V. and Meck, W. H. (2006). Interval timing with gaps and distracters: Evaluation of the ambiguity, switch, and time-sharing hypotheses. *Journal of Experimental Psychology: Animal Behavior Processes*, 32(3):329–338.

[56] Buhusi, C. V. and Meck, W. H. (2009). Relativity Theory and Time Perception: Single or Multiple Clocks? *PLoS ONE*, 4(7):e6268.

[57] Buonomano, D. V. and Karmakar, U. R. (2002). How do we tell time? *The Neuroscientist*, 8(1):42–51.

[58] Burle, B., Tandonnet, C., and Hasbroucq, T. (2010). 18 Excitatory and inhibitory motor mechanisms of temporal preparation. In Nobre, A. C. and Coull, J. T., editors, *Attention and Time*, pages 243–255. Oxford University Press, 1 edition.

[59] Cao, R., Bright, I. B., and Howard, M. (2024). Ramping cells in the rodent medial prefrontal cortex encode time to past and future events via real Laplace transform. *PNAS*, 121(38):e2404169121.

[60] Capizzi, M., Correa, A., and Sanabria, D. (2013). Temporal orienting of attention is interfered by concurrent working memory updating. *Neuropsychologia*, 51(2):326–339.

[61] Capizzi, M., Correa, A., Wojtowicz, A., and Rafal, R. (2015). Foreperiod priming in temporal preparation: Testing current models of sequential effects. *Cognition*, 134:39–49.

[62] Carleton, R. N., Norton, P. J., and Asmundson, G. J. (2007). Fearing the unknown: A short version of the Intolerance of Uncertainty Scale. *Journal of Anxiety Disorders*, 21(1):105–117.

[63] Carpenter, R. H. S. (2017). 4.3 Oculomotor Procrastination. In Fisher, D. F., Monty, R. A., and Senders, J. W., editors, *Eye Movements*, pages 237–246. Routledge, 1 edition.

[64] Carpenter, R. H. S. and Williams, M. L. L. (1995). Neural computation of log likelihood in control of saccadic eye movements. *Nature*, 377:59–62.

[65] Carpio, A., Dreher, J.-C., Ferrera, D., Galán, D., Mercado, F., and Obeso, I. (2024). Causal computations of supplementary motor area on spatial impulsivity. *Sci Rep*, 14:17040.

[66] Carrasco, M. (2011). Visual attention: The past 25 years. *Vision Research*, 51(13):1484–1525.

[67] Cavanagh, J. F., Wiecki, T. V., Kochar, A., and Frank, M. J. (2014). Eye tracking and pupillometry are indicators of dissociable latent decision processes. *Journal of Experimental Psychology: General*, 143(4):1476–1488.

[68] Cazettes, F., Reato, D., Morais, J. P., Renart, A., and Mainen, Z. F. (2021). Phasic Activation of Dorsal Raphe Serotonergic Neurons Increases Pupil Size. *Current Biology*, 31(1):192–197.e4.

[69] Chen, L. L., Hung, L. Y., Quinet, J., and Kosek, K. (2013). Cognitive regulation of saccadic velocity by reward prospect. *Eur J of Neuroscience*, 38(3):2434–2444.

[70] Cherng, Y.-G., Baird, T., Chen, J.-T., and Wang, C.-A. (2020). Background luminance effects on pupil size associated with emotion and saccade preparation. *Sci Rep*, 10(1):15718.

[71] Church, R. M. (1984). Properties of the Internal Clock". *Annals of the New York Academy of Sciences*, 423:566–582.

[72] Church, R. M. (2003). A Concise Introduction to Scalar Timing Theory. In Meck, W. H., editor, *Functional and neural mechanisms of interval timing*, pages 3–22. Routledge.

[73] Church, R. M. and Gibbon, J. (1982). Temporal generalization. *Journal of Experimental Psychology: Animal Behavior Processes*, 8(2):165–186.

[74] Connolly, J. D., Goodale, M. A., Goltz, H. C., and Munoz, D. P. (2005). fMRI Activation in the Human Frontal Eye Field Is Correlated With Saccadic Reaction Time. *Journal of Neurophysiology*, 94(1):605–611.

[75] Conway, C. M. (2020). How does the brain learn environmental structure? Ten core principles for understanding the neurocognitive mechanisms of statistical learning. *Neuroscience & Biobehavioral Reviews*, 112:279–299.

[76] Correa, A. (2010). 26 Enhancing behavioural performance by visual temporal orienting. In Nobre, A. C. and Coull, J. T., editors, *Attention and Time*, pages 357–370. Oxford University PressOxford, 1 edition.

[77] Corruble, E., Benyamina, A., Bayle, F., Falissard, B., and Hardy, P. (2003). Understanding impulsivity in severe depression? A psychometrical contribution. *Progress in Neuro-Psychopharmacology and Biological Psychiatry*, 27(5):829–833.

[78] Cosman, J. D., Lowe, K. A., Zinke, W., Woodman, G. F., and Schall, J. D. (2018). Prefrontal Control of Visual Distraction. *Current Biology*, 28(3):414–420.e3.

[79] Coull, J. T. (2009). Neural Substrates of Mounting Temporal Expectation. *PLoS Biol*, 7(8):e1000166.

[80] Coull, J. T. and Droit-Volet, S. (2018). Explicit Understanding of Duration Develops Implicitly through Action. *Trends in Cognitive Sciences*, 22(10):923–937.

[81] Coull, J. T., Korolczuk, I., and Morillon, B. (2024). The Motor of Time: Coupling Action to Temporally Predictable Events Heightens Perception. In Merchant, H. and De Lafuente, V., editors, *Neurobiology of Interval Timing*, pages 141–158. Springer International Publishing, 2 edition.

[82] Coull, J. T. and Nobre, A. C. (1998). Where and When to Pay Attention: The Neural Systems for Directing Attention to Spatial Locations and to Time Intervals as Revealed by Both PET and fMRI. *J. Neurosci.*, 18(18):7426–7435.

[83] Coull, J. T. and Nobre, A. C. (2008). Dissociating explicit timing from temporal expectation with fMRI. *Current Opinion in Neurobiology*, 18(2):137–144.

[84] Coull, J. T., Vidal, F., and Burle, B. (2016). When to act, or not to act: that's the SMA's question. *Current Opinion in Behavioral Sciences*, 8:14–21.

[85] Creelman, C. D. (1962). Human Discrimination of Auditory Duration. *Journal of the Acoustical Society of America*, 34(5):582–593.

[86] Crowe, D. A., Averbeck, B. B., and Chafee, M. V. (2010). Rapid Sequences of Population Activity Patterns Dynamically Encode Task-Critical Spatial Information in Parietal Cortex. *J. Neurosci.*, 30(35):11640–11653.

[87] Crowe, E. M., Los, S. A., Schindler, L., and Kent, C. (2021). Transfer effects in auditory temporal preparation occur using an unfilled but not filled foreperiod. *Quarterly Journal of Experimental Psychology*, 74(8):1432–1438.

[88] Cui, X., Stetson, C., Montague, P., and Eagleman, D. M. (2009). Ready…Go: Amplitude of the fMRI Signal Encodes Expectation of Cue Arrival Time. *PLoS Biol*, 7(8):e1000167.

[89] Dalley, J. W. and Robbins, T. W. (2017). Fractionating impulsivity: neuropsychiatric implications. *Nat Rev Neurosci*, 18(3):158–171.

[90] Daltrozzo, J. and Conway, C. M. (2014). Neurocognitive mechanisms of statistical-sequential learning: what do event-related potentials tell us? *Front. Hum. Neurosci.*, 8:437.

[91] Damsma, A., Schlichting, N., and van Rijn, H. (2021). Temporal Context Actively Shapes EEG Signatures of Time Perception. *J. Neurosci.*, 41(20):4514–4523.

[92] Damsma, A., Taatgen, N., De Jong, R., and Van Rijn, H. (2020). No evidence for an attentional bias towards implicit temporal regularities. *Atten Percept Psychophys*, 82(3):1136–1149.

[93] Damsma, A. and Van Rijn, H. (2017). Pupillary response indexes the metrical hierarchy of unattended rhythmic violations. *Brain and Cognition*, 111:95–103.

[94] Dankner, Y., Shalev, L., Carrasco, M., and Yuval-Greenberg, S. (2017). Prestimulus Inhibition of Saccades in Adults With and Without Attention-Deficit/Hyperactivity Disorder as an Index of Temporal Expectations. *Psychol Sci*, 28(7):835–850.

[95] Dassonville, P., Lewis, S. M., Foster, H. E., and Ashe, J. (1999). Choice and stimulus–response compatibility affect duration of response selection. *Cognitive Brain Research*, 7(3):235–240.

[96] De Berker, A. O., Rutledge, R. B., Mathys, C., Marshall, L., Cross, G. F., Dolan, R. J., and Bestmann, S. (2016). Computations of uncertainty mediate acute stress responses in humans. *Nat Commun*, 7(1):10996.

[97] De Corte, B. J., Akdoğan, B., and Balsam, P. D. (2022). Temporal scaling and computing time in neural circuits: Should we stop watching the clock and look for its gears? *Front. Behav. Neurosci.*, 16:1022713.

[98] De Gee, J. W., Colizoli, O., Kloosterman, N. A., Knapen, T., Nieuwenhuis, S., and Donner, T. H. (2017). Dynamic modulation of decision biases by brainstem arousal systems. *eLife*, 6:e23232.

[99] De Gee, J. W., Knapen, T., and Donner, T. H. (2014). Decision-related pupil dilation reflects upcoming choice and individual bias. *Proc. Natl. Acad. Sci. U.S.A.*, 111(5):3618–e625.

[100] de Hemptinne, C., Nozaradan, S., Duvivier, Q., Lefevre, P., and Missal, M. (2007). How Do Primates Anticipate Uncertain Future Events? *The Journal of Neuroscience*, 27(16):4334 – 4341.

[101] Degos, B., Ameqrane, I., Rivaud-Péchoux, S., Pouget, P., and Missal, M. (2018). Short-term temporal memory in idiopathic and Parkin-associated Parkinson's disease. *Sci Rep*, 8(1):7637.

[102] Degos, B., Pouget, P., and Missal, M. (2022). From anticipation to impulsivity in Parkinson's disease. *npj Parkinsons Dis.*, 8(1):125.

[103] Denison, R. N. (2024). Visual temporal attention from perception to computation. *Nat Rev Psychol*, 3(4):261–274.

[104] Di Stasi, L. L., Catena, A., Cañas, J. J., Macknik, S. L., and Martinez-Conde, S. (2013). Saccadic velocity as an arousal index in naturalistic tasks. *Neuroscience & Biobehavioral Reviews*, 37(5):968–975.

[105] Diamond, A. (2013). Executive Functions. *Annu. Rev. Psychol.*, 64(1):135–168.

[106] DiGirolamo, G. J., Patel, N., and Blaukopf, C. L. (2016). Arousal facilitates involuntary eye movements. *Exp Brain Res*, 234(7):1967–1976.

[107] Doherty, J. R., Rao, A., Mesulam, M. M., and Nobre, A. C. (2005). Synergistic Effect of Combined Temporal and Spatial Expectations on Visual Attention. *J. Neurosci.*, 25(36):8259–8266.

[108] Doya, K. (2000). Complementary roles of basal ganglia and cerebellum in learning and motor control. *Current Opinion in Neurobiology*, 10(6):732–739.

[109] Drążyk, D. and Missal, M. (2022). The oculomotor signature of expected surprise. *Sci Rep*, 12(1):2543.

[110] Drążyk, D. and Missal, M. (2023). How Does Temporal Blurring Alter Movement Timing? *eNeuro*, 10(9):ENEURO.0496–22.2023.

[111] Duma, G. M., Granziol, U., and Mento, G. (2020). Should I stay or should I go? How local-global implicit temporal expectancy shapes proactive motor control: An hdEEG study. *NeuroImage*, 220:117071.

[112] Duque, J., Greenhouse, I., Labruna, L., and Ivry, R. B. (2017). Physiological Markers of Motor Inhibition during Human Behavior. *Trends in Neurosciences*, 40(4):219–236.

[113] Duque, J. and Ivry, R. B. (2009). Role of Corticospinal Suppression during Motor Preparation. *Cerebral Cortex*, 19(9):2013–2024.

[114] Durstewitz, D. (2004). Neural representation of interval time:. *NeuroReport*, 15(5):745–749.

[115] Edelman, J. A. and Goldberg, M. E. (2001). Dependence of Saccade-Related Activity in the Primate Superior Colliculus on Visual Target Presence. *Journal of Neurophysiology*, 86(2):676–691.

[116] Ekman, P. and Friesen, W. V. (1971). Constants across cultures in the face and emotion. *Journal of Personality and Social Psychology*, 17(2):124–129.

[117] Evans, N. J. and Wagenmakers, E.-J. (2020). Evidence Accumulation Models: Current Limitations and Future Directions. *TQMP*, 16(2):73–90.

[118] Evenden, J. L. (1999). Varieties of impulsivity. *Psychopharmacology*, 146(4):348–361.

[119] Faouzi, J., Corvol, J.-C., and Mariani, L.-L. (2021). Impulse control disorders and related behaviors in Parkinson's disease: risk factors, clinical and genetic aspects, and management. *Current Opinion in Neurology*, 34(4):547–555.

[120] Forbes, S. H. (2015). Pupillometryr: an r package for preparing and analysing pupillometry data. *Journal of Open Source Software*, 5(50):2285.

[121] Forbes, S. H. (2023). Pupillometryr: an r package for preparing and analysing pupillometry data. *[manual]*.

[122] Franco, C. Y., Petok, J. R., Langley, J., Hu, X., and Bennett, I. J. (2021). Implicit associative learning relates to basal ganglia gray matter microstructure in young and older adults. *Behavioural Brain Research*, 397:112950.

[123] Freeston, M., Rheaume, J., Letarte, H., Dugas, M., and Ladouceur, R. (1994). Why do people worry? *Personality and Individual Differences*, 17(6):791–802.

[124] Friedman, D., Hakerem, G., Sutton, S., and Fleiss, J. L. (1973). Effect of stimulus uncertainty on the pupillary dilation response and the vertex evoked potential. *Electroencephalography and Clinical Neurophysiology*, 34(5):475–484.

[125] Friston, K., Kilner, J., and Harrison, L. (2006). A free energy principle for the brain. *Journal of Physiology-Paris*, 100(1-3):70–87.

[126] Gabay, S. and Henik, A. (2010). Temporal expectancy modulates inhibition of return in a discrimination task. *Psychonomic Bulletin & Review*, 17(1):47–51.

[127] Galley, N. (1989). Saccadic eye movement velocity as an indicator of (de)activation. A review and some speculations. *Journal of Psychophysiology*, 3(3):229–244.

[128] Gallistel, C. R. and Gibbon, J. (2000). Time, rate, and conditioning. *Psychological Review*, 107(2):289–344.

[129] Garraux, G., McKinney, C., Wu, T., Kansaku, K., Nolte, G., and Hallett, M. (2005). Shared Brain Areas But Not Functional Connections Controlling Movement Timing and Order. *J. Neurosci.*, 25(22):5290–5297.

[130] Gasser, T. (2005). Genetics of Parkinson's disease. *Current Opinion in Neurology*, 18:363–369.

[131] Geng, J. J., Blumenfeld, Z., Tyson, T. L., and Minzenberg, M. J. (2015). Pupil diameter reflects uncertainty in attentional selection during visual search. *Front. Hum. Neurosci.*, 9:435.

[132] Getty, D. J. (1975). Discrimination of short temporal intervals: A comparison of two models. *Perception & Psychophysics*, 18(1):1–8.

[133] Gibaldi, A. and Sabatini, S. P. (2021). The saccade main sequence revised: A fast and repeatable tool for oculomotor analysis. *Behav Res*, 53(1):167–187.

[134] Gibbon, J. (1977). Scalar Expectancy Theory and Weber's Law in Animal Timing. *Psychologcal Review*, 84(3):279–325.

[135] Gibbon, J., Church, R. M., and Meck, W. H. (1984). Scalar Timing in Memory. *Annals of the New York Academy of Sciences*, 423(1):52–77.

[136] Gibbons, H. and Rammsayer, T. H. (2004). Current-source density analysis of slow brain potentials during time estimation. *Psychophysiology*, 41(6):861–874.

[137] Godijn, R. and Kramer, A. F. (2008). Oculomotor capture by surprising onsets. *Visual Cognition*, 16(2-3):279–289.

[138] Godijn, R. and Theeuwes, J. (2003). Parallel allocation of attention prior to the execution of saccade sequences. *Journal of Experimental Psychology: Human Perception and Performance*, 29(5):882–896.

[139] Goossens, H. H. L. M. and Van Opstal, A. J. (2006). Dynamic Ensemble Coding of Saccades in the Monkey Superior Colliculus. *Journal of Neurophysiology*, 95(4):2326–2341.

[140] Goossens, H. H. L. M. and Van Opstal, A. J. (2012). Optimal Control of Saccades by Spatial-Temporal Activity Patterns in the Monkey Superior Colliculus. *PLoS Comput Biol*, 8(5):e1002508.

[141] Gottlieb, J. P., Kusunoki, M., and Goldberg, M. E. (1998). The representation of visual salience in monkey parietal cortex. *Nature*, 391(6666):481–484.

[142] Grabenhorst, M., Maloney, L. T., Poeppel, D., and Michalareas, G. (2021). Two sources of uncertainty independently modulate temporal expectancy. *Proc. Natl. Acad. Sci. U.S.A.*, 118(16):e2019342118.

[143] Grabenhorst, M., Michalareas, G., Maloney, L. T., and Poeppel, D. (2019). The anticipation of events in time. *Nat Commun*, 10(1):5802.

[144] Griffin, I., Miniussi, C., and Nobre, A. C. (2002). Multiple mechanisms of selective attention: differential modulation of stimulus processing by attention to space or time. *Neuropsychologia*, 40(13):2325–2340.

[145] Grondin, S. (2012). Violation of the scalar property for time perception between 1 and 2 seconds: Evidence from interval discrimination, reproduction, and categorization. *Journal of Experimental Psychology: Human Perception and Performance*, 38(4):880–890.

[146] Grondin, S. and Killeen, P. R. (2009). Tracking time with song and count: Different Weber functions for musicians and nonmusicians. *Attention, Perception & Psychophysics*, 71(7):1649–1654.

[147] Grujic, N., Polania, R., and Burdakov, D. (2024). Neurobehavioral meaning of pupil size. *Neuron*, 112(20):3381–3395.

[148] Haith, A. M., Reppert, T. R., and Shadmehr, R. (2012). Evidence for Hyperbolic Temporal Discounting of Reward in Control of Movements. *J. Neurosci.*, 32(34):11727–11736.

[149] Han, T. and Proctor, R. W. (2022). Revisiting variable-foreperiod effects: evaluating the repetition priming account. *Atten Percept Psychophys*, 84(4):1193–1207.

[150] Harnishfeger, K. (1995). Development of cognitive inhibition. In Dempster, F. N. and Corkill, A. J., editors, *Interference and Inhibition in Cognition and Behavior: Unifying Themes for Educational Psychology*, pages 176–199. Academic Press.

[151] Hartig, F. (2024). Dharma: Residual diagnostics for hierarchical (multi-level / mixed) regression models. *[manual]*.

[152] Harvey, C. D., Coen, P., and Tank, D. W. (2012). Choice-specific sequences in parietal cortex during a virtual-navigation decision task. *Nature*, 484(7392):62–68.

[153] Hayashi, M. J., Ditye, T., Harada, T., Hashiguchi, M., Sadato, N., Carlson, S., Walsh, V., and Kanai, R. (2015). Time Adaptation Shows Duration Selectivity in the Human Parietal Cortex. *PLoS Biol*, 13(9):e1002262.

[154] Heiney, S. A., Wohl, M. P., Chettih, S. N., Ruffolo, L. I., and Medina, J. F. (2014). Cerebellar-Dependent Expression of Motor Learning during Eyeblink Conditioning in Head-Fixed Mice. *J. Neurosci.*, 34(45):14845–14853.

[155] Herbst, S. K., Fiedler, L., and Obleser, J. (2018). Tracking Temporal Hazard in the Human Electroencephalogram Using a Forward Encoding Model. *eNeuro*, 5(2):ENEURO.0017–18.2018.

[156] Herbst, S. K. and Obleser, J. (2017). Implicit variations of temporal predictability: Shaping the neural oscillatory and behavioural response. *Neuropsychologia*, 101:141–152.

[157] Heys, J. G. and Dombeck, D. A. (2018). Evidence for a subcircuit in medial entorhinal cortex representing elapsed time during immobility. *Nat Neurosci*, 21(11):1574–1582.

[158] Hick, W. E. (1952). On the Rate of Gain of Information. *Quarterly Journal of Experimental Psychology*, 4(1):11–26.

[159] Hikosaka, O., Takikawa, Y., and Kawagoe, R. (2000). Role of the Basal Ganglia in the Control of Purposive Saccadic Eye Movements. *Physiological Reviews*, 80(3):953–978.

[160] Hollingworth, H. L. (1910). The Central Tendency of Judgment. *The Journal of Philosophy, Psychology and Scientific Methods*, 7(17):461–469.

[161] Horan, M., Daddaoua, N., and Gottlieb, J. (2019). Parietal neurons encode information sampling based on decision uncertainty. *Nat Neurosci*, 22(8):1327–1335.

[162] Horn, K. E. and Biittner-Ennever, A. (1994). Neurotransmitter Profile of Saccadic Omnipause Neurons in Nucleus Raphe lnterpositus. *Journal of Neuroscience*, 14(5):2032–2046.

[163] Horstmann, G. and Herwig, A. (2015). Surprise attracts the eyes and binds the gaze. *Psychon Bull Rev*, 22(3):743–749.

[164] Howard, M. W. and Eichenbaum, H. (2013). The hippocampus, time, and memory across scales. *Journal of Experimental Psychology: General*, 142(4):1211–1230.

[165] Hsu, T., Hsu, Y., Wang, H., and Wang, C. (2021). Role of the frontal eye field in human pupil and saccade orienting responses. *Eur J of Neuroscience*, 54(1):4283–4294.

[166] Hsu, T.-Y., Lee, H.-C., Lane, T. J., and Missal, M. (2019). Temporal Preparation, Impulsivity and Short-Term Memory in Depression. *Front. Behav. Neurosci.*, 13:258.

[167] Hyman, R. (1953). Stimulus information as a determinant of reaction time. *Journal of Experimental Psychology*, 45(3):188–196.

[168] Ikeda, T. and Hikosaka, O. (2007). Positive and Negative Modulation of Motor Response in Primate Superior Colliculus by Reward Expectation. *Journal of Neurophysiology*, 98(6):3163–3170.

[169] Irons, J. L., Jeon, M., and Leber, A. B. (2017). Pre-stimulus pupil dilation and the preparatory control of attention. *PLoS ONE*, 12(12):e0188787.

[170] Itti, L. and Baldi, P. (2009). Bayesian surprise attracts human attention. *Vision Research*, 49(10):1295–1306.

[171] Ivry, R. B. and Hazeltine, R. E. (1995). Perception and Production of Temporal Intervals Across a Range of Durations: Evidence for a Common Timing Mechanism. *Journal of Experimental Psychology: Human Perception and Performance*, 21(1):3–18.

[172] Jainta, S., Vernet, M., Yangand, Q., and Kapoula, Z. (2011). The pupil reflects motor preparation for saccades – even before the eye starts to move. *Front. Hum. Neurosci.*, 5:97.

[173] Janssen, P. and Shadlen, M. N. (2005). A representation of the hazard rate of elapsed time in macaque area LIP. *Nat Neurosci*, 8(2):234–241.

[174] Jazayeri, M. and Shadlen, M. N. (2010). Temporal context calibrates interval timing. *Nat Neurosci*, 13(8):1020–1026.

[175] Jennings, J. R. and Van Der Molen, M. W. (2005). Preparation for Speeded Action as a Psychophysiological Concept. *Psychological Bulletin*, 131(3):434–459.

[176] Jepma, M. (2010). The role of the noradrenergic system in the exploration-exploitation trade-off: a pharmacological study. *Front. Hum. Neurosci.*, 4:170.

[177] Jepma, M., Wagenmakers, E.-J., and Nieuwenhuis, S. (2012). Temporal expectation and information processing: A model-based analysis. *Cognition*, 122(3):426–441.

[178] Jin, W., Nobre, A. C., and Van Ede, F. (2020). Temporal Expectations Prepare Visual Working Memory for Behavior. *Journal of Cognitive Neuroscience*, 32(12):2320–2332.

[179] Joshi, S. and Gold, J. I. (2020). Pupil Size as a Window on Neural Substrates of Cognition. *Trends in Cognitive Sciences*, 24(6):466–480.

[180] Jurkowski, A. J., Stepp, E., and Hackley, S. A. (2005). Variable foreperiod deficits in Parkinson's disease: Dissociation across reflexive and voluntary behaviors. *Brain and Cognition*, 58(1):49–61.

[181] Kahneman, D. and Beatty, J. (1966). Pupil Diameter and Load on Memory. *Science*, 154(3756):1583–1585.

[182] Kalesnykas, R. and Hallett, P. (1987). The differentiation of visually guided and anticipatory saccades in gap and overlap paradigms. *Exp Brain Res*, 68(1):115–212.

[183] Kawagoe, R., Takikawa, Y., and Hikosaka, O. (1998). Expectation of reward modulates cognitive signals in the basal ganglia. *Nat Neurosci*, 1(5):411–416.

[184] Kiani, R. and Shadlen, M. N. (2009). Representation of Confidence Associated with a Decision by Neurons in the Parietal Cortex. *Science*, 324(5928):759–764.

[185] Kilavik, B. E., Roux, S., Ponce-Alvarez, A., Confais, J., Grün, S., and Riehle, A. (2009). Long-Term Modifications in Motor Cortical Dynamics Induced by Intensive Practice. *J. Neurosci.*, 29(40):12653–12663.

[186] Kipp, K. (2005). A Developmental Perspective on the Measurement of Cognitive Deficits in Attention-Deficit/Hyperactivity Disorder. *Biological Psychiatry*, 57(11):1256–1260.

[187] Kloosterman, N. A., Meindertsma, T., van Loon, A. M., Lamme, V. A. F., Bonneh, Y. S., and Donner, T. H. (2015). Pupil size tracks perceptual content and surprise. *Eur J Neurosci*, 41(8):1068–1078.

[188] Kobayashi, S. and Schultz, W. (2008). Influence of Reward Delays on Responses of Dopamine Neurons. *J. Neurosci.*, 28(31):7837–7846.

[189] Kononowicz, T. W. and Penney, T. B. (2016). The contingent negative variation (CNV): timing isn't everything. *Current Opinion in Behavioral Sciences*, 8:231–237.

[190] Kononowicz, T. W. and Van Rijn, H. (2011). Slow Potentials in Time Estimation: The Role of Temporal Accumulation and Habituation. *Front. Integr. Neurosci.*, 5:48.

[191] Kononowicz, T. W. and van Rijn, H. (2014). Decoupling Interval Timing and Climbing Neural Activity: A Dissociation between CNV and N1P2 Amplitudes. *Journal of Neuroscience*, 34(8):2931–2939.

[192] Kononowicz, T. W., van Rijn, H., and Meck, W. H. (2018). Timing and Time Perception: A Critical Review of Neural Timing Signatures Before, During, and After the To-Be-Timed Interval. *Stevens' Handbook of Experimental Psychology and Cognitive Neuroscience*, pages 1–38.

[193] Krishnamurthy, K., Nassar, M. R., Sarode, S., and Gold, J. I. (2017). Arousal-related adjustments of perceptual biases optimize perception in dynamic environments. *Nat Hum Behav*, 1(6):0107.

[194] Kveraga, K., Boucher, L., and Hughes, H. C. (2002). Saccades operate in violation of Hick's law. *Exp Brain Res*, 146(3):307–314.

[195] Kóbor, A., Kardos, Z., Horváth, K., Janacsek, K., Takács, A., Csépe, V., and Nemeth, D. (2021). Implicit anticipation of probabilistic regularities: Larger CNV emerges for unpredictable events. *Neuropsychologia*, 156:107826.

[196] Laeng, B., Sirois, S., and Gredebäck, G. (2012). Pupillometry: A Window to the Preconscious? *Perspect Psychol Sci*, 7(1):18–27.

[197] Lakens, D. (2017). Equivalence tests: A practical primer for t-tests, correlations, and meta-analyses. *Social Psychological and Personality Science*, 8(4):355–362.

[198] Lakens, D., Scheel, A. M., and Isager, P. M. (2018). Equivalence Testing for Psychological Research: A Tutorial. *Advances in Methods and Practices in Psychological Science*, 1(2):259–269.

[199] Lakens, D. (2025). Toster: Equivalence tests: A practical primer for t-tests, correlations, and meta-analyses. *[manual]*.

[200] Land, M. F. and Hayhoe, M. (2001). In what ways do eye movements contribute to everyday activities? *Vision Research*, 41(25-26):3559–3565.

[201] Land, M. F. and McLeod, P. (2000). From eye movements to actions: how batsmen hit the ball. *Nat Neurosci*, 3(12):1340–1345.

[202] Lavín, C., San Martín, R., and Rosales Jubal, E. (2014). Pupil dilation signals uncertainty and surprise in a learning gambling task. *Front. Behav. Neurosci.*, 7:218.

[203] Lawlor, J., Zagala, A., Jamali, S., and Boubenec, Y. (2023). Pupillary dynamics reflect the impact of temporal expectation on detection strategy. *iScience*, 26(2):106000.

[204] Lebon, F., Greenhouse, I., Labruna, L., Vanderschelden, B., Papaxanthis, C., and Ivry, R. B. (2016). Influence of Delay Period Duration on Inhibitory Processes for Response Preparation. *Cereb. Cortex*, 26(6):2461–2470.

[205] Lee, K.-M., Keller, E. L., and Heinen, S. J. (2005). Properties of saccades generated as a choice response. *Exp Brain Res*, 162(3):278–286.

[206] Lejeune, H. (1998). Switching or gating? The attentional challenge in cognitive models of psychological time. *Behavioural Processes*, 44(2):127–145.

[207] Lejeune, H. and Wearden, J. H. (2009). Vierordt's *The Experimental Study of the Time Sense* (1868) and its legacy. *European Journal of Cognitive Psychology*, 21(6):941–960.

[208] Lenth, R. (2025). emmeans: Estimated marginal means, aka least-squares means. *[manual]*.

[209] Li, B., Chen, Y., Xiao, L., Liu, P., and Huang, X. (2017). Duration adaptation modulates EEG correlates of subsequent temporal encoding. *NeuroImage*, 147:143–151.

[210] Lindskog, M., Nyström, P., and Gredebäck, G. (2021). Can the Brain Build Probability Distributions? *Front. Psychol.*, 12:596231.

[211] Liversedge, S. P. and Findlay, J. M. (2000). Saccadic eye movements and cognition. *Trends in Cognitive Sciences*, 4(1):6–14.

[212] Los, S. A. (2010). 21 Foreperiod and sequential effects: theory and data. In Nobre, A. C. and Coull, J. T., editors, *Attention and Time*, pages 289–302. Oxford University PressOxford, 1 edition.

[213] Los, S. A. (2013). The role of response inhibition in temporal preparation: Evidence from a go/no-go task. *Cognition*, 129(2):328–344.

[214] Los, S. A. (2014). Outlines of a multiple trace theory of temporal preparation. *Frontiers in Psychology*, 5:1058.

[215] Los, S. A. and Heslenfeld, D. J. (2005). Intentional and Unintentional Contributions to Nonspecific Preparation: Electrophysiological Evidence. *Journal of Experimental Psychology: General*, 134(1):52–72.

[216] Los, S. A., Knol, D. L., and Boers, R. M. (2001). The foreperiod effect revisited: conditioning as a basis for nonspecifc preparation. *Acta Psychologica*, 106:121–145.

[217] Los, S. A., Kruijne, W., and Meeter, M. (2017). Hazard versus history: Temporal preparation is driven by past experience. *Journal of Experimental Psychology: Human Perception and Performance*, 43(1):78–88.

[218] Los, S. A., Nieuwenstein, J., Bouharab, A., Stephens, D. J., Meeter, M., and Kruijne, W. (2021). The warning stimulus as retrieval cue: The role of associative memory in temporal preparation. *Cognitive Psychology*, 125:101378.

[219] Loued-Khenissi, L. and Preuschoff, K. (2020). Information Theoretic Characterization of Uncertainty Distinguishes Surprise From Accuracy Signals in the Brain. *Front. Artif. Intell.*, 3:5.

[220] Luce, R. D. (1991). 8 Distributions of Simple Decision Latencies. In Braodbent, D. E., McGaugh, J. L., Mackintosh, N. J., Posner, M. I., Tulving, E., and Weiskrantz, L., editors, *Response times: their role in inferring elementary mental organization*, pages 122–175. Oxford University Press, 1 edition.

[221] Lüdecke, D., Ben-Shachar, M. S., Patil, I., Waggoner, P., and Makowski, D. (2021). Performance: an r package for assessment, comparison and testing of statistical models. *Journal of Open Source Software*, 6(60):3139.

[222] Lüdecke, D. and Ben-Shachar, M. S. and Patil, I. and Waggoner, P. and Makowski, D. (2025a). Parameters: Extracting, computing and exploring the parameters of statistical models using r. *[manual]*.

[223] Lüdecke, D. and Ben-Shachar, M. S. and Patil, I. and Waggoner, P. and Makowski, D. (2025b). Performance: an r package for assessment, comparison and testing of statistical models. *[manual]*.

[224] Ma, W. J. and Jazayeri, M. (2014). Neural Coding of Uncertainty and Probability. *Annu. Rev. Neurosci.*, 37(1):205–220.

[225] Macar, F. and Besson, M. (1985). Contingent negative variation in processes of expectancy, motor preparation and time estimation. *Biological Psychology*, 21(4):293–307.

[226] Macar, F. and Vidal, F. (2003). The CNV peak: An index of decision making and temporal memory. *Psychophysiology*, 40(6):950–954.

[227] Macar, F., Vidal, F., and Casini, L. (1999). The supplementary motor area in motor and sensory timing: evidence from slow brain potential changes. *Experimental Brain Research*, 125(3):271–280.

[228] MacAskill, M. R. and Anderson, T. J. (2016). Eye movements in neurodegenerative diseases. *Current Opinion in Neurology*, 29(1):61–68.

[229] MacDonald, C. J., Lepage, K. Q., Eden, U. T., and Eichenbaum, H. (2011). Hippocampal "Time Cells" Bridge the Gap in Memory for Discontiguous Events. *Neuron*, 71(4):737–749.

[230] MacKay, A. and Juola, J. F. (2007). Are spatial and temporal attention independent? *Perception & Psychophysics*, 69(6):972–979.

[231] MacLeod, C. M. (2007). 1 The concept of inhibition in cognition. In Gorfein, D. S. and MacLeod, C. M., editors, *Inhibition in cognition.*, pages 3–23. American Psychological Association, Washington.

[232] Mahanama, B., Jayawardana, Y., Rengarajan, S., Jayawardena, G., Chukoskie, L., Snider, J., and Jayarathna, S. (2022). Eye Movement and Pupil Measures: A Review. *Front. Comput. Sci.*, 3:733531.

[233] Manohar, S. G., Chong, T. T.-J., Apps, M. A., Batla, A., Stamelou, M., Jarman, P. R., Bhatia, K. P., and Husain, M. (2015). Reward Pays the Cost of Noise Reduction in Motor and Cognitive Control. *Current Biology*, 25(13):1707–1716.

[234] Maris, E. and Oostenveld, R. (2007). Nonparametric statistical testing of EEG- and MEG-data. *Journal of Neuroscience Methods*, 164(1):177–190.

[235] Massar, S. A. A., Sasmita, K., Lim, J., and Chee, M. W. L. (2018). Motivation alters implicit temporal attention through sustained and transient mechanisms: A behavioral and pupillometric study. *Psychophysiology*, 55(12):e13275.

[236] Matell, M. S. and Meck, W. H. (2000). Neuropsychological mechanisms of interval timing behavior. *Bioessays*, 22(1):94–103.

[237] Matell, M. S. and Meck, W. H. (2004). Cortico-striatal circuits and interval timing: coincidence detection of oscillatory processes. *Cognitive Brain Research*, 21(2):139–170.

[238] Mathôt, S. (2018). Pupillometry: Psychology, Physiology, and Function. *Journal of Cognition*, 1(1):16.

[239] Mathôt, S., Fabius, J., Van Heusden, E., and Van der Stigchel, S. (2018). Safe and sensible preprocessing and baseline correction of pupil-size data. *Behav Res*, 50(1):94–106.

[240] Matthews, W. J. and Grondin, S. (2012). On the replication of Kristofferson's (1980) quantal timing for duration discrimination: some learning but no quanta and not much of a Weber constant. *Atten Percept Psychophys*, 74(5):1056–1072.

[241] Matthews, W. J. and Meck, W. H. (2016). Temporal cognition: Connecting subjective time to perception, attention, and memory. *Psychological Bulletin*, 142(8):865–907.

[242] Mattiesing, R. M., Kruijne, W., Meeter, M., and Los, S. A. (2017). Timing a week later: The role of long-term memory in temporal preparation. *Psychon Bull Rev*, 24(6):1900–1905.

[243] Mazzoni, P., Hristova, A., and Krakauer, J. W. (2007). Why Don't We Move Faster? Parkinson's Disease, Movement Vigor, and Implicit Motivation. *J. Neurosci.*, 27(27):7105–7116.

[244] McDougal, D. H. and Gamlin, P. D. (2015). Autonomic Control of the Eye. *Comprehensive Physiology*, 5(1):439–473.

[245] Meermeier, A., Gremmler, S., Richert, K., Eckermann, T., and Lappe, M. (2017). The reward of seeing: Different types of visual reward and their ability to modify oculomotor learning. *Journal of Vision*, 17(12):11.

[246] Mello, G. B. M., Soares, S., and Paton, J. J. (2015). A Scalable Population Code for Time in the Striatum. *Current Biology*, 25(9):1113–1122.

[247] Mento, G., Tarantino, V., Sarlo, M., and Bisiacchi, P. S. (2013). Automatic Temporal Expectancy: A High-Density Event-Related Potential Study. *PLoS ONE*, 8(5):e62896.

[248] Merchant, H., Harrington, D. L., and Meck, W. H. (2013). Neural Basis of the Perception and Estimation of Time. *Annu. Rev. Neurosci.*, 36(1):313–336.

[249] Milliken, B., Lupiáñez, J., Roberts, M., and Stevanovski, B. (2003). Orienting in space and time: Joint contributions to exogenous spatial cuing effects. *Psychonomic Bulletin & Review*, 10(4):877–883.

[250] Milstein, D. M. and Dorris, M. C. (2007). The Influence of Expected Value on Saccadic Preparation. *J. Neurosci.*, 27(18):4810–4818.

[251] Missal, M. and Keller, E. L. (2002). Common Inhibitory Mechanism for Saccades and Smooth-Pursuit Eye Movements. *Journal of Neurophysiology*, 88(4):1880–1892.

[252] Mita, A., Mushiake, H., Shima, K., Matsuzaka, Y., and Tanji, J. (2009). Interval time coding by neurons in the presupplementary and supplementary motor areas. *Nat Neurosci*, 12(4):502–507.

[253] Miura, K. and Optican, L. M. (2006). Membrane channel properties of premotor excitatory burst neurons may underlie saccade slowing after lesions of omnipause neurons. *J Comput Neurosci*, 20(1):25–41.

[254] Miyashita, K., Rand, M. K., Miyachi, S., and Hikosaka, O. (1996). Anticipatory saccades in sequential procedural learning in monkeys. *Journal of Neurophysiology*, 76(2):1361–1366.

[255] Mostofsky, S. H., Schafer, J. G. B., Abrams, M. T., Goldberg, M. C., Flower, A. A., Boyce, A., Courtney, S. M., Calhoun, V. D., Kraut, M. A., Denckla, M. B., and Pekar, J. J. (2003). fMRI evidence that the neural basis of response inhibition is task-dependent. *Cognitive Brain Research*, 17(2):419–430.

[256] Moustafa, A. A., Chakravarthy, S., Phillips, J. R., Gupta, A., Keri, S., Polner, B., Frank, M. J., and Jahanshahi, M. (2016). Motor symptoms in Parkinson's disease: A unified framework. *Neuroscience & Biobehavioral Reviews*, 68:727–740.

[257] Muhammed, K., Dalmaijer, E., Manohar, S., and Husain, M. (2020). Voluntary modulation of saccadic peak velocity associated with individual differences in motivation. *Cortex*, 122:198–212.

[258] Mulder, M., Van Maanen, L., and Forstmann, B. U. (2014). Perceptual decision neurosciences – A model-based review. *Neuroscience*, 277:872–884.

[259] Munoz, D. P. and Everling, S. (2004). Look away: the anti-saccade task and the voluntary control of eye movement. *Nat Rev Neurosci*, 5(3):218–228.

[260] Munoz, D. P. and Wurtz, R. H. (1995). Saccade-related activity in monkey superior colliculus. I. Characteristics of burst and buildup cells. *Journal of Neurophysiology*, 73(6):2313–2333.

[261] Murphy, P. R., Vandekerckhove, J., and Nieuwenhuis, S. (2014). Pupil-Linked Arousal Determines Variability in Perceptual Decision Making. *PLoS Comput Biol*, 10(9):e1003854.

[262] Nachev, P., Kennard, C., and Husain, M. (2008). Functional role of the supplementary and pre-supplementary motor areas. *Nat Rev Neurosci*, 9(11):856–869.

[263] Naghibi, N., Jahangiri, N., Khosrowabadi, R., Eickhoff, C. R., Eickhoff, S. B., Coull, J. T., and Tahmasian, M. (2024). Embodying Time in the Brain: A Multi-Dimensional Neuroimaging Meta-Analysis of 95 Duration Processing Studies. *Neuropsychol Rev*, 34(1):277–298.

[264] Nassar, M. R., Rumsey, K. M., Wilson, R. C., Parikh, K., Heasly, B., and Gold, J. I. (2012). Rational regulation of learning dynamics by pupil-linked arousal systems. *Nat Neurosci*, 15(7):1040–1046.

[265] Ng, K. K., Tobin, S., and Penney, T. B. (2011). Temporal Accumulation and Decision Processes in the Duration Bisection Task Revealed by Contingent Negative Variation. *Front. Integr. Neurosci.*, 5:77.

[266] Niemi, P. (1979). Stimulus intensity effects on auditory and visual reaction processes. *Acta Psychologica*, 43(4):299–312.

[267] Niemi, P. and Naatanen, R. (1981). Foreperiod and simple reaction time. *Psychological Bulletin*, 89(1):133–162.

[268] Nobre, A. C. (2001). Orienting attention to instants in time. *Neuropsychologia*, 39(12):1317–1328.

[269] Nobre, A. C., Correa, A., and Coull, J. T. (2007). The hazards of time. *Current Opinion in Neurobiology*, 17(4):465–470.

[270] Nobre, A. C. and van Ede, F. (2018). Anticipated moments: temporal structure in attention. *Nat Rev Neurosci*, 19(1):34–48.

[271] Nombela, C., Rittman, T., Robbins, T. W., and Rowe, J. B. (2014). Multiple Modes of Impulsivity in Parkinson's Disease. *PLoS ONE*, 9(1):e85747.

[272] Noorani, I. and Carpenter, R. H. S. (2016). The LATER model of reaction time and decision. *Neuroscience & Biobehavioral Reviews*, 64:229–251.

[273] Notaro, G., Van Zoest, W., Altman, M., Melcher, D., and Hasson, U. (2019). Predictions as a window into learning: Anticipatory fixation offsets carry more information about environmental statistics than reactive stimulus-responses. *Journal of Vision*, 19(2):8.

[274] Näätänen, R. (1971). Non-aging fore-periods and simple reaction time. *Acta Psychologica*, 35(4):316–327.

[275] Ofir, N. and Landau, A. N. (2022). Neural signatures of evidence accumulation in temporal decisions. *Current Biology*, 32(18):4093–4100.e6.

[276] Oostenveld, R. and Fries, P. and Maris, E. and Schoffelen, J. M. (2021). Fieldtrip: Open source software for advanced analysis of meg, eeg, and invasive electrophysiological data. *[manual]*.

[277] Optican, L. M. and Pretegiani, E. (2017). What stops a saccade? *Phil. Trans. R. Soc. B*, 372(1718):20160194.

[278] O'Reilly, J. X. (2013). Making predictions in a changing world—inference, uncertainty, and learning. *Front. Neurosci.*, 7:105.

[279] O'Reilly, J. X., McCarthy, K. J., Capizzi, M., and Nobre, A. C. (2008). Acquisition of the Temporal and Ordinal Structure of Movement Sequences in Incidental Learning. *Journal of Neurophysiology*, 99(5):2731–2735.

[280] Oswal, A., Ogden, M., and Carpenter, R. H. S. (2007). The Time Course of Stimulus Expectation in a Saccadic Decision Task. *Journal of Neurophysiology*, 97(4):2722–2730.

[281] Otero-Millan, J., Optican, L. M., Macknik, S. L., and Martinez-Conde, S. (2018). Modeling the Triggering of Saccades, Microsaccades, and Saccadic Intrusions. *Front. Neurol.*, 9:346.

[282] Palmieri, H. and Carrasco, M. (2024). Task demand mediates the interaction of spatial and temporal attention. *Sci Rep*, 14(1):9228.

[283] Pasquereau, B. and Turner, R. S. (2015). Dopamine neurons encode errors in predicting movement trigger occurrence. *Journal of Neurophysiology*, 113(4):1110–1123.

[284] Pastalkova, E., Itskov, V., Amarasingham, A., and Buzsáki, G. (2008). Internally Generated Cell Assembly Sequences in the Rat Hippocampus. *Science*, 321(5894):1322–1327.

[285] Paton, J. J. and Buonomano, D. V. (2018). The Neural Basis of Timing: Distributed Mechanisms for Diverse Functions. *Neuron*, 98(4):687–705.

[286] Patton, J. H., Stanford, M. S., and Barratt, E. S. (1995). Factor structure of the barratt impulsiveness scale. *J. Clin. Psychol.*, 51(6):768–774.

[287] Payzan-LeNestour, E. and Bossaerts, P. (2012). Do not Bet on the Unknown Versus Try to Find Out More: Estimation Uncertainty and "Unexpected Uncertainty" Both Modulate Exploration. *Front. Neurosci.*, 6:150.

[288] Perugini, A., Ditterich, J., and Basso, M. A. (2016). Patients with Parkinson's Disease Show Impaired Use of Priors in Conditions of Sensory Uncertainty. *Current Biology*, 26(14):1902–1910.

[289] Pfeuffer, C. U., Aufschnaiter, S., Thomaschke, R., and Kiesel, A. (2020). Only time will tell the future: Anticipatory saccades reveal the temporal dynamics of time-based location and task expectancy. *Journal of Experimental Psychology: Human Perception and Performance*, 46(10):1183–1200.

[290] Pfeuffer, C. U., Kiesel, A., and Huestegge, L. (2016). A look into the future: Spontaneous anticipatory saccades reflect processes of anticipatory action control. *Journal of Experimental Psychology: General*, 145(11):1530–1547.

[291] Pfeuty, M., Ragot, R., and Pouthas, V. (2005). Relationship between cnv and timing of an upcoming event. *Neuroscience Letters*, 382(1–2):106–111.

[292] Pineda-Pardo, J. A., Obeso, I., Guida, P., Dileone, M., Strange, B. A., Obeso, J. A., Oliviero, A., and Foffani, G. (2019). Static magnetic field stimulation of the supplementary motor area modulates resting-state activity and motor behavior. *Commun Biol*, 2(1):397.

[293] Piras, F. and Coull, J. T. (2011). Implicit, Predictive Timing Draws upon the Same Scalar Representation of Time as Explicit Timing. *PLoS ONE*, 6(3):e18203.

[294] Pouget, P., Murthy, A., and Stuphorn, V. (2017). Cortical control and performance monitoring of interrupting and redirecting movements. *Phil. Trans. R. Soc. B*, 372(1718):20160201.

[295] Praamstra, P., Kourtis, D., Kwok, H. F., and Ostenveld, R. (2006). Neurophysiology of Implicit Timing in Serial Choice Reaction-Time Performance. *Journal of Neuroscience*, 26(20):5448–5455.

[296] Preuschoff, K. (2011). Pupil dilation signals surprise: evidence for noradrenaline's role in decision making. *Front. Neurosci.*, 5:115.

[297] Proctor, R. W. and Schneider, D. W. (2018). Hick's law for choice reaction time: A review. *Quarterly Journal of Experimental Psychology*, 71(6):1281–1299.

[298] Protopapa, F., H, M. J., Kulashekhar, S., van der Zwaag, W., Battistella, G., Murray, M. M., Kanai, R., and Bueti, D. (2019). Chronotopic maps in human supplementary motor area. *PLoS Biol*, 17(3):e3000026.

[299] Rammsayer, T. and Ulrich, R. (2001). Counting models of temporal discrimination. *Psychonomic Bulletin & Review*, 8(2):270–277.

[300] Ranganath, C. and Rainer, G. (2003). Neural mechanisms for detecting and remembering novel events. *Nat Rev Neurosci*, 4(3):193–202.

[301] Ratcliff, R. (1978). A Theory of Memory Retrieval. *Psychological Review*, 85(2):59–108.

[302] Ratcliff, R. and Smith, P. L. (2004). A Comparison of Sequential Sampling Models for Two-Choice Reaction Time. *Psychological Review*, 111(2):333–367.

[303] Ratcliff, R., Smith, P. L., Brown, S. D., and McKoon, G. (2016). Diffusion Decision Model: Current Issues and History. *Trends in Cognitive Sciences*, 20(4):260–281.

[304] Reimer, J., McGinley, M. J., Liu, Y., Rodenkirch, C., Wang, Q., McCormick, D. A., and Tolias, A. S. (2016). Pupil fluctuations track rapid changes in adrenergic and cholinergic activity in cortex. *Nat Commun*, 7(1):13289.

[305] Ren, Y., Allenmark, F., Müller, H. J., and Shi, Z. (2021). Variation in the "coefficient of variation": Rethinking the violation of the scalar property in time-duration judgments. *Acta Psychologica*, 214:103263.

[306] Reppert, T. R., Lempert, K. M., Glimcher, P. W., and Shadmehr, R. (2015). Modulation of Saccade Vigor during Value-Based Decision Making. *J. Neurosci.*, 35(46):15369–15378.

[307] Rescorla, R. A. and Wagner, A. R. (1972). A Theory of Pavlovian Conditioning: Variations in the Effectiveness of Reinforcement and Nonreinforcement. *Classical conditioning II: Current research and theory*, Appleton-Century-Crofts.(New York):64–99.

[308] Richer, F. and Beatty, J. (1987). Contrasting Effects of Response Uncertainty on the Task-Evoked Pupillary Response and Reaction Time. *Psychophysiology*, 24(3):258–262.

[309] Rohenkohl, G., Gould, I. C., Pessoa, J., and Nobre, A. C. (2014). Combining spatial and temporal expectations to improve visual perception. *Journal of Vision*, 14(4):8–8.

[310] Rolando, F., Kononowicz, T. W., Duhamel, J.-R., Doyère, V., and Wirth, S. (2024). Distinct neural adaptations to time demand in the striatum and the hippocampus. *Current Biology*, 34(1):156–170.e7.

[311] Rolke, B. and Hofmann, P. (2007). Temporal uncertainty degrades perceptual processing. *Psychonomic Bulletin & Review*, 14(3):522–526.

[312] Rosenthal, R. (1994). Parametric measures of effect size. In Cooper, H. M. and Hedges, L. V., editors, *The handbook of research synthesis*, pages 231–244. Russell Sage Foundation, New York, NY.

[313] Rucker, J. C., Ying, S. H., Moore, W., Optican, L. M., Büttner-Ennever, J., Keller, E. L., Shapiro, B. E., and Leigh, R. J. (2011). Do brainstem omnipause neurons terminate saccades? *Annals of the New York Academy of Sciences*, 1233(1):48–57.

[314] Rueda-Orozco, P. E., Hidalgo-Balbuena, A. E., González-Pereyra, P., Martinez-Montalvo, M. G., and Báez-Cordero, A. S. (2024). The Interactions of Temporal and Sensory Representations in the Basal Ganglia. In Merchant, H. and De Lafuente, V., editors, *Neurobiology of Interval Timing*, pages 141–158. Springer International Publishing, 2 edition.

[315] Ruediger, S. and Scanziani, M. (2020). Learning speed and detection sensitivity controlled by distinct cortico-fugal neurons in visual cortex. *eLife*, 9:e59247.

[316] Sakurai, K., Li, H., Inamura, N., Masuoka, N., and Hisatsune, T. (2020). OPEN Relationship between elevated. *Scientific Reports*, 10:21032.

[317] Salet, J. M., Kruijne, W., and Van Rijn, H. (2021). Implicit learning of temporal behavior in complex dynamic environments. *Psychon Bull Rev*, 28(4):1270–1280.

[318] Salet, J. M., Kruijne, W., van Rijn, H., Los, S. A., and Meeter, M. (2022). FMTP: A unifying computational framework of temporal preparation across time scales. *Psychological Review*, 129(5):911–948.

[319] Sassenhagen, J. and Draschkow, D. (2019). Cluster-based permutation tests of MEG/EEG data do not establish significance of effect latency or location. *Psychophysiology*, 56(6):e13335.

[320] Satterthwaite, T. D., Green, L., Myerson, J., Parker, J., Ramaratnam, M., and Buckner, R. L. (2007). Dissociable but inter-related systems of cognitive control and reward during decision making: Evidence from pupillometry and event-related fMRI. *NeuroImage*, 37:15.

[321] Schiller, P. H., True, S. D., and Conway, J. L. (1980). Deficits in eye movements following frontal eye-field and superior colliculus ablations. *Journal of Neurophysiology*, 44(6):1175–1189.

[322] Schreiber, L., Odlaug, B. L., and Grant, J. E. (2011). Impulse Control Disorders: Updated Review of Clinical Characteristics and Pharmacological Management. *Front. Psychiatry*, 2:1.

[323] Scudder, C., Kaneko, C., and Fuchs, A. (2002). The brainstem burst generator for saccadic eye movements. *Experimental Brain Research*, 142(4):439–462.

[324] Sedaghat-Nejad, E., Herzfeld, D. J., and Shadmehr, R. (2019). Reward Prediction Error Modulates Saccade Vigor. *J. Neurosci.*, 39(25):5010–5017.

[325] Sedaghat-Nejad, E., Pi, J. S., Hage, P., Fakharian, M. A., and Shadmehr, R. (2022). Synchronous spiking of cerebellar Purkinje cells during control of movements. *Proc. Natl. Acad. Sci. U.S.A.*, 119(14):e2118954119.

[326] Seibold, V. C., Stepper, M. Y., and Rolke, B. (2020). Temporal attention boosts perceptual effects of spatial attention and feature-based attention. *Brain and Cognition*, 142:105570.

[327] Seideman, J. A., Stanford, T. R., and Salinas, E. (2018). Saccade metrics reflect decision-making dynamics during urgent choices. *Nat Commun*, 9(1):2907.

[328] Selya, A. S. (2012). A practical guide to calculating Cohen's f2, a measure of local effect size, from PROC MIXED. *Frontiers in Psychology*, 3:1.

[329] Shadmehr, R., Reppert, T. R., Summerside, E. M., Yoon, T., and Ahmed, A. A. (2019). Movement Vigor as a Reflection of Subjective Economic Utility. *Trends in Neurosciences*, 42(5):323–336.

[330] Shalev, N. and Nobre, A. C. (2022). Eyes wide open: Regulation of arousal by temporal expectations. *Cognition*, 224:105062.

[331] Shannon, C. E. (1948). A mathematical theory of communication. *The Bell system Technical Journal*, 27(3):379–424.

[332] Sharma, J., Sugihara, H., Katz, Y., Schummers, J., Tenenbaum, J., and Sur, M. (2015). Spatial Attention and Temporal Expectation Under Timed Uncertainty Predictably Modulate Neuronal Responses in Monkey V1. *Cereb. Cortex*, 25(9):2894–2906.

[333] Sheridan, M. R. and Flowers, K. A. (1990). MOVEMENT VARIABILITY AND BRADYKINESIA IN PARKINSON'S DISEASE. *Brain*, 113(4):1149–1161.

[334] Shin, J. C. and Ivry, R. B. (2002). Concurrent learning of temporal and spatial sequences. *Journal of Experimental Psychology: Learning, Memory, and Cognition*, 28(3):445–457.

[335] Siegel, M., Buschman, T. J., and Miller, E. K. (2015). Cortical information flow during flexible sensorimotor decisions. *Science*, 348(6241):1352–1355.

[336] Simen, P. (2018). 8 Reaction time analysis for interval timing research. In Vatakis, A., Balcı, F., Di Luca, M., and Correa, A., editors, *Timing and Time Perception: Procedures, Measures, and Applications*, pages 165–177. BRILL, Boston, 1 edition.

[337] Simen, P., Vlasov, K., and Papadakis, S. (2016). Scale (in)variance in a unified diffusion model of decision making and timing. *Psychological Review*, 123(2):151–181.

[338] Simmonds, D. J., Pekar, J. J., and Mostofsky, S. H. (2008). Meta-analysis of Go/No-go tasks demonstrating that fMRI activation associated with response inhibition is task-dependent. *Neuropsychologia*, 46(1):224–232.

[339] Smalianchuk, I., Jagadisan, U. K., and Gandhi, N. J. (2018). Instantaneous Midbrain Control of Saccade Velocity. *J. Neurosci.*, 38(47):10156–10167.

[340] Snijders, T. A. B. and Bosker, R. J. (2012). 6 Testing and Model Specification. In *Multilevel analysis: an introduction to basic and advanced multilevel modeling*, pages 148–164. Sage, Los Angeles, 2 edition.

[341] Sparks, D. L. (2002). The brainstem control of saccadic eye movements. *Nat Rev Neurosci*, 3(12):952–964.

[342] Spitzer, R. L., Kroenke, K., Williams, J. B. W., and Löwe, B. (2006). A Brief Measure for Assessing Generalized Anxiety Disorder: The GAD-7. *Arch Intern Med*, 166(10):1092.

[343] Starkweather, C. K., Gershman, S. J., and Uchida, N. (2018). The Medial Prefrontal Cortex Shapes Dopamine Reward Prediction Errors under State Uncertainty. *Neuron*, 98(3):616–629.e6.

[344] Steinborn, M. B. and Langner, R. (2012). Arousal modulates temporal preparation under increased time uncertainty: Evidence from higher-order sequential foreperiod effects. *Acta Psychologica*, 139(1):65–76.

[345] Steinborn, M. B., Rolke, B., Bratzke, D., and Ulrich, R. (2008). Sequential effects within a short foreperiod context: Evidence for the conditioning account of temporal preparation. *Acta Psychologica*, 129(2):297–307.

[346] Steinemann, N. A., Stine, G. M., Trautmann, E. M., Zylberberg, A., Wolpert, D. M., and Shadlen, M. N. (2024). Direct observation of the neural computations underlying a single decision.

[347] Stewart, E. E. M., Valsecchi, M., and Schütz, A. C. (2020). A review of interactions between peripheral and foveal vision. *Journal of Vision*, 20(12):2.

[348] Stine, G. M., Trautmann, E. M., Jeurissen, D., and Shadlen, M. N. (2023). A neural mechanism for terminating decisions. *Neuron*, 111(16):2601–2613.e5.

[349] Strauch, C., Wang, C.-A., Einhäuser, W., Van Der Stigchel, S., and Naber, M. (2022). Pupillometry as an integrated readout of distinct attentional networks. *Trends in Neurosciences*, 45(8):635–647.

[350] Stuphorn, V. and Schall, J. D. (2006). Executive control of countermanding saccades by the supplementary eye field. *Nat Neurosci*, 9(7):925–931.

[351] Stuphorn, V., Taylor, T. L., and Schall, J. D. (2000). Performance monitoring by the supplementary eye ®eld. *Nature Neuroscience*, 408.

[352] Summerfield, C. and Egner, T. (2009). Expectation (and attention) in visual cognition. *Trends in Cognitive Sciences*, 13(9):403–409.

[353] Taatgen, N. and Van Rijn, H. (2011). Traces of times past: Representations of temporal intervals in memory. *Mem Cogn*, 39(8):1546–1560.

[354] Takikawa, Y., Kawagoe, R., and Hikosaka, O. (2002). Reward-Dependent Spatial Selectivity of Anticipatory Activity in Monkey Caudate Neurons. *Journal of Neurophysiology*, 87(1):508–515.

[355] Tal-Perry, N. and Yuval-Greenberg, S. (2021). Prestimulus inhibition of eye movements reflects temporal expectation rather than time estimation. *Atten Percept Psychophys*, 83(6):2473–2485.

[356] Tal-Perry, N. and Yuval-Greenberg, S. (2022). The Spatiotemporal Link of Temporal Expectations: Contextual Temporal Expectation Is Independent of Spatial Attention. *J. Neurosci.*, 42(12):2516–2523.

[357] Teichert, T., Grinband, J., and Ferrera, V. (2016). The importance of decision onset. *Journal of Neurophysiology*, 115(2):643–661.

[358] Teufel, C. and Fletcher, P. C. (2020). Forms of prediction in the nervous system. *Nat Rev Neurosci*, 21(4):231–242.

[359] Theeuwes, J., Huang, C., Frings, C., and Van Moorselaar, D. (2024). Statistical learning of motor preparation. *Journal of Experimental Psychology: Human Perception and Performance*, 50(2):152–162.

[360] Thiel, C. M. and Fink, G. R. (2008). Effects of the cholinergic agonist nicotine on reorienting of visual spatial attention and top-down attentional control. *Neuroscience*, 152(2):381–390.

[361] Thier, P. and Markanday, A. (2019). Role of the Vermal Cerebellum in Visually Guided Eye Movements and Visual Motion Perception. *Annu. Rev. Vis. Sci.*, 5(1):247–268.

[362] Thura, D., Cos, I., Trung, J., and Cisek, P. (2014). Context-Dependent Urgency Influences Speed–Accuracy Trade-Offs in Decision-Making and Movement Execution. *J. Neurosci.*, 34(49):16442–16454.

[363] Tiganj, Z., Cromer, J. A., Roy, J. E., Miller, E. K., and Howard, M. W. (2018). Compressed Timeline of Recent Experience in Monkey Lateral Prefrontal Cortex. *Journal of Cognitive Neuroscience*, 30(7):935–950.

[364] Tiganj, Z., Jung, M. W., Kim, J., and Howard, M. W. (2017). Sequential Firing Codes for Time in Rodent Medial Prefrontal Cortex. *Cerebral Cortex*, 27(12):5663–5671.

[365] Tobler, P. N., Fiorillo, C. D., and Schultz, W. (2005). Adaptive Coding of Reward Value by Dopamine Neurons. *Science*, 307(5715):1642–1645.

[366] Tomassini, A., Pollak, T. A., Edwards, M. J., and Bestmann, S. (2019). Learning from the past and expecting the future in Parkinsonism: Dopaminergic influence on predictions about the timing of future events. *Neuropsychologia*, 127:9–18.

[367] Treisman, M. (1963). Temporal discrimination and the indifference interval: Implications for a model of the "internal clock". *Psychological Monographs: General and Applied*, 77(13):1–31.

[368] Trillenberg, P., Verleger, R., Wascher, E., Wauschkuhn, B., and Wessel, K. (2000). CNV and temporal uncertainty with 'ageing' and 'non-ageing' S1–S2 intervals. *Clinical Neurophysiology*, 111(7):1216–1226.

[369] Turcano, P., Jacobson, J., Ghoniem, K., Mullan, A., Camerucci, E., Stang, C., Piat, C., Bower, J. H., and Savica, R. (2024). Impulse control disorders and use of dopamine agonists in early onset Parkinson's disease. *Front. Neurol.*, 15:1404904.

[370] Ulrich, R., Nitschke, J., and Rammsayer, T. (2006). Crossmodal temporal discrimination: Assessing the predictions of a general pacemaker-counter model. *Perception & Psychophysics*, 68(7):1140–1152.

[371] Urai, A. E., Braun, A., and Donner, T. H. (2017). Pupil-linked arousal is driven by decision uncertainty and alters serial choice bias. *Nat Commun*, 8(1):14637.

[372] Usher, M., Olami, Z., and McClelland, J. L. (2002). Hick's Law in a Stochastic Race Model with Speed–Accuracy Tradeoff. *Journal of Mathematical Psychology*, 46(6):704–715.

[373] Vallesi, A. (2010). 22 Neuro-anatomical substrates of foreperiod effects. In Nobre, A. C. and Coull, J. T., editors, *Attention and Time*, pages 303–316. Oxford University Press, 1 edition.

[374] Vallesi, A., Arbula, S., and Bernardis, P. (2014). Functional dissociations in temporal preparation: Evidence from dual-task performance. *Cognition*, 130(2):141–151.

[375] Vallesi, A., Lozano, V., and Correa, A. (2013). Dissociating temporal preparation processes as a function of the inter-trial interval duration. *Cognition*, 127(1):22–30.

[376] Vallesi, A., McIntosh, A. R., and Stuss, D. T. (2009). Temporal preparation in aging: A functional MRI study. *Neuropsychologia*, 47(13):2876–2881.

[377] Vallesi, A. and Shallice, T. (2007). Developmental dissociations of preparation over time: Deconstructing the variable foreperiod phenomena. *Journal of Experimental Psychology: Human Perception and Performance*, 33(6):1377–1388.

[378] Van Der Wel, P. and Van Steenbergen, H. (2018). Pupil dilation as an index of effort in cognitive control tasks: A review. *Psychon Bull Rev*, 25(6):2005–2015.

[379] Van Ede, F., Rohenkohl, G., Gould, I., and Nobre, A. C. (2020). Purpose-Dependent Consequences of Temporal Expectations Serving Perception and Action. *J. Neurosci.*, 40(41):7877–7886.

[380] Van Elswijk, G., Kleine, B. U., Overeem, S., and Stegeman, D. F. (2007). Expectancy Induces Dynamic Modulation of Corticospinal Excitability. *Journal of Cognitive Neuroscience*, 19(1):121–131.

[381] van Rijn, H., Kononowicz, T. W., Meck, W. H., Ng, K. K., and Penney, T. B. (2011). Contingent negative variation and its relation to time estimation: a theoretical evaluation. *Front. Integr. Neurosci.*, 5:91.

[382] Vangkilde, S., Coull, J. T., and Bundesen, C. (2012). Great expectations: Temporal expectation modulates perceptual processing speed. *Journal of Experimental Psychology: Human Perception and Performance*, 38(5):1183–1191.

[383] Vangkilde, S., Petersen, A., and Bundesen, C. (2013). Temporal expectancy in the context of a theory of visual attention. *Phil. Trans. R. Soc. B*, 368(1628):20130054.

[384] Visalli, A., Capizzi, M., Ambrosini, E., Kopp, B., and Vallesi, A. (2021). Electroencephalographic correlates of temporal Bayesian belief updating and surprise. *NeuroImage*, 231:117867.

[385] Voeten, C. C. (2023). permutes: Permutation tests for time series data. *[manual]*.

[386] Voon, V., Mehta, A. R., and Hallett, M. (2011). Impulse control disorders in Parkinson's disease: recent advances. *Current Opinion in Neurology*, 24(4):324–330.

[387] Walter, W., Cooper, R., Aldridge, V., McCallum, W. C., and Winter, A. L. (1964). Contingent Negative Variation: An Electric Sign Of Sensorimotor Association And Expectancy In The Human Brain. *Nature*, 203:380–384.

[388] Wang, C.-A. and Munoz, D. P. (2015). A circuit for pupil orienting responses: implications for cognitive modulation of pupil size. *Current Opinion in Neurobiology*, 33:134–140.

[389] Wang, C.-A., Nguyen, K. T., and Juan, C.-H. (2021). Linking Pupil Size Modulated by Global Luminance and Motor Preparation to Saccade Behavior. *Neuroscience*, 476:90–101.

[390] Wascher, E., Verleger, R., Jaskowski, P., and Wauschkuhn, B. (1996). Preparation for action: an ERP study about two tasks provoking variability in response speed. *Psychophysiology*, 33(3):262–272.

[391] Wearden, J. (2016). A Brief History of Time Perception. In Wearden, J., editor, *The Psychology of Time Perception*, pages 1–11. Palgrave Macmillan UK, London.

[392] Wearden, J. H. and Lejeune, H. (2008). Scalar Properties in Human Timing: Conformity and Violations. *Quarterly Journal of Experimental Psychology*, 61(4):569–587.

[393] Weinbach, N., Shofty, I., Gabay, S., and Henik, A. (2015). Endogenous temporal and spatial orienting: Evidence for two distinct attentional mechanisms. *Psychon Bull Rev*, 22(4):967–973.

[394] Wiener, M. and Thompson, J. C. (2015). Repetition enhancement and memory effects for duration. *NeuroImage*, 113:268–278.

[395] Wierda, S. M., van Rijn, H., Taatgen, N. A., and Martens, S. (2012). Pupil dilation deconvolution reveals the dynamics of attention at high temporal resolution. *Proc. Natl. Acad. Sci. U.S.A.*, 109(22):8456–8460.

[396] Williams, J. N. (2020). The Neuroscience of Implicit Learning. *Language Learning*, 70(S2):255–307.

[397] Wittmann, M. and van Wassenhove, V. (2009). The experience of time: neural mechanisms and the interplay of emotion, cognition and embodiment. *Phil. Trans. R. Soc. B*, 364(1525):1809–1813.

[398] Wolf, C. and Lappe, M. (2021). Vision as oculomotor reward: cognitive contributions to the dynamic control of saccadic eye movements. *Cogn Neurodyn*, 15(4):547–568.

[399] Wolpert, D. M. and Flanagan, J. R. (2001). Motor prediction. *Current Biology*, 11(18):R729–R732.

[400] Woodrow, H. (1914). The measurement of attention. *Psychological Monographs*, 17:i–158.

[401] Yu, A. J. and Dayan, P. (2005). Uncertainty, Neuromodulation, and Attention. *Neuron*, 46(4):681–692.

[402] Zhang, J., Nombela, C., Wolpe, N., Barker, R. A., and Rowe, J. B. (2016). Time on timing: Dissociating premature responding from interval sensitivity in Parkinson's disease. *Movement Disorders*, 31(8):1163–1172.

[403] Zénon, A. (2019). Eye pupil signals information gain. *Proceedings of the Royal Society B*, 286:20191593.